TECHNICAL UNIVERSITY OF CRETE, GREECE

Mineral Resources Engineering Department

Biochar production from agricultural waste and environmental application

Kaliakatsou Georgia

Dipl. Engineer

Chania, 2016

Abstract

In this work, three types of biomass, pecan shells (Pe), sawdust (Sd) or pistachio shells (Pl) were subjected to slow pyrolysis for the production of biochar. Pyrolysis was carried out over a temperature range of 250–550 °C for one hour using a heating rate of 10 °C·min^{-1} and the quality of the produced biochars was assessed by evaluating their main properties, namely pH, volatile matter, char and C, H, N, O, S, content. The pyrolysis yield was also examined. Thermogravimetric analysis (TG), X-ray diffraction (XRD), Fourier Transform Infrared Spectroscopy (FTIR) and Scanning Electron Microscopy (SEM) were used for the identification of the morphology and structure of the produced biochar. The biochars were studied for their potential to adsorb either heavy metals in flasks or phenols in both flasks and fixed-bed columns. In order to improve the efficiency of biochar, activation was carried out with the use of KOH or FeCl$_3$. The potential of biochars in terms of phenols adsorption in acidic or basic solutions was also studied.

Keywords

Biochar, activated carbon, pecan shells, sawdust, pistachio shells, adsorption, heavy metals, phenols

Papers

The following papers were produced from my thesis work

Komnitsas, K., Zaharaki, D., Bartzas, G., Kaliakatsou, G., Kritikaki, A.: Efficiency of pecan shells and sawdust biochar on Pb and Cu adsorption, Desalination and Water Treatment, 57(7): 3237-46 (2016)

Zaharaki, D., Kaliakatsou, G., Kritikaki, A., Bartzas, G., Komnitsas, K.: Quality of biochar produced from pyrolysis of pecan shells and sawdust, 4th International Symposium on Green Chemistry, Environment, Health and Development, 24-26 (2014)

Περίληψη

Σε αυτή τη μελέτη βιομάζες διαφορετικής προέλευσης, δηλαδή κελύφη καρυδιών πεκάν (Pe), πριονίδι πεύκου (Sd) και κελύφη φυστικιών Αίγινης (Pl) χρησιμοποιήθηκαν για την παραγωγή βιοεξανθρακώματος (biochar) με αργή πυρόλυση σε θερμοκρασιακό εύρος από 250 έως 550 °C. Ο ρυθμός θέρμανσης ήταν 10 °C·min⁻¹, ενώ η πυρόλυση για κάθε θερμοκρασία διήρκησε μία ώρα. Η ποιότητα των παραγόμενων βιοεξανθρακωμάτων εκτιμήθηκε αξιολογώντας τις βασικές του ιδιότητες όπως είναι το pH, καθώς και το ποσοστό άνθρακα (C), υδρογόνου (H), αζώτου (N), οξυγόνου (O) και θείου (S) στο βιοεξανθράκωμα. Μελετήθηκε ακόμη η απόδοση της πυρόλυσης, η οποία μειώνεται κυρίως με την αύξηση της θερμοκρασίας πυρόλυσης και δευτερευόντως με την αύξηση του χρόνου πυρόλυσης. Παράγοντες όπως τα λιγνοκυτταρινικά συστατικά της βιομάζας δύνανται να έχουν επιρροή στην απόδοση της πυρόλυσης. Το pH, η ηλεκτρική αγωγιμότητα (EC) και το ποσοστό άνθρακα βρέθηκε ότι αυξάνονται με την αύξηση της θερμοκρασίας, ενώ το ποσοστό οξυγόνου βρέθηκε ότι μειώνεται.

Ακόμη, για την εξακρίβωση της μορφολογίας και της δομής του παραγόμενου βιοεξανθρακώματος χρησιμοποιήθηκαν τεχνικές όπως θερμοβαρυμετρική ανάλυση (TG), περίθλαση ακτινών X (XRD), φασματοσκοπία υπερύθρου με χρήση μετασχηματισμού Fourier (FTIR) και ηλεκτρονική μικροσκοπία σάρωσης (SEM). Όλα τα φάσματα που προέκυψαν από την ανάλυση των βιομαζών (Pe, Sd και Pl) ήταν χαρακτηριστικά οξυγονωμένων υδρογονανθράκων, ενώ παρατηρήθηκε απώλεια των ομάδων αυτών λόγω της αποσύνθεσης της κυτταρίνης και ημικυτταρίνης κατά την πυρόλυση.

Τα παραγόμενα προϊόντα εξετάστηκαν για την ικανότητά τους να προσροφούν βαρέα μέταλλα από υδατικά διαλύματα σε πειράματα που πραγματοποιήθηκαν σε κωνικές φιάλες. Τα βιοεξανθρακώματα από τα κελύφη πεκάν και το πριονίδι απορροφούν πιο αποτελεσματικά το μόλυβδο και το κάδμιο από ότι το χαλκό ή το κοβάλτιο. Ο μόλυβδος απομακρύνεται πολύ περισσότερο από το βιοεξανθράκωμα από κελύφη πεκάν (98.5 %) σε σύγκριση με το βιοεξανθράκωμα από πριονίδι (72.5 %), ενώ για το χαλκό, το κάδμιο και το κοβάλτιο το βιοεξανθράκωμα από πριονίδι φάνηκε ότι είναι καλύτερος προσροφητής. Γενικότερα, φάνηκε ότι όσο πιο υψηλή είναι η συγκέντρωση του προσροφητή τόσο υψηλότερη είναι η προσρόφηση των βαρέων μετάλλων και ότι το μεγαλύτερο ποσοστό απομάκρυνσης των ιόντων των μετάλλων πραγματοποιήθηκε σε όλες τις περιπτώσεις μέχρι τις δύο πρώτες ώρες. Επιπλέον, φαίνεται ότι υπάρχει μία κρίσιμη συγκέντρωση προσροφητή για τον καλύτερο δυνατό ρυθμό προσρόφησης των μετάλλων στο βιοεξανθράκωμα η οποία εξαρτάται από τη δομή του βιοεξανθρακώματος και τα την ιοντική ακτίνα των μετάλλων. Το κινητικό μοντέλο ψευδο-δεύτερης τάξης βρέθηκε ότι ταιριάζει καλύτερα στα δεδομένα προσρόφησης των μετάλλων και επομένως ο κύριος μηχανισμός προσρόφησής τους από το βιοεξανθράκωμα είναι η χημική προσρόφηση των δισθενών ιόντων των μετάλλων πάνω στις πολικές δραστικές ομάδες του βιοεξανθρακώματος. Οι χαρακτηριστικές αυτές ομάδες περιλαμβάνουν υδροξύλια και καρβοξύλια στα οποία τα μέταλλα συγκρατώνται μέσω της συμπλοκοποίησης ή της ανταλλαγής ιόντων, ενώ για βιοεξανθρακώματα παραγόμενα σε υψηλότερες θερμοκρασίες η κύρια διεργασία που κυρίως καθορίζει την προσρόφηση των μετάλλων είναι η διασωματιδιακή διάχυση των μετάλλων μέσα στους πόρους. Άλλοι παράγοντες που σχετίζονται με την προσρόφηση των ιόντων μετάλλων είναι οι απελευθερωμένες ιοντικές ρίζες (π.χ. CO_3^{2-}) από ορυκτά τα οποία ενυπάρχουν στο βιοεξανθράκωμα, καθώς επίσης και η υψηλή περιεκτικότητα του βιοεξανθρακώματος σε άνθρακα. Ο βαθμός εκρόφησης που εμφανίζουν τα βαρέα μέταλλα σχετίζεται με τη δομή του βιοεξανθρακώματος και τη φύση των βαρέων μετάλλων και όχι με το διάλυμα που χρησιμοποιείται για την εκρόφησή τους (HCl ή HNO_3). Ύστερα από 24 ώρες εκρόφησης, το βιοεξανθράκωμα από κελύφη πεκάν, υπό τη χρήση HNO_3 ως μέσου εκρόφησης παρουσίασε τη χαμηλότερη εκρόφηση μετάλλου (63.3 % εκρόφηση μολύβδου), ενώ το βιοεξανθράκωμα από πριονίδι τη μέγιστη εκρόφηση του μετάλλου με χρήση του ίδιου μέσου εκρόφησης (100 % εκρόφηση μολύβδου). Οι ικανότητες προσρόφησης που προκύπτουν για τα βιοεξανθρακώματα μετά τη δεύτερη προσρόφηση αποκάλυψαν ότι το βιοεξανθράκωμα από πριονίδι που έχει ήδη χρησιμοποιηθεί μία φορά για την προσρόφηση μετάλλου είναι καλύτερο προσροφητικό υλικό για εκ νέου χρήση από ότι το αντίστοιχο βιοεξανθράκωμα από κελύφη πεκάν.

Τα παραγόμενα βιοεξανθρακώματα εξετάστηκαν και για την ικανότητά τους να απορροφούν φαινόλες από υδατικά διαλύματα σε κωνικές φιάλες αλλά και σε στήλες σταθερής κλίνης. Επιπλέον, έγινε σύγκριση της προσρόφησης των φαινολών από τα υδατικά διαλύματα σε κωνικές φιάλες, με pH μεταξύ 4.55 και 5.82, με την προσρόφηση σε αντίστοιχα όξινα (pH 4) ή βασικά (pH 9) υδατικά διαλύματα. Σύγκριση έγινε επίσης και με την προσρόφηση φαινολών από υδατικά διαλύματα σε κωνικές φυάλες όπου το βιοεξανθράκωμα που χρησιμοποιήθηκε είχε προηγουμένως τροποποιηθεί με καυστικό κάλιο (KOH) ή χλωριούχο σίδηρο ($FeCl_3$). Η υψηλότερη συγκέντρωση βιοεξανθρακώματος οδήγησε σε αυξημένο ποσοστό προσρόφησης. Το μεγαλύτερο ποσοστό απομάκρυνσης των φαινολών από υδατικό διάλυμα σε κωνικές φυάλες έφτασε το 70 % όταν χρησιμοποιήθηκε συγκέντρωση βιοεξανθρακώματος από πριονίδι ίση με 5 g·L⁻¹. Όταν διαφορετικοί ρύποι είναι ο στόχος της προσρόφησης, διαφορετικοί συνδυασμοί μηχανισμών προσρόφησης εμπλέκονται. Έτσι, ο χρόνος

ισορροπίας για την προσρόφηση των φαινολών ήταν μεγαλύτερος από αυτόν για την προσρόφηση βαρέων μετάλλων. Χρειάστηκαν, δηλαδή 48 ώρες για να επέλθει ισορροπία, ενώ μέχρι το πρώτο εικοσιτετράωρο είχε πραγματοποιηθεί το 67.4 έως και 98.6 % της συνολικής προσρόφησης από όλους τους προσροφητές που χρησιμοποιήθηκαν. Πιστεύεται ότι οι βασικοί παράγοντες που επηρεάζουν την προσρόφηση των φαινολών είναι κυρίως ο συνδυασμός της επιφάνειας των μικροπόρων, η δομή των πόρων και οι δραστικές επιφανειακές ομάδες παρά η ειδική επιφάνεια από μόνη της. Όμοια με την περίπτωση προσρόφησης μετάλλων, το κινητικό μοντέλο ψευδο-δεύτερης τάξης βρέθηκε ότι ταιριάζει καλύτερα στα δεδομένα προσρόφησης των φαινολών και επομένως ο κύριος μηχανισμός προσρόφησής τους από το βιοεξανθράκωμα είναι η χημική προσρόφηση των φαινολών σε ιοντική μορφή πάνω στις πολικές δραστικές ομάδες του βιοεξανθρακώματος, όπως είναι, σύμφωνα με την FTIR ανάλυση, οι καρβοξυλικές ομάδες και οι ομάδες που περιέχουν υδροξύλιο. Φαίνεται παρόλα αυτά ότι υπάρχει προτεραιότητα των φαινολών να εισχωρούν στους πόρους όταν η συγκέντρωση του προσροφητή είναι χαμηλή. Επιπλέον, φαίνεται ότι στα βιοεξανθρακώματα από κελύφη πεκάν και από πριονίδι προσδένονται πρώτα τα πρωτόνια (H^+) και δευτερευόντως οι φαινόλες πιθανότατα εξηγώντας επίσης το μεγαλύτερο διάστημα που απαιτείται για να επιτευχθεί συγκέντρωση ισορροπίας κατά την προσρόφηση φαινολών σε σχέση με την προσρόφηση μετάλλων.

Η κατανομή των μοριακών και ιονισμένων φαινολών ποικίλει καθώς το pH του διαλύματος μεταβάλλεται. Παρόλα αυτά, σε αυτή τη μελέτη η μεταβολή του pH του αρχικού διαλύματος δεν επηρέασε την προσρόφηση των φαινολών στο βιοεξανθράκωμα, πιθανότατα λόγω της ρυθμιστικής ικανότητας του βιοεξανθρακώματος. Από περιβαλλοντική άποψη φαίνεται πάντως ότι τα βιοεξανθρακώματα όχι μόνο μπορούν να χρησιμοποιηθούν για τη μείωση των συγκεντρώσεων βαρέων μετάλλων και φαινολών από υδατικά διαλύματα αλλά και για τη ρύθμιση του pH τους επιτυγχάνοντας έως και 43 % μεταβολή του pH στο διάλυμα που χρησιμοποιήθηκε βιοεξανθράκωμα από πριονίδι.

Στα πειράματα που διεξήχθησαν στις στήλες σταθερής κλίνης, το βιοεξανθράκωμα από πριονίδι είναι πιο αποδοτικό στη συνεχόμενη προσρόφηση φαινολών από ότι τα βιοεξανθρακώματα από κελύφη πεκάν και φυστικιών Αιγίνης επειδή έως και 79 % λιγότερη ποσότητα του πρώτου βιοεξανθρακώματος χρησιμοποιείται για αποτελέσματα προσρόφησης κοντά στο 55 %.

Το βιοεξανθράκωμα το οποίο τροποποιήθηκε με ΚΟΗ παρουσίασε χαμηλότερο ποσοστό προσρόφησης φαινολών από το βιοεξανθράκωμα που δεν τροποποιήθηκε, λόγω της παρεμπόδισης των ενεργών θέσεων από τα μόρια ΚΟΗ που παρέμειναν προσκολλημένα πάνω στο βιοεξανθράκωμα και λόγω της διαβρωτικής ικανότητας του αντιδραστηρίου αυτού. Φαίνεται ότι πρέπει να εξεταστεί περαιτέρω η διεργασία της τροποποίησης.

Για το βιοεξανθράκωμα από κελύφη φυστικιών Αιγίνης το οποίο τροποποιήθηκε με διάλυμα χλωριούχου σιδήρου το ποσοστό απομάκρυνσης των φαινολών ήταν υψηλότερο από αυτό του βιοεξανθρακώματος που δεν τροποποιήθηκε, ενώ για τα υπόλοιπα βιοεξανθρακώματα η προσρόφηση ήταν παρόμοια. Οι λειτουργικές ομάδες που φαίνεται να συνεισφέρουν στην προσρόφηση των φαινολών με την ανάπτυξη ηλεκτροστατικών δυνάμεων που αναπτύσσονται μεταξύ προσροφητή και προσροφούμενης ουσίας είναι οι καρβοξυλικές ομάδες, και οι ομάδες που περιέχουν υδροξύλιο όπως είναι και ο γκαιτίτης (FeOOH). Παρόλα αυτά, τα βιοεξανθρακώματα τα οποία εμποτίζονται με χλωριούχο σίδηρο έχουν ευεργετική επίδραση σε χαμηλά pH και επομένως ο εμποτισμός του βιοεξανθρακώματος με χλωριούχο σίδηρο δεν είναι κατάλληλη διαδικασία εάν η στοχευόμενη προσροφούμενη ουσία έχει υψηλό pKa, όπως οι φαινόλες.

Η ειδική επιφάνεια και η δομή των πόρων του βιοεξανθρακώματος εξαρτώνται από τη φύση της πρώτης ύλης και μπορεί να είναι τελείως διαφορετικά όταν το βιοεξανθράκωμα παράγεται σε διαφορετικές θερμοκρασίες ή όταν υπόκειται στη διεργασία της τροποποίησης. Επιπλέον, οι ιδιότητες του βιοεξανθρακώματος διαφέρουν από αυτές του τροποποιημένου βιοεξανθρακώματος, παρότι και τα δύο είναι υλικά πλούσια σε άνθρακα. Όταν τα βιοεξανθρακώματα παράγονται σε υψηλότερες θερμοκρασίες τότε η ειδική επιφάνεια αυξάνεται φτάνοντας τα 298.7 $m^2 \cdot g^{-1}$. Η αύξηση αυτή οφείλεται στις χημικές αλλαγές που σημβαίνουν στην επιφάνεια του βιοεξανθρακώματος κατά την πυρόλυσή τους σε υψηλότερες θερμοκρασίες, όπως είναι η αποσύνθεση των οργανικών δεσμών και η ανάπτυξη της αρωματικότητας στα βιοεξανθρακώματα τα οποία οδηγούν στη δημιουργία μικρο- και μακρο-πόρων.

Όλα τα πορίσματα που προέκυψαν από αυτή τη μελέτη είναι σημαντικά για την επιλογή βιοεξανθρακωμάτων και τροποποιημένων βιοεξανθρακωμάτων κατάλληλων για εφαρμογή σε υδατικά συστήματα για την προσρόφηση βαρέων μετάλλων και φαινολών. Παρόλα αυτά, η άμεση συσχέτιση και σύγκριση των πειραματικών αποτελεσμάτων προσρόφησης με τη βιβλιογραφία είναι πολύπλοκη εξαιτίας της ποικιλίας των πειραματικών συνθηκών και παραμέτρων. Ένας μεγάλος αριθμός συμπληρωματικών πειραμάτων και η σταδιακή ταξινόμηση των συμπερασμάτων θα βοηθήσουν στο μέλλον.

Λέξεις κλειδιά: Βιοεξανθράκωμα, ενεργοποιημένος άνθρακας, πεκάν κελύφη, πριονίδι, κελύφη φυστικιών Αιγίνης, προσρόφηση, βαρέα μέταλλα, φαινόλες

Acknowledgements

Contents

Tables list

Figures list

Abbreviations

Pe:	Pecan shells
Sd:	Sawdust
Pl:	Pistachio shells

Pe250:	Pecan shells biochar pyrolyzed at 250 °C
Sd250:	Sawdust biochar pyrolyzed at 250 °C
Pl250:	Pistachio shells biochar pyrolyzed at 250 °C

Pe350:	Pecan shells biochar pyrolyzed at 350 °C
Sd350:	Sawdust biochar pyrolyzed at 350 °C
Pl350:	Pistachio shells biochar pyrolyzed at 350 °C

Pe450:	Pecan shells biochar pyrolyzed at 450 °C
Sd450:	Sawdust biochar pyrolyzed at 450 °C
Pl450:	Pistachio shells biochar pyrolyzed at 450 °C

Pe550:	Pecan shells biochar pyrolyzed at 550 °C
Sd550:	Sawdust biochar pyrolyzed at 550 °C
Pl550:	Pistachio shells biochar pyrolyzed at 550 °C

y_P:	Pyrolysis yield
VM:	Volatile matter
FTIR:	Fourier Transform Infrared Spectroscopy
XRD:	X-ray diffraction
SEM:	Scanning Electron Microscopy
TG:	Thermogravimetric analysis

PePhe:	Solution of 100 mg·L^{-1} phenols agitated with Pe350
SdPhe:	Solution of 100 mg·L^{-1} phenols agitated with Sd350
PlPhe:	Solution of 100 mg·L^{-1} phenols agitated with Pl350

Pe10Phe:	10 mg·L^{-1} phenols percolated through mixture of 50-50 v/v quartz sand to Pe350 in 100 mL column
Sd10Phe:	10 mg·L^{-1} phenols percolated through mixture of 50-50 v/v quartz sand to Sd350 in 100 mL column
C10Phe:	Control column, 10 mg·L^{-1} phenols percolated through quartz sand in 100 mL in 100 mL column

Pe200Phe:	200 mg·L^{-1} phenols percolated through mixture of 75-25 v/v quartz sand to Pe350 in 1000 mL column
Sd200Phe:	200 mg·L^{-1} phenols percolated through mixture of 75-25 v/v quartz sand to Sd350 in 1000 mL column
Pl200Phe:	200 mg·L^{-1} phenols percolated through mixture of 75-25 v/v quartz sand to Pl350 in 1000 mL column

Pe20Phe:	20 mg·L^{-1} phenols percolated through mixture of 75-25 v/v quartz sand to Pe350 in 1000 mL column
Sd20Phe:	20 mg·L^{-1} phenols percolated through mixture of 75-25 v/v quartz sand to Sd350 in 1000 mL column
Pl20Phe:	20 mg·L^{-1} phenols percolated through mixture of 75-25 v/v quartz sand to Pl350 in 1000 mL column

PeA350-KOH:	Pe350 impregnated with 1M KOH, 20:500 w/v ratio of biochar to activator
SdA350-KOH:	Sd350 impregnated with 1M KOH, 20:500 w/v ratio of biochar to activator
PlA350-KOH:	Pl350 impregnated with 1M KOH, 20:500 w/v ratio of biochar to activator

PeA350-FeCl$_3$:   Pe350 impregnated with 1M FeCl$_3$, 20:500 w/v ratio of biochar to activator
SdA350-FeCl$_3$:   Sd350 impregnated with 1M FeCl$_3$, 20:500 w/v ratio of biochar to activator
PIA350-FeCl$_3$:   PI350 impregnated with 1M FeCl$_3$, 20:500 w/v ratio of biochar to activator

1. Introduction

Due to the raising public concern about sustainable development, researchers are considering the management of anthropogenic activities. Biodegradable non-toxic organic solid by-products/wastes, such as agricultural wastes and horticultural residues, livestock manures, municipal wastes are potential feedstock materials for biochar production. Biochar is a carbon-rich, fine-grained, porous substance, which is produced by thermal decomposition of organic material under oxygen-limited conditions (pyrolysis) and at relatively low temperatures (<700 °C) *(Lehmann and Joseph, 2009; Sohi et al., 2009)*, where the carbon content of the woody biomass cannot combust without oxygen and so it is reduced to biochar *(http://www.swarmhub.co.uk/downloads/pdf/carbon_project/introduction_biochar.pdf)*. Pyrolysis of organic material results in the production of three products, namely gas, oil and biochar, but only the last one will be the topic in this study.

Biochar can be produced by several thermo chemical processes; conventional carbonization or slow pyrolysis, fast pyrolysis, flash carbonization, and gasification. The terms fast and slow pyrolysis are indicative of the time in which vapors are driven off the biomass in the reaction vessel. Fast pyrolysis occurs at moderate temperatures, with very short vapor residence times, whereas slow pyrolysis requires a relatively long vapor residence time *(Sparkes and Stoutjesdijk, 2011)*. In general, fast pyrolysis (600- 700 °C) produces biochars with highly aromatic nature and well-organized C layers, but with fewer H and O functional groups due to dehydration and deoxygenation of the biomass *(Ahmad et al., 2014; Uchimiya et al., 2011)* and potentially with lower ion exchange capacity *(Novak et al., 2009)*. On the other hand, slow pyrolysis (300- 400 °C) produces biochars with more diversified organic character, including aliphatic and cellulose type structures and contain more C–O and C–H functional groups *(Rajapaksha et al., 2016)*. Among all processes, slow pyrolysis has the advantage that its conditions can be optimized to maximize the production of either gases, oils or biochars depending on the required product *(Sánchez et al., 2009)*. Furthermore, slow pyrolysis minimizes the risk of releasing dioxins and harmful polyaromatic hydrocarbons.

Biochar yield and quality varies and depends on the type of the raw material and the pyrolysis conditions (principally pyrolysis temperature, heating rate, pressure, and residence time at the pyrolysis temperature). Pyrolysis yield has been found to range from 8 to even 77% at low pyrolysis temperatures (250- 300 °C) *(Dai et al., 2013; Ding et al., 2014)* for various raw materials. The increase of pyrolysis temperature decreases the biochar yield which can range from 25 to 46 % because the high temperatures allow the thermal cracking of hydrocarbon materials. As a consequence low pyrolysis temperature is ideal for high biochar yield but finding the exact temperature for each raw material used for biochar production demands separate experiments. Lignocellulosic materials are composed of cellulose and at a lesser extend of hemicellulose and lignin and the proportion of these constituents differ from biomass to biomass *(Kan et al., 2016)*. Interactions among these components affect the final performance of pyrolysis product. Heating rate influences the nature and composition of the final product, as at low heating rates the possibility of secondary pyrolysis reaction may be prevented, while at high heating rates gaseous and liquid yield is more favorable than biochar yield. For instance, increase of the heating rate from 30 to 50 °C·min^{-1} decreased the biochar yield for a temperature range of 400 to 600 °C *(Tripathi et al., 2016)*. Increase in residence time increases the biochar yield at high temperatures, while decreases the biochar yield at low temperatures as reported in the review of *Tripathi et al. (2016)*. The particle size of biomass could delay the rate at which the heat is transferred to inner biomass and this could increase biochar yield. However, other researchers have found no significant increase, reduction, or even reduction and subsequently increase of biochar yield with the increase of particle size *(Tripathi et al., 2016)*. When the feedstock is very fine, agglomeration may take place in higher temperatures and this may in turn affect the porosity of the final product.

Residence time not only affects biochar yield but it also influences the quality and characteristics of biochar by promoting the development of micro-and macro-pores. Longer residence time has been reported to enhance the pore size in biochar. Moreover, increase of pyrolysis temperature increases biochar porosity as well due to the transformation of aliphatic C structures to aromatic C structures *(Gray et al., 2014)*. The porous structure is one of the most important characteristics of biochar which has been proved to play a significant role in contaminants adsorption. Biochar particles have large surface area and thus more available adsorption sites. Impurities such as ash content and metal oxides as well as acidic oxygen functional groups such as carboxylic lactonic and amine groups could favor adsorption process in aqueous solution *(Machida et al., 2006)*.

Carbon content has been found to increase after pyrolysis of raw material *(Angin et al., 2013)*, while the increase of pressure inside the reactor can increase further the carbon content in biochar *(Tripathi et al., 2016)*. On the other hand, hydrogen and oxygen content are found to decrease when

raw material is pyrolyzed *(Angin et al., 2013)*. The existence of hydrogen and oxygen is of great importance for contaminants adsorption because they are key parts of the oxygen functional groups, which are responsible for surface interactions between pollutants and biochar via ion exchange and complexation *(Cao et al., 2010; Zhenyu et al., 2015)*. pH increases with the increase of pyrolysis temperature *(Dai et al., 2013)* and there is a great positive correlation with the ash content in biochars. Various analyses such as X-ray diffraction (XRD), scanning electron microscopy (SEM), and Fourier Transform Infrared (FTIR) analyses have been conducted in order to determine differences in biochar properties.

Water pollution by heavy metals discharged from industrial effluents has been causing a worldwide concern during recent years, as most of industrial pollutants in groundwater may cause harmful elevated concentrations in humans and animals through food chain and even cause death. Heavy metals tend to accumulate in living organisms as they are not biodegradable, unlike organic contaminants. Toxic heavy metals of particular concern during treatment of industrial wastewaters include copper, lead, cadmium and much less hazardous cobalt the effects of which have been investigated extensively.

Copper compounds are found at mining, livestock farms, pesticide production, chemical industry and metal piping and even if small amount of copper is essential to all living organisms as a trace dietary mineral, presence in large quantities may be dangerous for eyes, skin, respiratory system, liver, kidneys with increased risk for Wilson's disease and can cause anemia, stomach and intestinal irritation *(Singh et al., 2011)*. Elevated copper levels have also been linked to worsening symptoms of Alzheimer's disease *(Brewer and MACN, 2009)*, *(Brewer, 2012)*. Maximum contamination level of copper in drinking water is defined at 2 mg·L^{-1} *(WHO)*.

Lead is used in building construction, lead-acid batteries, bullets and shot, weights, as part of solders, pewters, fusible alloys, pesticide and as a radiation shield. It can be also found in automobile emission, mining, burning of coal and smoking *(Singh et al., 2011)*. Lead is a highly poisonous metal (whether inhaled or swallowed) and can harm almost every organ and system in the human body, especially the nervous system and the brain with mental retardation in children, development delay, fatal infant encephalopathy, congenital paralysis, sensor neural deafness and causes blood disorders, namely, liver and kidney damage, *(Singh et al., 2011)*. Permissible level of lead contamination of drinking water is set at 0.01 mg·L^{-1} *(WHO)*.

Cadmium occurs as a minor component in most zinc ores and therefore is a byproduct of zinc production. Cadmium was used for a long time as corrosion-resistant plating on steel and cadmium compounds are used as red, orange and yellow pigments, to color glass and stabilize plastic. It has been also used in welding, electroplating, pesticide, fertilizers, Cd and Ni batteries and nuclear fission plants *(Singh et al., 2011)*. One of its few new uses is in cadmium telluride solar panels. Similarly to previous heavy metals, cadmium is a harmful element for respiratory system, prostate, blood and as a drinking water pollutant, kidneys is its main target organ. Cadmium can cause bone defects (osteomalacia, osteoporosis), increased blood pressure, gastrointestinal disorder, foot or wrist palsy and even prostatic, lung and bone marrow cancer *(CDC; Singh et al., 2011)*. Permissible level is set at 0.003 mg·L^{-1} *(WHO)*.

Cobalt is primarily used as the metal, in the preparation of magnetic, wear-resistant and high-strength alloys. Its compounds cobalt silicate and cobalt (II) aluminate ($CoAl_2O_4$, cobalt blue) give a distinctive deep blue color to glass, ceramics, inks, paints and varnishes. A radioisotope of cobalt is commercially important as it is used as a radioactive tracer and for the production of high energy gamma rays. Cobalt is an essential element for life in minute amounts as it is a key constituent of vitamin B12 for all animals *(Barceloux, 1999)*. However, cobalt has been incriminated in cardiomyopathies in Quebec beer drinkers (addition of cobalt compounds to stabilize beer foam) as well as in a person exposed to industrial cobalt and in patients on maintenance hemodialysis with and without cobalt therapy *(Manifold et al., 1978)*.

Phenols, another component discharged from industrial effluents, are produced on a large scale (about 7 billion kg·yr^{-1}) from petroleum. It is an important industrial commodity as a precursor to many materials and useful compounds *(Weber et al., 2016)*. It is primary used to synthesize plastics and related materials. Phenol and its chemical derivatives are essential for production of polycarbonates, epoxies, bakelite, nylon, detergents, antioxidants, and pesticides, dyes, herbicides such as phenoxy herbicides, and numerous pharmaceutical drugs. They pose serious danger when entering the food chain as water pollutants. Phenols affect the taste and odor of fish and drinking water only just at very low concentration *(Mohan et al., 2014)*. It has been reported that 14 to 140 mg/kg (equivalent to a 70-kg worker being exposed to 167 to 1,670 ppm for 30 minutes, assuming a breathing rate of 50 liters per minute and 100% absorption) is the lethal oral dose *(Deichmann and Gerarde 1969; Lefaux, 1978)*. Permissible level of phenols contamination of drinking water in Greece is set at 5μg·L^{-1} (*Υγειονομική διάταξη Υ2/2600/21-6-2001*). Groundwater can be a potential source for an intense exposure to all the above contaminants because of arbitrary disposal and inappropriate waste management. Therefore, it is

necessary to develop low-cost and effective methods able to reduce the presence of these pollutants in water.

According to the International Biochar Initiative (IBI), biochar can be used for both agricultural and environmental gains. The agricultural management introduced by green revolution to meet the food requirements reduced soil organic carbon, a principal factor for soil fertility. Use of fertilizers for productivity improvement leads to dependency, causes pollution and does little to maintain soil organic carbon, while applications of biochar for agricultural improvement might not need to be very frequent compared with fertilizers, compost or manures. Biochar can provide an effective means for the enhancement of C sequestration in soil *(Abdel-Fattah et al., 2015)*. When biochar application was compared to raw feedstock application into soil, only 2- 5 % of the added carbon was respired in biochar treatments, whereas about 80% of the added carbon in feedstock treatments was respired during the nearly 2 years of an incubation experiment *(Hansen et al., 2016)*. Plants grown on soils may be limited among other reasons by deficiencies of N, P, K, reduced nutrient cycling and reduced uptake of nutrients by plant roots and finally by inhibition of root growth *(Marschner, 2012)*. Biochar and compost soil amendments significantly improved uptake of N, P and K by barley plants in *Agegnehu et al. (2016)* research. Consequently, in the same research, they found the highest yield and the highest chlorophyll content in leaves and the number of productive tillers significantly increased. Furthermore, biochar application in soil did not affect aggregate stability, a principal structure also responsible for soil fertility *(Hansen et al., 2016)*. Moreover, switchgrass derived biochars significantly improved, almost doubled, moisture storage capacity in soils *(Novak et al. 2013)* compared with the control ones, while a smaller increase of 11 % was also observed in the past by *Karhu et al. (2011)*. Greenhouse gas emissions apart from CO_2 mentioned before, are also found to be reduced when biochar is added to soil. Researchers found net reduction in greenhouse gas accounted mainly by the consistent decrease in N_2O emission across rice and wheat growing cycles by 10-20 % when biochar was used as soil amendment *(Zhang et al., 2013)*. In another research, biochar addition increased the average cumulative CH_4 uptake by soil by 96% due to increased soil aeration as a result of increased porosity which decreases CH_4 production and/or increases CH_4 oxidation in soil *(Karhu et al., 2011)*.

In aqueous systems, while the use of activated carbon is well known and has been shown to be very effective in removal of metal contaminants via adsorption, it is not as ubiquitous as it might be due to the high cost of production. Alternatively, biochar has been extensively examined in last years for its potential to immobilize contaminants in water *(Ahmad et al., 2014; Rajapaksha et al., 2016)*. Biochars have been observed to reduce heavy metals in water to more than 95% of the initial Cr^{+3}, Cd^{+2} and Pb^{+2}, Zn^{2+} and Cu^{2+} *(Agrafioti et al., 2014; Lao et al., 2005; Doumer et al., 2016)*, up to 89% of Cr^{+6} and 53% of As^{+5} *(Agrafioti et al., 2014)* and up to 70 % of Hg^{+2} *(Tang et al., 2015)*. Biochar, this novel low-cost carbonaceous material has been reported to even improve the removal efficiency of heavy metals from aqueous environment compared with the traditional adsorbents like activated carbon due to its large surface area, unique porosity as well as the abundance of functional groups on the surface *(Ahmad et al., 2014)* which enhance the metal sorption affinity and capacity of biochar through cation exchange and surface complexation *(Rajapaksha et al., 2016)*. As heavy metal pollutants often coexist in wastewater and contaminated soil, their competitive sorption as well as the mobilities of single versus multiple heavy metal species has become a global concern *(Uchimiya et al., 2011; Han et al., 2013)*. Thus, further competitive adsorption studies are necessary in order to accurately estimate the heavy metal adsorption capacity of biochar in natural environments and the competitive adsorption of heavy metals. In addition, biochar has been also used for the removal of other inorganic contaminants such as nitrates (NO_3^-) *(Niandou et al., 2013)*, phosphate PO_3^{-4} and ammonium NH^{+4} *(Zeng et al., 2013)*.

Biochar has been found effective in removal and/or immobilization of many complex organic compounds in water such as herbicides atrazine and metolachlor *(Niandou et al., 2013)*, industrial solvent trichloroethylene *(Ahmad et al., 2012)*, pesticide dibromochloropropane (DBCP) *(Klasson et al., 2013)* and other compounds, namely pentachlorophenol *(Lang et al., 2014)*, naphthalene and 1-naphthol *(Chen and Chen, 2009)*, phenanthrene, bisphenol A (BPA) and 17a-ethinyl estradiol (EE2) *(Sun et al., 2011)* and results could be as good as those obtained from activated carbon. Only recently removal of phenols by biochar was examined *(Han et al., 2013)*. Among environmental gains, biochar is a promising filter of percolating soil water (to immobilize pollutants of surface and groundwater bodies) *(Barrow, 2012)*. For instance, trials in China with biochar applied up to 1.0 % by weight to soils contaminated with agrochemicals reportedly resulted in the sequestration or breakdown of pollutants and their reduced uptake by plants *(Xiang-Yang Yu et al., 2009)*. Where raw material produces contaminated biochar unsuitable for food crops loaded biochar could be simply land-filled, a less technically challenging strategy than releasing wastes arbitrarily. However, the low desorption yields reported in *Doumer et al. (2016)* confirm that the sorption process was largely irreversible and that the biochars could be used in decontamination applications. A lot of researches have to be done to see the effects of various biochars on biosphere after their use for various contaminants reduction.

The practical applications of conventional biochar for contaminant immobilization and removal however need further improvements. Recent attention has focused on modification of biochar with novel structures and surface properties in order to improve its remediation efficacy and environmental benefits. Although, modification of biochar using various techniques requires additional cost, it is likely to result in changes in its surface properties including surface area, surface charge, functional groups, and pore volume and distribution *(Rajapaksha et al., 2016)*. Biochar modifications involve various methods, namely chemical such as, acid treatment (H_3PO_4, H_2SO_4, H_2O_2,), base treatment (KOH, NaOH), chemical oxidation (HNO_3, $KMnO_4$), amination, surfactant modification, impregnation of mineral sorbents ($FeCl_3$) and magnetic modification or physical modification such as steam activation *(Rajapaksha et al., 2016)*. *Wu et al. (2015)* modified biochar using $FeCl_3$ in order to enhance sludge dewaterability, while the sorption behavior of developed sorbents under various agents and specifically ferric chloride for contaminants removal from the water are examined in another research *(Gopal et al., 2004)*. Applicability and performance of modification methods depend on the type of contaminants (inorganic/organic, anionic/cationic, hydrophilic/hydrophobic, polar/non-polar), environmental conditions, remediation goals, and use purpose *(Rajapaksha et al., 2016)*. Moreover, experimental conditions, such as pH conditions, have been reported to influence the final adsorptive efficiency of biochars *(Abdel-Fattah et al., 2015; Peng et al., 2016)*.

Chemical modification can be conducted in either one step or two steps. In first case, carbonization and modification are achieved simultaneously, while in the second case either carbonization or activation precedes. Addition of base is one of the main treatments for chemical modification. Researchers have treated the pristine biochars using potassium hydroxide (KOH) to modify their surface properties *(Jin et al., 2014; Jin et al., 2016; Dehkhoda et al., 2016)*. According to the literature, chemical activation using KOH produced activated carbon with high surface area (900–3000 $m^2 \cdot g^{-1}$) *(Dehkhoda et al., 2016)* with mostly microporous structure (i.e., >85% of total pore volume). KOH-modified biochar was reported to have tetracycline (a more complex organic contaminant than phenols) adsorption capacity 58.52 $mg \cdot g^{-1}$, significantly larger than most studies 4.3–54 $mg \cdot g^{-1}$ due to its larger surface area *(Liu et al., 2012)*. Potassium species (K_2O, K_2CO_3) may be formed during activation as a result of intercalation of K^+ in the layer of the crystallites that form the condensed C structure. These species may diffuse into the internal structure of biochar matrix widening existing pores and creating new pores of the product *(Rajapaksha et al., 2016)*. More pores in biochars may 'trap' more organic molecules. Hence, efficient adsorption of organic pollutants on biochars can be achieved by increasing their surface area and optimizing their pore size distribution. Besides the specific surface area and porosity, the alkali biochar showed higher carbon and oxygen content than the raw biochar, mainly because of the elevated removal of inorganic matter, e.g. ash content *(Liu et al., 2011)*.

As also reported elsewhere, activation of precarbonized precursors with KOH could enhance the surface hydroxyl groups and henceforth the O content and surface basicity *(Rajapaksha et al., 2016)*. *Niandou et al. (2013)* also mentioned that base activation led to the development of biochar with surface charges suitable for adsorption of anionic species. The enhancement of organic pollutant adsorption by biochar has been mainly attributed to the oxygen-containing functional groups which interact with organic pollutant via hydrogen binding and complexation *(Liu et al., 2012)*. The structure of biochars is believed to be similar to that of activated carbon (AC), which consists of short stacks of small graphite-like sheets arranged in a highly disordered form *(Liu et al., 2012)*. The graphite-like structure can act as a π-acceptor, while the molecule of the organic pollutant with the aromatic ring structure that *Liu et al. (2012)* used can act as an electron donor, therefore the π–π electron donor–acceptor interaction can form between biochar and the organic pollutant molecule. In addition, the O of C–O bonds on biochar surface contain unpaired electrons and can be considered as electron donors, while the aromatic ring can serve as an electron acceptor. Therefore, an organic pollutant could act either like a donor or like an acceptor on the electron donor–acceptor interaction, depending on its form (anionic or cationic) in solution and consequently on solution pH. Once the alkali modification of biochar may change surface area as well as the amount and types of functional groups on the surface of biochar, it can enhance the adsorption capability of biochar as well. Thus, using such modified biochar to adsorb phenols might offer a simple, low-cost and efficient approach for phenols removal from wastewater.

As far as phenols adsorption onto biochar in relation with pH solution is concerned, *Panumati et al. (2008)* found greater adsorption capacity of phenols at pH 2 than at pH 12. At pH 2 the surfaces of activated carbons are protonated and have acidic surfaces with positive charges. Phenol behaves as a weak base that interacts with the acidic surface of activated carbons by dispersion electron donor-acceptor interaction *(Panumati et al., 2008)*. In contrary, at pH 12 the surfaces of activated carbons have negative charges and the molecules of phenol are in the form of the phenolic anion. These cause electrostatic repulsion between the surfaces and phenolic anions. However, *Liu et al., (2012)* mention that although the pH could be an important factor influencing adsorption of organic pollutants on biochar by electrostatic attraction, few differences of electrostatic attraction between biochar and

pollutants were observed under natural environmental pH conditions because of the buffering effect of biochars.

Biochar might present low pollutant adsorption due to large negative surface charge. One method to increase the adsorption capacity is to introduce metal (hydr)oxides, mainly iron (hydr)oxides, into porous biochar. Iron (hydr)oxides, such as goethite, haematite, ferrihydrite, and akaganeite, can be produced by the precipitation of ferric salts and occur naturally in mineral forms. Iron (hydr)oxides have a high affinity toward oxyanion ions and are very selective in the adsorption process. *Li et al. (2016)* found that activation with HCl, for protonation of biochar, and coating with iron ($FeCl_3 \cdot 6H_2O$) leads to increased biochar oxygen content and thus to the generation of more available activated sites on biochar surface that can significantly increase nitrate or phosphate biochar adsorption capacity. Similarly to *Li et al. (2016)*, the adsorption of other ionic contaminants by iron coated biochar could be investigated. Akaganeite can be formed in the ferric chloride solutions because of the interaction of chloride ions with the surface of the hydrous iron. In this case, amorphous $FeOOH$ can be the active substance of biochar *(Li et al., 2016)*. The Fe^{3+} ion has a high charge-to-size ratio because of its high positive charge and small ion radius. This condition leads to significant hydrolytic action of Fe^{3+} in a water solution. Similarly, complexes of iron coated biochar in a water solution are hydrolyzed to [C-$Fe(OH_2)_5]^{+3}_{(s)}$ and pursuant to hydrolytic reactions low pH favors the resistance of this initial form of the hydrolyzed complexes. Increase of pH would lead to [C-$Fe(OH_2)_4(OH)]^{+2}_{(s)}$ and [C-$Fe(OH_2)_3(OH)]^{+}_{(s)}$ *(Li et al., 2016)*. Hence, iron coated biochars in low pH are expected to have better adsorption capacity than at higher pH.

The objectives of this study were to address if three different woody feedstock materials, namely pecan shells from the region of Chania, Greece, sawdust from local carpentry and pistachio shells obtained from Aegina island, Greece, could be promising raw materials for biochars able to remove heavy metals Cu, Pb, Cd and Co and phenols from contaminated solutions. Biochar characteristics corresponding to pyrolysis conditions namely pyrolysis yield, pH, volatile matter, and C, H, S, N are investigated. Thermogravimetric analysis (TG), X-ray diffraction (XRD), Fourier Transform Infrared Spectroscopy (FTIR) and Scanning Electron Microscopy (SEM) were used in order to identify the morphology and structure of the produced biochars. Moreover, their behavior in adsorption is examined under different conditions of pH and experimental layouts in flasks and columns. Activated biochars were also examined for their phenols adsorption capability.

2. Materials and methods

2.1. Feedstocks preparation

Pecan shells (Pe) obtained from trees cultivated in the region of Chania, Crete, Greece and sawdust (Sd) obtained from local carpentry, as well as pistachio shells (PI) obtained from Aegina island, Greece were subjected to pyrolysis for the production of biochar. The pecan and pistachio shells were soaked for 2 hours in warm water and washed out under flowing water in order to remove any impurities and salt respectively. Then, wet shells were left to dry in room temperature for 2 days (Fig. 1) and thereafter were oven-dried at 40 °C for 24 h (ON-O2, MEDLINE). Sawdust was not treated before pyrolysis. Pecan and pistachio shells and sawdust were stocked airtight in plastic bags until their use.

2.2. Characterization of feedstocks and biochars

Moisture content was estimated for sawdust, pecan and pistachio shells. The oven (ON-O2, MEDLINE) was preheated to 110 °C and samples of feedstock materials (6- 7g) were left to dry for 24 h. After 24 h heating, the samples were weighted and the moisture content was equal to the calculated % sample weight loss.

Then, feedstocks and biochars were subjected to the following chemical analyses using a ratio w/v of material to deionized water 1: 10; pH and Eh (oxidation–reduction potential) with a Hanna 211 pH/Eh meter and EC (Electrical Conductivity) with a Hanna EC215 conductivity meter. For these measurements, used materials were grinded in doses (e.g. 50 g) for 2 min with a FRITSCH mill rotating rings.

Initially, laboratory experiments were conducted in order to examine pyrolysis yield variation depending on pyrolysis temperature, pyrolysis time and particle size of feedstock material. For this reason, pecan shells were milled to ≤2 cm. Moreover, FRITSCH mill rotating rings were used for further grinding of pecan shells for 30 seconds, 1 and 2 minutes. Henceforth, samples would be referred to as Pe, Pe0.5, Pe1 and Pe2 respectively. Then, pyrolysis of small quantities (~50 g) of feedstocks was carried out in a modified laboratory furnace, N-8L SELECTA (Fig. 1), at temperatures varying between 250–550 °C, using porcelain capsules. Nitrogen was fed in the oven at a rate 100

mL·min^{-1} for 60 min to remove air. Pyrolysis yield (y$_P$) was determined for all pecan shell (Pe, Pe0.5, Pe1, Pe2) biochars produced at pyrolysis temperatures of 250, 350, 450 and 550 °C from the % weight loss after heating. The biochar samples are hereafter referred to as Pe250, Pe0.5(250), Pe1(250), Pe2(250) and so forth. The heating rate was maintained at 10 °C·min^{-1} and the retention time of the feedstock in each temperature was 60 min. Pyrolysis of Sd for 60 min was also carried out for all pyrolysis temperatures and the same heating rate of 10 °C·min^{-1}. Sawdust biochar would be similarly to pecan shell biochars referred to as Sd250, Sd350, Sd450 and Sd550. The influence of pyrolysis time on pyrolysis yield was also examined. Both feedstocks, Pe and Sd were pyrolyzed at pyrolysis temperatures of 250, 350, 450 and 550 °C with no retention time. The heating rate was maintained at 10 °C·min^{-1}. After completion of pyrolysis, biochars were removed from the oven when the temperature decreased to approximately 200 °C. Then, products were placed into dehumidifier until temperature decreased to room temperature.
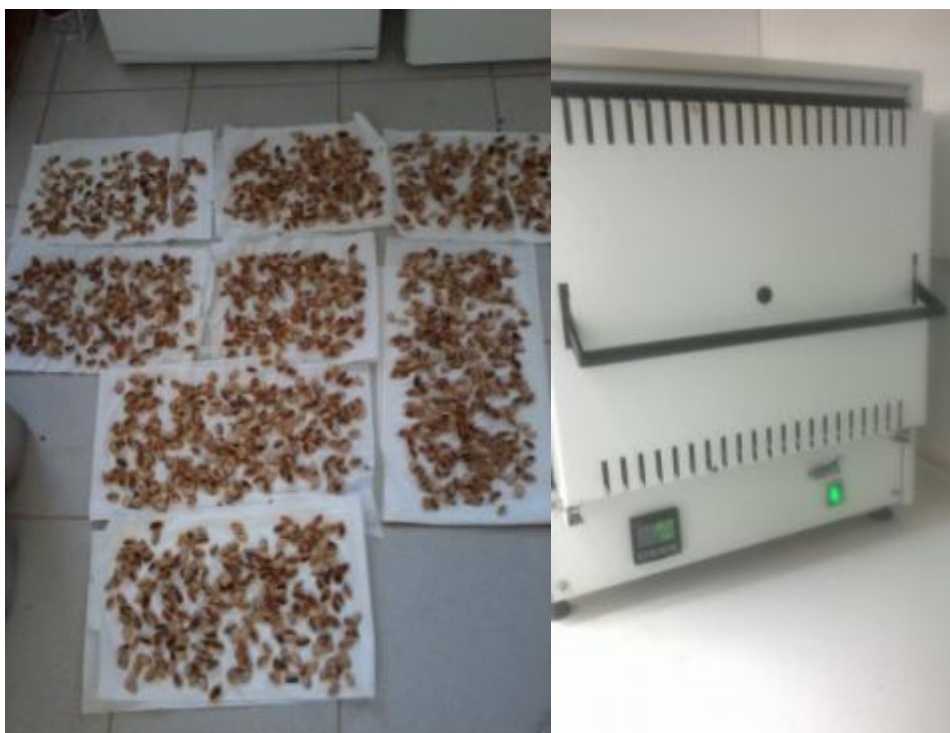
Fig. 1. Preparation of pistachio nut shells; drying at room temperature. Modified laboratory furnace, N-8L SELECTA (left to right)

Elemental C, H, N and S analysis was carried out in a Flash 2000 Elemental Analyzer Thermo Scientific calibrated using BBOT standards (2,5-Bis(5-tert-butyl-2-benzo-oxazol-2-yl) thiophene) containing carbon for the following selected biochars: Pe, Pe350, Pe550, Sd, Sd350 and Sd550. All biochars were milled in doses (e.g. 50 g) for 1 min prior to CHNS analysis.

Biochars were subjected to thermogravimetric analysis (TG) using a differential thermogravimetric analyzer Diamond DTA-TG of Perkin Elmer (temperature measurement precision of ±2 °C, microbalance sensitivity <5 µg). The rate and % weight loss for each sample were determined continuously as a function of time or temperature, under dynamic conditions, in the range of 40-850 °C. The experiments were carried out at atmospheric pressure, under nitrogen atmosphere, with a flow rate of 100 mL·min^{-1} and a linear heating rate of 10 °C·min^{-1}. Volatile matter (VM) and char content were also determined. All experiments were carried out in duplicate.

Surface area was measured using a NOVA Surface Area Analyzer (Quantachrome instruments). In addition, Fourier Transform Infrared Spectroscopy (FTIR), X-ray diffraction (XRD) and Scanning Electron Microscopy (SEM) were used for the identification of the morphology and structure of selected produced biochar. FTIR analysis was carried out using a Perkin-Elmer Spectrum 1000 (USA); for the production of the pellets each sample was mixed with KBr at a ratio 1:100 w/w. The spectra were recorded from 4000 to 400 cm^{-1} by 1801 scans at 2 cm^{-1} resolution. XRD analysis was performed using a Bruker D8 Advance diffractometer with a Cu tube and a scanning range from 3° to 70° 2θ with a step 0.03° and 4 sec/step measuring time. Qualitative analysis was carried out using the Diffracplus software (Bruker AXS) and the PDF database. SEM analysis was carried out with a JEOL 6380LV scanning electron microscope equipped with an EDS INCA microanalysis system with low vacuum, pressure 30 Pa, voltage 20 kV and 10 to 12 mm sample distance (working distance) from the detector.

2.3. Experimental methodology to assess biochar adsorption potential

2.3.1. Shake flask experiments

Biochars' potential to adsorb heavy metals was first examined in flask experiments. Two solutions of 100 mL were prepared by dissolving the required quantities of heavy metal salts ($Cu(NO_3)_2 \cdot 3H_2O$, $Pb(NO_3)_2$, $Co(NO_3)_2 \cdot 6H_2O$ and $Cd(NO_3)_2 \cdot 4H_2O$) in distilled water. The first solution contained 10 mg·L^{-1} of each metal (Cu, Pb, Co, Cd) and the second one 25 mg·L^{-1} of each metal. Interferences because of simultaneous existence of these heavy metals in solutions did not give us valid results when concentration of each ion was determined. For this reason, henceforth mono-metal solutions were prepared with a concentration of 100 mg·L^{-1}. Thus, 400 mL of the mono-metal solutions (100 mg·L^{-1}) and biochars (0.1, 0.5, 1 and 5 g·L^{-1}) were agitated at 230 rpm with a vibromatic rocking mixer (Fig. 2) until equilibrium was reached (24 h). The experiment was performed at room temperature at pH 4.55 to 5.82 and the selected biochars, Pe350 and Sd350, were milled to ≤0.5 mm. At various sampling times (5 and 30 min, 1, 2, 6 and 24 h) 20 mL of liquid samples were withdrawn and filtered through Whatman filters (0.45 μm) in order to separate solids from liquids (Fig. 3). 20 mL of deionized water were added in order to replenish the lost volume. The filtered solutions were analyzed for their Cu, Pb, Co and Cd concentrations using a Lamotte SMART3 colorimeter, while the residual biochars on the filters (cake) were left to dry overnight in an oven and stored for future use. Based on the concentration results at each sampling time and for each adsorbent concentration, % adsorption of each heavy metal ion is calculated. Furthermore, based on equilibrium concentrations, Freundlich and Langmuir models have been checked for their feasibility to describe adsorption. Moreover, the heavy metal sorption kinetics was investigated.

Fig. 2. Vibromatic rocking mixer for shaking conical vials in all experiments

The following series of experiments was conducted in order to examine the potential of biochars to adsorb phenols. Thus, solutions of 200 mL containing 100 mg·L^{-1} phenols with pH 6.69 were shaken with 0.1, 0.2, 0.5 and 1 g (0.5, 1, 2.5 and 5 g·L^{-1} respectively) of biochars Pe350, Sd350 or Pl350 at 130 rpm for up to 48 h on a reciprocating shaker at room temperature (~20°C). Moreover, in order to examine pH influence on phenols adsorption a new series of experiments was conducted using 0.01 N HCl and 0.01 N NaOH solutions for pH adjustment of the 100 mg·L^{-1} phenol solution. Thus, Pe350, Sd350 or Pl350 were added in phenols solutions of initial pH 4 or 9 at a biochar concentration of 5 g·L^{-1} to examine their ability to reduce phenols concentration. Samples would be referred to as Pe4Phe, Pe9Phe and so forth. Aliquots of aqueous samples (10 mL) were withdrawn, filtered and phenols concentration was determined at 15 min and 2, 4, 6, 24, 48 h. 10 mL of deionized water were added in order to replenish the lost volume.

Fig. 3. Aqueous solutions filtration with Whatman filters (0.45 μm)

It is worth mentioning that pH, Eh and EC of the biochars and solutions before and after all the adsorption experiments were measured in order to record any significant changes.

2.3.2. Desorption experiments

The residual biochars Pe350 and Sd350 (loaded biochars) derived from Pb (maximum % metal adsorption) and Cu adsorption experiment with adsorbent concentration 5 g·L^{-1} as described above, were used for desorption experiment in order to assess their reuse potential. Thus, for each biochar, two desorption experiments were carried out, one with 0.1 N HCl solution and the other one with 0.1 N HNO$_3$ solution. The solutions were agitated for 24 h. Filtration was used in order to remove solids from liquids and the remaining liquids were analyzed for their Pb or Cu concentration. Solids were left to dry for 24 h in an oven and thereafter were used for second adsorption experiments involving agitation of 5 g·L^{-1} loaded biochars with 100 mg·L^{-1} solution of Pb or Cu for 24 h. Filtration was used again in order to remove solids from liquids. The remaining Pb or Cu concentrations in the liquids were determined again.

2.3.3. Column experiments

Biochars' potential for removing phenols was also examined with fixed-bed column experiments. Experiments were conducted at room temperature in 100 mL open-top transparent plexiglas free draining columns of internal diameter 2 cm and height 20 cm filled with 50-50 v/v quartz sand to biochar and w/w 90:4.5 g for quartz sand to Sd350 and 64:29 g for quartz sand to Pe350. Pecan shells biochar was ground to ≤4 mm prior to use, with a final particle size distribution of 67 % between 2 and 4 mm, 25 % between 1 and 2 mm, 5 % between 0.5 and 1mm, while for sawdust biochar particle distribution in these fractions accounts for 28, 36 and 19 % respectively. A control column was also set, filled only with quartz sand (135 g). The respective mixtures were packed into their respective columns after homogenization. The prepared columns were hereafter referred to as Sd10Phe, Pe10Phe and C10Phe respectively. Then, a solution of 10 mg·L^{-1} phenols (indicative waste disposal limit in Greece, 2 mg·L^{-1}) was allowed to percolate through the column from the top. Columns' bottom was blocked with triplicate parafilm and solution addition continued until the upper level of the reactive bed was reached. Thus, 57 mL were added to Sd10Phe column and 35 mL to Pe10Phe and C10Phe. On first and third day 2 mL of the effluent solution were successively sampled from each column with a syringe for phenol concentration determination using a Lamotte SMART3 colorimeter. The same procedure was repeated for the clean-up of a solution containing COD (150 mg·L^{-1} from CH$_3$COOH) (disposal limit in Greece, 15 g·L^{-1}) or PO$_4$ (60mg·L^{-1} from KH$_2$PO$_4$) (disposal limit in Greece, 30 mg·L^{-1}).

Thereafter, a new experiment series was set in order to estimate the removal of phenols from solutions using 1000 mL transparent plexiglas columns of internal diameter 5 cm and height 45 cm. The filling of the columns included placement of glass wool at the bottom and subsequently 1 cm in height of quartz sand. Then, in the first case columns were filled with 75-25 v/v quartz sand to biochar with w/w ratio 607:99 g for quartz sand to Pe350 and 847:17.5 g for quartz sand to Sd350, filling 30 cm in height of the column. In second case, 50-50 v/v quartz sand to biochar Pe350, Sd350 or PI350 were mixed. The respective mixtures included w/w ratio 699:142 g for quartz sand to Pe350, 503:30 g for quartz sand to Sd350 and 722:129 g for quartz sand to PI350 (Fig. 4). Pe350 was ground to ≤4 mm prior to use as mentioned before, while pistachio shells biochar was ground to 0.5 mm with a final particle size distribution of 6 % between 0.063 and 0.5 mm and 25 % between 0.025 and 0.063 mm. Phenol solution of 200 mg·L^{-1} with a flow rate 0.01 mL·sec^{-1} and 20 mg·L^{-1} were pumped up-flow in

the columns respectively, from 20 L plastic vessels using peristaltic pumps (OMEGA FPU251 type) (Fig. 4). Samples hereafter referred to Pe200Phe, Sd200Phe, Pl200Phe and Pe20Phe, Sd20Phe, Pl20Phe respectively. Fig. 4 and 5 show the experimental layout of Pe20Phe and Sd20Phe. Establishment of a 2 cm layer of quartz sand at the top of the columns prevented the loss of biochar due to solution flow through the columns.

Fig. 4. Layout of column experiments Pe20Phe and Sd20Phe and use of OMEGA FPU251 peristaltic pumps

Fig. 5. Pe20Phe and Sd20Phe (left to right) (Plexiglas columns Hight/Diameter: 45/5 (cm/cm); biochar: quartz sand 50:50 (v/v); initial phenol concentration 20 mg·L^{-1})

At the input and output of columns, pH was measured in order to record any significant changes in phenols solution pH. 10 mL of the effluent solution were collected after 24 h from the top of each column for phenol concentration determination while effluent volume was also determined. For 50-50 v/v filled columns these measurements took place for 14 days.

2.3.4. Modification of biochars

The selected biochars Pe350, Sd350 or PI350 were mixed and stirred with 1M KOH (potassium hydroxide) solution or 1M $FeCl_3$ (iron (III) chloride) solution with w/v ratio of biochar to activator 20:500 (g/mL). Activation was carried out in 800 mL conical flasks for 3 h. The resulting solids after activation were filtered and rinsed by distilled water several times in order to leach out the activating agent, until discolored drainage solution was shown. Finally, they were dried for 24 h at 90°C, and hereafter referred to PeA350, SdA350 and PIA350. The adsorbent concentration with maximum % adsorption (5 $g \cdot L^{-1}$ in this study) was used for the following sorption experiments with activated biochars. Solutions of 200 mL containing 100 $mg \cdot L^{-1}$ phenols with pH 6.88 were shaken with 1 g of activated biochar at 130 rpm for up to 120 h on a reciprocating shaker at room temperature. Aliquots of aqueous samples (10 mL) were withdrawn, filtered and measured for their phenols concentration at 15 min and 2, 6, 24, 48, 72 and 120 h. 10 mL of deionized water were added in order to replenish the lost volume. The suspension pH was measured before and after the experiment.

3. Results

3.1. Characterization of feedstocks and biochars

The moisture content of pecan and pistachio shells and sawdust was calculated at 14.3, 2.2 and 8.4 % respectively. Table 1 presents the granulometry percentages of the ground samples accordingly with the time of grinding, namely 30 seconds (Pe0.5), 1 min (Pe1) and 2 min (Pe2). In Table 2 the respective pyrolysis yields are presented.

Table 1. Granulometry percentages of ground pecan shell samples

	Pe0.5 (%)	Pe1 (%)	Pe2 (%)
>2 mm	3	0	0
2-0.25 mm	85	78	63
<0.25 mm	12	22	37
Total	100	100	100

Pyrolysis yield (y_P) was determined for all pecan shells (Pe, Pe0.5, Pe1, Pe2) and sawdust biochars produced at pyrolysis temperatures of 250, 350, 450, 550 °C using the following equation;

Pyrolysis yield (y_P) (%) = 100 × (weight of biochar) / (weight of feedstock) (1)

As it is shown in Table 2, pyrolysis yield decreases substantially (e.g. from 77 to 7.9 % for Sd) as pyrolysis temperature increases. Particularly, pyrolysis yield decreases more from 250 to 350 °C (~ 30 %) than from 450 to 550 °C for all biochars produced. This decrease in pyrolysis yield obtained at temperatures lower than 400 °C is due to the destruction of the cellulose and hemicelluloses, while at temperatures higher than 400 °C is due to condensation of aliphatic compounds and loss of volatiles CH_4, H_2 and CO *(Agrafioti, 2014)*. The different reduction in pyrolysis yield from 250 to 350 °C among Pe, Sd and PI biochars is attributed to different lignocellulosic composition of the three feedstocks (greater reduction for Sd and PI than for Pe biochars). In addition, Sd biochars showed lower pyrolysis yields than Pe and PI biochars for the entire temperature range, except 250 °C, where Sd showed the highest pyrolysis yield. Moreover, as far as particle size of feedstocks is concerned, it seems that there is no need for grinding before pyrolysis because no remarkable difference in pyrolysis yield is observed for samples Pe, Pe0.5, Pe1 and Pe2 pyrolyzed at same temperatures. Therefore, the following experiments included only Pe samples for estimating the effect of pyrolysis time on pyrolysis yield.

Table 2. Characterization of Pe, Sd, Pl and the produced biochars

Feedstock material	Biochar	y_P, %	moisture content, %	pH	EC, mS/cm	Eh, mV	VM, %	Char, %	Surface area, $m^2 \cdot g^{-1}$	% C	%H	%N	%O
Pe		-	14.3	5.8	0.32	75.8	71.3	28.7	-	47.4	5.4	0.4	46.8
60 min retention time													
	Pe250	74.2		5.2	0.31	123.6	56.2	43.8	3.2	54.6	4.3	0.6	40.5
	Pe0.5(250)	74.7											
	Pe1(250)	66.4											
	Pe2(250)	69.7											
	Pe350	44.5		4.9	0.19	129.9	40.9	59.1	3.2	65.6	3.0	0.6	30.8
	Pe0.5(350)	45.0											
	Pe1 (350)	42.8											
	Pe2 (350)	39.6											
	Pe 450	30.3		6.8	0.39	38.5	37.4	62.6	165.4	74.8	2.1	0.6	22.6
	Pe0.5(450)	30.9											
	Pe1(450)	30.1											
	Pe2(450)	27.3											
	Pe550	21.7		6.9	0.46	12.8	23.0	77.0	298.7	76.4	1.9	0.6	21.1
	Pe0.5(550)	23.2											
	Pe1 (550)	20.2											
	Pe2 (550)	18.6											
no retention time													
	Pe250	92.1		4.7	0.26	144.4							
	Pe350	61.7		5.0	0.20	132.8							
	Pe450	38.9											
	Pe550	28.7											
Sd		-	8.4	5.7	0.38	79.5	89.6	10.4	-	46.7	5.8	0.1	47.4
60 min retention time													
	Sd250	77.0		4.7	0.18	153.7	67.2	32.8	2.5	52.3	3.5	0.5	43.7
	Sd350	30.6		3.8	0.20	197.0	42.9	57.1	2.6	63.2	2.1	0.3	34.4
	Sd450	13.8		5.0	0.22	122.0	38.5	61.5	66.8	66.8	1.8	0.2	31.2
	Sd550	7.9		6.6	0.32	25.0	35.7	64.2	84.6	68.0	1.5	0.5	30.0
no retention time													
	Sd250	90.8		4.5	0.19	146.0							
	Sd350	48.7		4.5	0.20	145.0							
	Sd450	27.8											
	Sd550	18.3											
Pl		-	2.2	4.3	7.7		86.0	14.0	12.4	45.9	6.0	0.4	47.6
60 min retention time													
	Pl250	72.9		4.7	13.1		70.9	29.1	27.1	54.2	5.3	0.4	40.1
	Pl350	31.6		5.1	21.5		48.1	51.9	50.2	70.0	3.3	0.2	26.5
	Pl450	31.4		6.7	25.9		44.1	55.9	54.2	75.0	2.8	0.2	22.0
	Pl550	28.4		7.2	29.7		28.3	71.7	69.9	77.3	2.1	0.2	20.4

It is seen for both Pe and Sd biochars that greater pyrolysis yield is observed as pyrolysis time reduces ranging from 92.1 to 28.7 % for Pe biochars and 90.8 to 18.3 % for Sd biochars for no retention time instead of 77 to 7.9 % and 74.2 to 21.7 %, respectively, for 60 min retention time. This probably means that the desired product (biochar) is not ready after less than 60 min pyrolysis time, because pyrolysis reactions are not completed (increase of pyrolysis time upon a certain time does not result to further reduction of pyrolysis yield as *Agrafioti (2014)* supported). Moreover, the influence of pyrolysis time on pyrolysis yield is secondary to the influence of pyrolysis temperature; 92.1 % with no retention time instead of 74.2 % with 60 min retention time for Pe250, whereas 74.2 % for Pe250 instead of 45 % for Pe350 both with 60 min retention time.

Results in Table 2 indicate that pH as well as EC increase slightly as pyrolysis temperature increases. pH was acidic to neutral for all feedstocks and biochars produced; 4.7- 5.8 for Pe and Pe biochars, 3.8- 6.6 for Sd and Sd biochars, 4.3- 7.2 for PI and PI biochars. EC was higher for PI and PI biochars ranging from 7.7 to 29.7 mS·cm^{-1}, while EC of the other feedstocks and biochars ranged from 0.18 to 0.46 mS·cm^{-1}. On the other hand, Eh was found to reduce as temperature increases ranging from 123 to 12.8 mV and 153.7 to 25 mV for Pe350 and Sd350 respectively.

Volatile matter content decreases with the increase of pyrolysis temperature, while the char content exhibited an opposite trend as expected. Increased pyrolysis temperature (from 250 to 550 °C) results in substantial decrease of the volatile matter (VM) content (from 71.3 to 23% for Pe biochars, 89.6 to 35.7% for Sd biochars and 86 to 28.3 % for PI biochars). Increase of pyrolysis temperature results also in increased char content reaching 77, 64.2 and 71.7 % at 550 °C, for Pe, Sd, and PI biochars respectively.

For all biochars, increase of pyrolysis temperature results in an increase of surface area. Particularly, sharp increase of surface area is observed at pyrolysis temperatures over 350 °C. The surface area showed the greatest increase as temperature increased from 350 to 450 °C with the maximum increase observed for Pe biochars. Maximum surface area was measured 298.7 m^2·g^{-1} for Pe550 more than double greater than that of Sd550 (84.6 m^2·g^{-1}) and even higher than that of PI550 (69.9 m^2·g^{-1}). The progressive increase in biochar surface area at higher temperatures may be attributed to the decomposition of organic substances as also *Ding et al. (2014)* mentioned. As it is mentioned in previous research *(Komnitsas et al., 2015)*, porosity increases also at higher temperatures due to the transformation of aliphatic C structures to aromatic C structures.

The results of ultimate elemental analysis of the feedstocks and chosen biochars are given also in Table 2. The carbon content increased as pyrolysis temperature increased reaching up to 77.3 % for PI550 followed by Pe550 (76.4 %) and Sd550 (68 %). The hydrogen content indicated the opposite change trend as expected ranging from 5.4 to 1.9, 5.8 to 1.5 and 6 to 2.1 for Pe, Sd and PI feedstocks and the respective biochars. Furthermore, since the sulfur content was below the detection limit, for all biochars in this study, they could be used in adsorption and purification processes. Nitrogen content was almost stable with the increase of pyrolysis temperature for Pe, Sd and PI biochars. The oxygen content was subsequently calculated as the difference and was found to decrease with the increase of temperature as expected from approximate 40 % to approximate 20 % for all biochars produced.

3.2. Heavy metal adsorption onto biochar and activated carbon

3.2.1. Effect of contact time and biochar dosage on heavy metals adsorption

Adsorption dynamics of the Pe350 and Sd350 toward Cu, Pb, Cd and Co were measured as a function of contact time and adsorbent concentration 0.1- 5 g·L^{-1} at room temperature (~20 °C) using 100 mg·L^{-1} heavy metal solutions for 24 h at initial pH for all cases from 4.55 to 5.82. Sampling was done at various times, namely 5 and 30 min, 1, 2, 6 and 24 h. The % adsorption of each heavy metal and for each adsorbent concentration is calculated using the following equation:

$$\% \text{ Adsorption} = \frac{C_o - C_i}{C_o} \times 100 \quad (2)$$

where C_o is the initial concentration of each heavy metal (mg·L^{-1}) and C_i the concentration of each heavy metal at each interval time.

The results are presented in Fig. 6, 7, 8 and 9 while in detail are exhibited in Table 3. The contact time was determined at 24 h for all solutions in order to establish equilibrium. The adsorption of Cu, Pb, Cd and Co increased rapidly within the first 30 min, followed by a gradual increase up to 24 h.
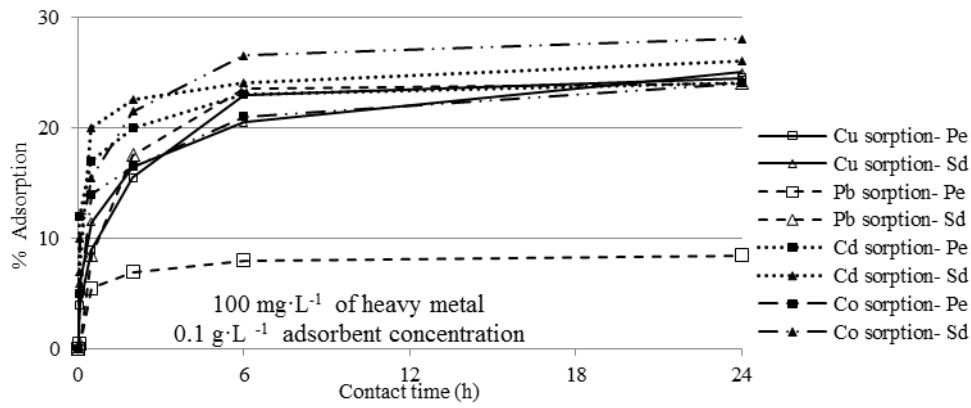
Fig. 6. The effect of contact time on heavy metal (Cu, Pb, Cd, Co) adsorption for adsorbent (Pe350 and Sd350) concentration 0.1 g·L^{-1}
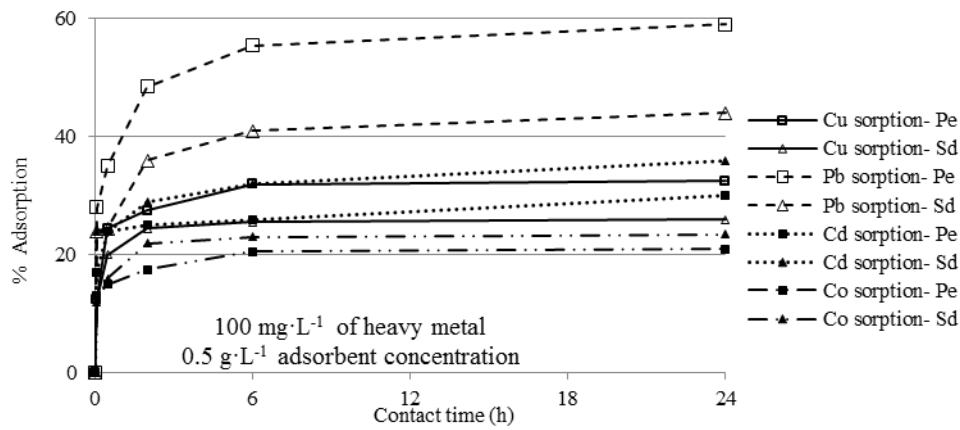
Fig. 7. The effect of contact time on heavy metal (Cu, Pb, Cd, Co) adsorption for adsorbent (Pe350 and Sd350) concentration 0.5 g·L^{-1}.
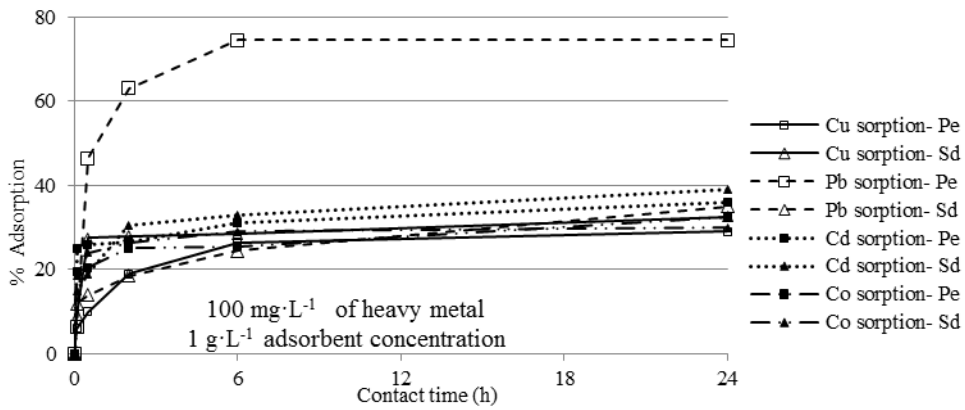
Fig. 8. The effect of contact time on heavy metal (Cu, Pb, Cd, Co) adsorption for adsorbent (Pe350 and Sd350) concentration 1 g·L^{-1}.
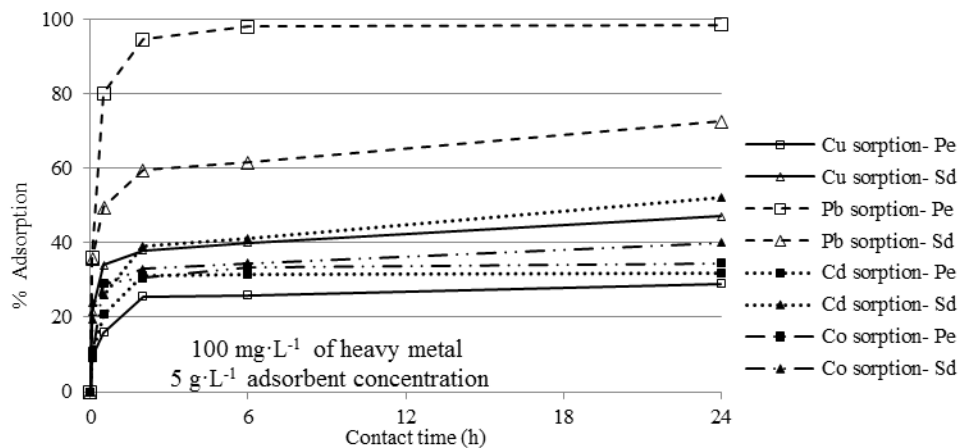
Fig. 9. The effect of contact time on heavy metal (Cu, Pb, Cd, Co) adsorption for adsorbent (Pe350 and Sd350) concentration 5 g·L^{-1}.

The increase in adsorption at the initial stage is due to the large number of vacant adsorption sites, which become saturated with time and as a consequence adsorption is less efficient afterwards and is also assigned to slow migration of heavy metal into pore spaces inside the biochars *(Ding et al., 2014; Elaigwu et al., 2013)*. Most of the metal ion removal occurred within 2 h accounting for 95.9, 85.6 and 82.1 % of total Pb^{2+} adsorption by Pe350 (5 and 1 g·L^{-1}) and by Sd350 (5 g·L^{-1}) respectively.

As far as adsorbent concentration is concerned, it is deduced from Table 3 and Fig. 10 that in general the higher the adsorbent concentration, the higher the % adsorption of heavy metal. This is not valid with Cu and Cd adsorption onto Pe350 where maximum % adsorption is observed for 0.5 and 1 g·L^{-1} respectively and Co adsorption onto Pe350 where reduction in % adsorption was observed at 0.5 g·L^{-1}. Furthermore, reduction in % adsorption of Pb and Co onto Sd350 was observed for 1 and 0.5 g·L^{-1} respectively. As it is also deduced from Table 3, both biochars adsorb more effectively Pb and Cd than Cu and Co for all adsorbent concentrations except for 0.1 g·L^{-1} that Pb shows the lowest adsorption among all heavy metals. These irregularities indicate that the number of adsorption sites play a predominant role in adsorption of heavy metals but are not the only ones. Particularly, as far as heavy metals are concerned, Pb is much better removed by Pe350 compared to Sd350 at 1 and 5 g·L^{-1} adsorbent concentration (74.5 and 98.5 % adsorption for Pe350 compared to 35 and 72.5 % adsorption respectively for Sd350). Maximum % adsorption was observed for Pb, at adsorbent concentration 5 followed by 1 g·L^{-1} for Pe350; 98.5 and 74.5 % respectively. Next highest % adsorption was observed for Pb, at adsorbent concentration 5 g·L^{-1} for Sd350 (72.5 %). Regarding the other metals, Cd and Co are better adsorbed on Sd biochar at all adsorbent concentrations and Cu on Sd biochar at all adsorbent concentrations, except for 0.5 g·L^{-1} where Pe biochar adsorb better.
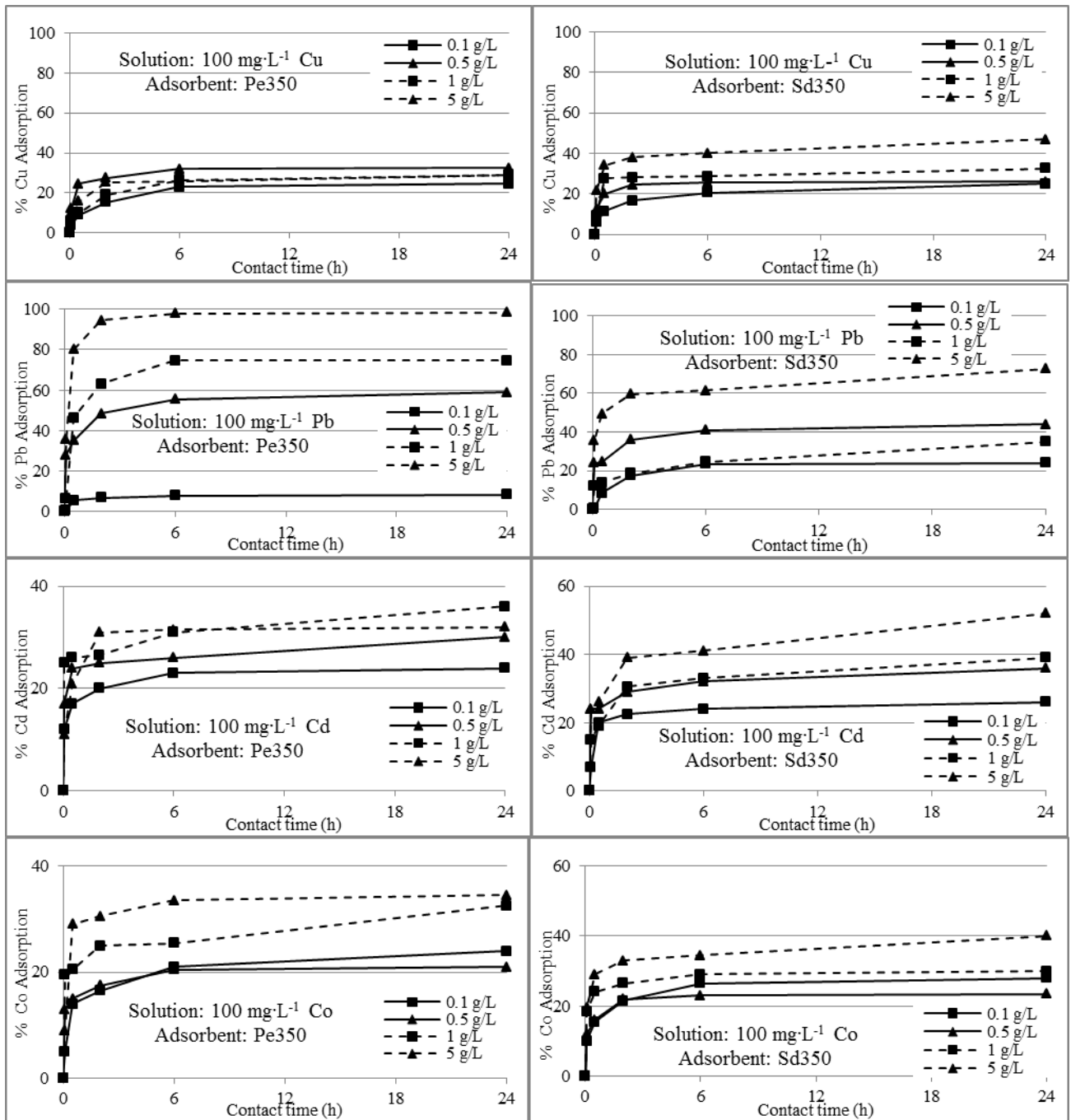
Fig. 10. The effect of adsorbent (Pe350 and Sd350) concentration (0.1 g·L^{-1}, 0.5 g·L^{-1}, 1 g·L^{-1}, 5 g·L^{-1}) on heavy metal (Cu, Pb, Cd, Co) adsortpion.

Table 3. % Adsorption of heavy metals at each sampling time for each adsorbent concentration

Adsorbent	Adsorbent Concentration, $g \cdot L^{-1}$	Time, h	% Cu adsorption	% Pb adsorption	% Cd adsorption	% Co adsorption
Pe350	0.1	0.08	4.0	0.5	12.0	5.0
		0.5	9.0	5.5	17.0	14.0
		2	15.5	7.0	20.0	16.5
		6	23.0	8.0	23.0	21.0
		24	24.5	8.5	24.0	24.0
	0.5	0.08	12.5	28.0	17.0	13.0
		0.5	24.5	35.0	24.0	15.0
		2	27.5	48.5	25.0	17.5
		6	32.0	55.5	26.0	20.5
		24	32.5	59.0	30.0	21.0
	1	0.08	6.0	6.5	25.0	19.5
		0.5	10.0	46.5	26.0	20.5
		2	19.0	63.0	26.5	25.0
		6	26.5	74.5	31.0	25.5
		24	29.0	74.5	36.0	32.5
	5	0.08	9.5	36.0	11.0	9.0
		0.5	16.0	80.0	21.0	29.0
		2	25.5	94.5	31.0	30.5
		6	26.0	98.0	31.5	33.5
		24	29.0	98.5	32.0	34.5
Sd350	0.1	0.08	6.0	0.5	7.0	10.0
		0.5	11.5	8.5	20.0	15.5
		2	16.5	17.5	22.5	21.5
		6	20.5	23.5	24.0	26.5
		24	25.0	24.0	26.0	28.0
	0.5	0.08	12.5	24.0	24.0	12.0
		0.5	20.0	24.5	24.0	16.0
		2	24.5	36.0	29.0	22.0
		6	25.5	41.0	32.0	23.0
		24	26.0	44.0	36.0	23.5
	1	0.08	9.0	12.0	15.0	18.5
		0.5	27.5	14.0	19.0	24.0
		2	28.0	18.5	30.5	26.5
		6	28.5	24.5	33.0	29.0
		24	32.5	35.0	39.0	30.0
	5	0.08	21.5	35.5	24.0	19.5
		0.5	34.0	49.5	26.0	29.0
		2	38.0	59.5	39.0	33.0
		6	40.0	61.5	41.0	34.5
		24	47.0	72.5	52.0	40.0

It should be mentioned, that for all heavy metals and adsorbent concentrations examined, pH values of the solutions during the experiments did not vary considerably prior to and after adsorption (Table 4), and thus it can be assumed that solution pH variation did not have a significant impact on heavy metal adsorption mechanisms.

Table 4. pH, Eh and EC of biochars (Pe350, Sd350) and solutions of each heavy metal (100 mg·L^{-1}) mixed with each adsorbent concentration (0.1, 0.5, 1 and 5 g·L^{-1}) for 24 h.

	Adsorbent concentration g·L^{-1}	Adsorbent		Cu			Pb			Cd			Co		
					24h adsorption			24h adsorption			24h adsorption			24h adsorption	
		Pe350	Sd350	Initial	Pe350	Sd350	Initial	Pe350	Sd350	Initial	Pe350	Sd350	Initial	Pe350	Sd350
pH	0.1	4.9	3.8	4.98	5.03	4.61	4.65	4.67	4.33	5.59	5.74	5.02	5.82	5.48	5.14
	0.5			5.02	4.65	4.23	4.72	4.49	3.96	5.59	5.42	4.76	5.48	5.56	4.92
	1			4.59	4.84	3.86	4.55	4.36	3.62	5.24	5.15	4.17	5.05	4.99	4.30
	5			5.02	5.20	3.45	4.72	5.25	3.53	5.59	5.38	4.11	5.48	5.55	4.21
Eh. mV	0.1	129.9	197.0	120.4	116.7	141.8	134.2	138.4	159.2	76.6	76.1	118.4	87.2	90.0	114.7
	0.5			119.9	140.1	165.9	137.4	149.2	180.7	85.4	92.8	135.0	103.0	86.8	132.7
	1			143.3	132.4	191.5	145.5	154.1	202.3	106.0	109.7	172.0	116.5	116.1	170.0
	5			119.9	121.4	212.9	137.4	108.2	207.3	85.4	94.8	174.0	103.0	87.7	165.8
EC. ms·cm^{-1}	0.1	0.19	0.2	0.37	0.33	0.25	0.26	0.22	0.22	0.22	0.19	0.19	0.42	0.36	0.36
	0.5			0.41	0.34	0.36	0.28	0.22	0.25	0.23	0.20	0.19	0.44	0.36	0.36
	1			0.39	0.32	0.25	0.28	0.14	0.13	0.24	0.13	0.14	0.44	0.24	0.23
	5			0.41	0.36	0.45	0.28	0.23	0.33	0.23	0.21	0.22	0.44	0.37	0.37

Slight reduction in solution pH is attributed to H^{+1} release after coordination between groups of COOH or OH with metal ions *(Wang et al., 2014)*. Eh and EC where not found to differ notably as well.

Subsequently, the difference betwee the initial concentration (Co) and the equilibrium concentration (Ce) in $mg \cdot L^{-1}$ was multiplied by the volume of solution in L and then divided by the amount of adsorbent (g), thus giving us the adsorption capacity which divided by the contact time of 24 h gives the adsorption rates (in $mg_{adsorbate} \cdot g_{adsorbent}^{-1} \cdot h^{-1}$) for all combinations of adsorbent materials, adsorbent concentrations and adsorbed heavy metals (Fig.11). The equation used was the following:

$$q_t = \frac{(C_0 - C_e)V}{mt} \ (3)$$

In all cases, it is worth mentioning that the higher the adsorbent concentration the lower the adsorption rate, despite the fact that the higher the adsorbent concentration the higher the % adsorption as mentioned in previous section. This result showed that as the adsorbent concentration increases, the number of heavy metal bonds on biochars increases (increased % adsorption), but adsorption rate decreases. It is worth mentioning though that the adsorption rate of Pb onto Pe350 is far lower than those of the other heavy metals' onto both biochars at 0.1 $g \cdot L^{-1}$ adsorbent concentration because of the competition of Pb ions, with the higher ionic radius among all heavy metals examined in this study, to be adsorbed by biochars as it is discussed in next sections. The 0.5 $g \cdot L^{-1}$ adsorbent concentration seems to be crucial for the best adsorption rate of Pb onto Pe350, while for the other combinations of heavy metals and biochars the crucial adsorbent concentration maybe 0.1 $g \cdot L^{-1}$ or less. The higher adsorption rates of all metals and adsorbent concentrations were observed for Sd350(Co), Pe350(Cu) and Sd350(Cd), namely 11.58, 10.68 and 10.67$mg \cdot g^{-1} \cdot h^{-1}$ respectively.
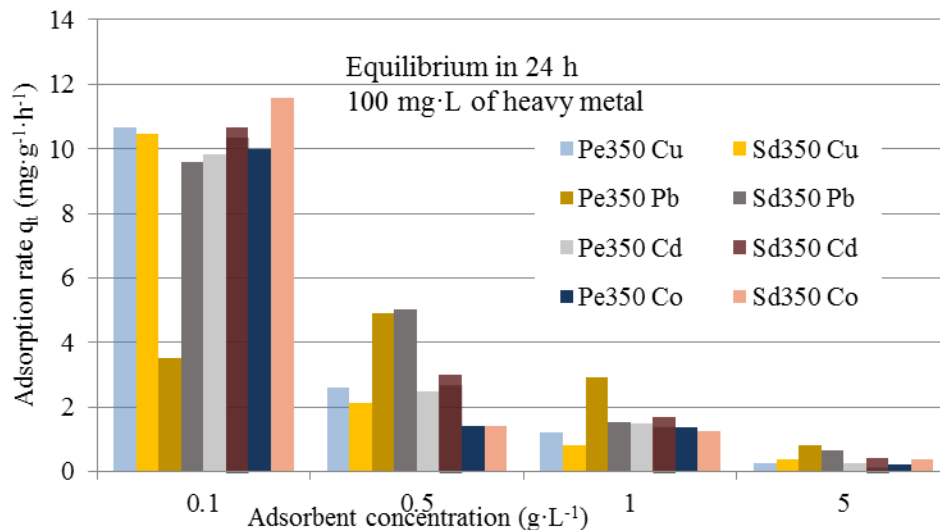
Fig. 11. Adsorption rates ($mg \cdot g^{-1} \cdot h^{-1}$) of Cu, Pb, Cd and Cu (concentration 100 $mg \cdot L^{-1}$) for adsorbent (Pe350 and Sd350) concentrations 0.1, 0.5, 1 and 5 $g \cdot L^{-1}$

3.2.2. Kinetic studies

Further analysis of adsorption of Cu, Pb, Cd and Co was conducted using the following kinetic models:

1. Pseudo-first order model (Lagergren):
The non-linear form of the model is given by

$$\frac{dq_t}{dt} = k_1 (q_e - q_t) \qquad (4) \text{ and can be presented as follows:}$$

$$\log(q_e - q_t) = \log q_e - \frac{k_1 t}{2.303} \qquad (5)$$

where q_t and q_e are the sorption capacity (µg/g) of the adsorbent at time t (h) and at equilibrium, respectively and k_1 is the pseudo-first order sorption rate constant (h^{-1}).

2. Pseudo-second order model (Lagergren):
The non-linear form of the model is given by

$$\frac{dq_t}{dt} = k_2 (q_e - q_t)^2$$ (6) and can be presented as follows:

$$\frac{t}{q_t} = \frac{1}{k_2 q_e^2} + \frac{t}{q_e}$$ (7)

where q_t and q_e are defined earlier, and k_2 is the pseudo-second order sorption rate constant ($g \cdot \mu g^{-1} \cdot h^{-1}$). The q_e and constant k_1 can be calculated from the plot between $\log(q_e - q_t)$ versus t. Similarly, the q_e and constant k_2 can be calculated from the plot of t/q_t versus t. Table 5 and 6 exhibit the model parameters for the pseudo-first-order and pseudo-second-order kinetics.

Table 5. Pseudo-first-order kinetic model parameters for the adsorption of heavy metal (Cu, Pb, Cd or Co) onto Pe350 or Sd350 (0.1, 0.5, 1 or 5 $g \cdot L^{-1}$).

Adsorbent	Heavy metal	Adsorbent concentration, $g \cdot L^{-1}$	$q_{e\ (Exp)}$, $mg \cdot g^{-1}$	Model q_e, $mg \cdot g^{-1}$	K_1, $1 \cdot h^{-1}$	R^2
Pe350	Cu	0.1	245.0	217.3	0.45	0.995
		0.5	65.0	38.8	0.62	0.941
		1	29.0	24.5	0.39	0.987
		5	5.8	3.4	0.34	0.707
	Pb	0.1	85.0	58.3	0.44	0.873
		0.5	118.0	70.4	0.41	0.899
		1	74.5	63.9	0.90	0.918
		5	19.7	9.5	0.81	0.906
	Cd	0.1	240.0	130.8	0.45	0.892
		0.5	60.0	25.4	0.23	0.483
		1	36.0	16.2	0.21	0.544
		5	6.4	3.2	0.66	0.790
	Co	0.1	240.0	169.7	0.31	0.877
		0.5	42.0	22.0	0.53	0.919
		1	32.5	16.2	0.17	0.476
		5	6.9	3.5	0.51	0.797
Sd350	Cu	0.1	250.0	184.6	0.25	0.885
		0.5	52.0	23.7	0.58	0.834
		1	32.5	14.6	0.26	0.438
		5	9.4	4.7	0.24	0.591
	Pb	0.1	240.0	233.9	0.64	0.999
		0.5	88.0	51.0	0.38	0.875
		1	35.0	25.8	0.16	0.823
		5	14.5	7.4	0.24	0.603
	Cd	0.1	260.0	136.1	0.36	0.702
		0.5	72.0	33.9	0.26	0.673
		1	39.0	24.9	0.27	0.775
		5	10.4	6.3	0.20	0.667
	Co	0.1	280.0	193.2	0.44	0.955
		0.5	47.0	23.3	0.58	0.857
		1	30.0	12.9	0.46	0.817
		5	8.0	3.9	0.25	0.599

Table 6. Pseudo-second-order kinetic model parameters for the adsorption of heavy metal (Cu, Pb, Cd or Co) onto Pe350 or Sd350 (0.1, 0.5, 1 or 5 $g \cdot L^{-1}$).

Adsorbent	Heavy metal	Adsorbent concentration C_A, $g \cdot L^{-1}$	$q_{e\,(Exp)}$, $mg \cdot g^{-1}$	Model q_e, $mg \cdot g^{-1}$	k_2, $g \cdot \mu g^{-1} \cdot h^{-1}$	R^2
Pe350	Cu	0.1	245.0	250.0	5.33	0.999
		0.5	65.0	50.0	133.33	1.000
		1	29.0	33.3	30.00	0.999
		5	5.8	5.0	571.43	1.000
	Pb	0.1	85.0	250.0	5.33	0.999
		0.5	118.0	125.0	21.33	1.000
		1	74.5	100.0	16.67	0.999
		5	19.7	20.0	500.00	1.000
	Cd	0.1	240.0	250.0	16.00	1.000
		0.5	60.0	50.0	66.67	0.999
		1	36.0	50.0	66.67	0.999
		5	6.4	5.0	1333.33	1.000
	Co	0.1	240.0	250.0	5.33	0.999
		0.5	42.0	50.0	80.00	1.000
		1	32.5	33.3	45.00	0.996
		5	6.9	10.0	333.33	1.000
Sd350	Cu	0.1	250.0	250.0	5.33	0.998
		0.5	52.0	50.0	200.00	1.000
		1	32.5	33.3	90.00	0.999
		5	9.4	10.0	200.00	0.998
	Pb	0.1	240.0	250.0	2.29	0.981
		0.5	88.0	100.0	25.00	1.000
		1	35.0	33.3	22.50	0.989
		5	14.5	14.3	163.33	0.998
	Cd	0.1	260.0	250.0	16.00	1.000
		0.5	72.0	100.0	20.00	0.999
		1	39.0	33.3	90.00	0.998
		5	10.4	11.1	115.71	0.996
	Co	0.1	280.0	250.0	16.00	1.000
		0.5	47.0	50.0	133.33	1.000
		1	30.0	33.3	150.00	1.000
		5	8.0	10.0	200.00	0.999

The results indicated that the pseudo-second-order kinetic model fit the data better than the pseudo-first-order kinetic model. The pseudo-second-order model exhibited correlation coefficient (R^2) values higher than 0.996 with the most of them to be equal to 0.999 or 1, except for Pb adsorption onto 0.1 and 1 $g \cdot L^{-1}$ Sd350 ($R^2 = 0.981$ and 0.989 respectively). On the other hand, the pseudo-first-order kinetic model exhibited lower R^2 values ranging from 0.995 to even very low 0.438, except for Pb adsorption onto 0.1 $g \cdot L^{-1}$ Sd350 where R^2 was higher ($R^2 = 0.999$) than that of pseudo-second-order kinetic model. Moreover, experimental q_e values were comparable with q_e values obtained from pseudo-second-order kinetic model, while differed for pseudo-first-order kinetic model as expected.

Under the assumptions of the pseudo-second-order model, the rate-limiting step may be the chemical adsorption that involves chemical bonding between divalent metal ions and polar functional groups on the adsorbent and the reaction rate is proportional to the number of active sites (functional groups) present on the adsorbent surface *(Elaigwu et al., 2013; Mohan et al., 2011)*.

Table 7 presents the equilibrium concentrations of heavy metals for each adsorbent concentration. Based on equilibrium concentrations regarding adsorption of Cu, Pb, Cd and Co using Pe350 or Sd350 in a solution containing 100 mg·L^{-1} Cu, Pb, Cd or Co, Langmuir and Freundlich isotherms have been used to describe adsorption (Table 8). The Langmuir model assumes that the adsorbent has a fixed number of adsorption sites, at equilibrium the adsorbed metal formed a single layer (monolayer adsorption), the surface is homogeneous and finally there is no interaction between the adsorbed molecules. Langmuir isotherm is the most commonly used linear expression to correlate the concentration of solute in liquid phase with the concentration of solute in the solid phase at equilibrium conditions. The linearized Langmuir isotherm is described by the following equation;

$$C_e/q_e = 1/(Ka·q_{max}) + C_e/q_{max} \qquad (8)$$

where C_e (mg·L^{-1}) is the equilibrium concentration of metal ion in solution, q_e (mg·g^{-1}) is the uptake of metal per unit weight of adsorbent in equilibrium, q_{max} is the maximum adsorption capacity of the adsorbent (mg·g^{-1}) for the formation of a monolayer surface and Ka (L·mg^{-1}) is the Langmuir constant related to the energy of the adsorption.

On the other hand, the Freundlich adsorption model is based on the assumption that the surface of the adsorbent is heterogeneous, the adsorption on the surface is chemical and laminate and that the concentration of the metal adsorbed onto the adsorbent surface increases with the concentration of the metal in solution. The Freundlich isotherm is linearized to the following equation;

$$logq_e = logK_f + (1/n)logC_e \qquad (9)$$

where q_e (mg·g^{-1}) is the uptake of metal per unit weight of adsorbent in equilibrium, C_e (mg·L^{-1}) is the equilibrium concentration of metal ion in solution, K_f (L·g^{-1}) is the constant related to the adsorption capacity of the adsorbent and 1/n is the constant related to the adsorption intensity.

Table 7. Equilibrium heavy metal concentration (24 h) in each solution

Adsorbent	Adsorbent concentration, g·L^{-1}	Cu concentration, mg·L^{-1}	Pb concentration, mg·L^{-1}	Cd concentration, mg·L^{-1}	Co concentration, mg·L^{-1}
Pe350	0.1	75.5	91.5	76.0	76.0
	0.5	67.5	41.0	70.0	79.0
	1	71.0	25.5	64.0	67.5
	5	71.0	1.5	68.0	65.5
Sd350	0.1	75.0	76.0	74.0	72.0
	0.5	74.0	56.0	64.0	76.5
	1	67.5	65.0	61.0	70.0
	5	53.0	27.5	48.0	60.0

The Langmuir isotherm constants q_{max} and Ka can be calculated from the plot between C_e/q_e versus C_e. Similarly, the Freundlich isotherm constants K_F and 1/n can be calculated from the plot of $logq_e$ versus $logCe$.

Table 8. Langmuir and Freundlich isotherm parameters and correlation coefficients for the adsorption of Cu, Pb, Cd and Co onto Pe350 and Sd350.

	Langmuir			Freundlich		
	R^2	q_{max}	Ka	R^2	1/n	$logK_F$
Pe350 (Cu)	0.013	-5.155	-0.011	0.162	13.758	-23.880
Pe350 (Pb)	0.962	90.090	0.584	0.876	0.412	1.260
Pe350 (Cd)	0.102	-3.251	-0.012	0.438	13.871	-23.909
Pe350 (Co)	0.496	-2.252	-0.013	0.505	11.405	-19.579
Sd350 (Cu)	0.969	-4.468	-0.013	0.765	7.381	-11.816
Sd350 (Pb)	0.383	-40.984	-0.010	0.681	2.217	-2.057
Sd350 (Cd)	0.914	-5.828	-0.014	0.974	7.338	-11.381
Sd350 (Co)	0.808	-2.448	-0.013	0.490	9.945	-16.685

From Table 8, it was observed that the calculated Langmuir isotherm parameters and their corresponding R^2 values showed a better fit for Pe350(Pb), Sd350(Cu) and Sd350(Co), while in case of Sd350 (Cd) Freundlich isotherm was found to be the best-fitting isotherm followed by Langmuir isotherm. For the remaining adsorption schemes Pe350(Cu), Pe350(Cd), Pe350(Co) and Sd350(Pb) neither Langmuir nor Freundlich isotherms were found to fit. Therefore, results indicated monolayer adsorption of Pb, Cu and Co onto biochars (onto Pe350 for Pb and onto Sd350 for Co and Cu), while laminate adsorption of Cd onto Sd350.

The essential characteristics of the Langmuir adsorption isotherm parameter can be used to predict the affinity between the sorbate and sorbent using a dimensionless constant called separation factor or equilibrium parameter R_L which is defined by

$$R_L = \frac{1}{1 + K_a \times C_o} \qquad (10)$$

Where Ka is defined earlier and C_o is the initial contaminant concentration.

Fig. 12 below illustrates the linearized isotherms best-fitted to experimental data of equilibrium concentration.
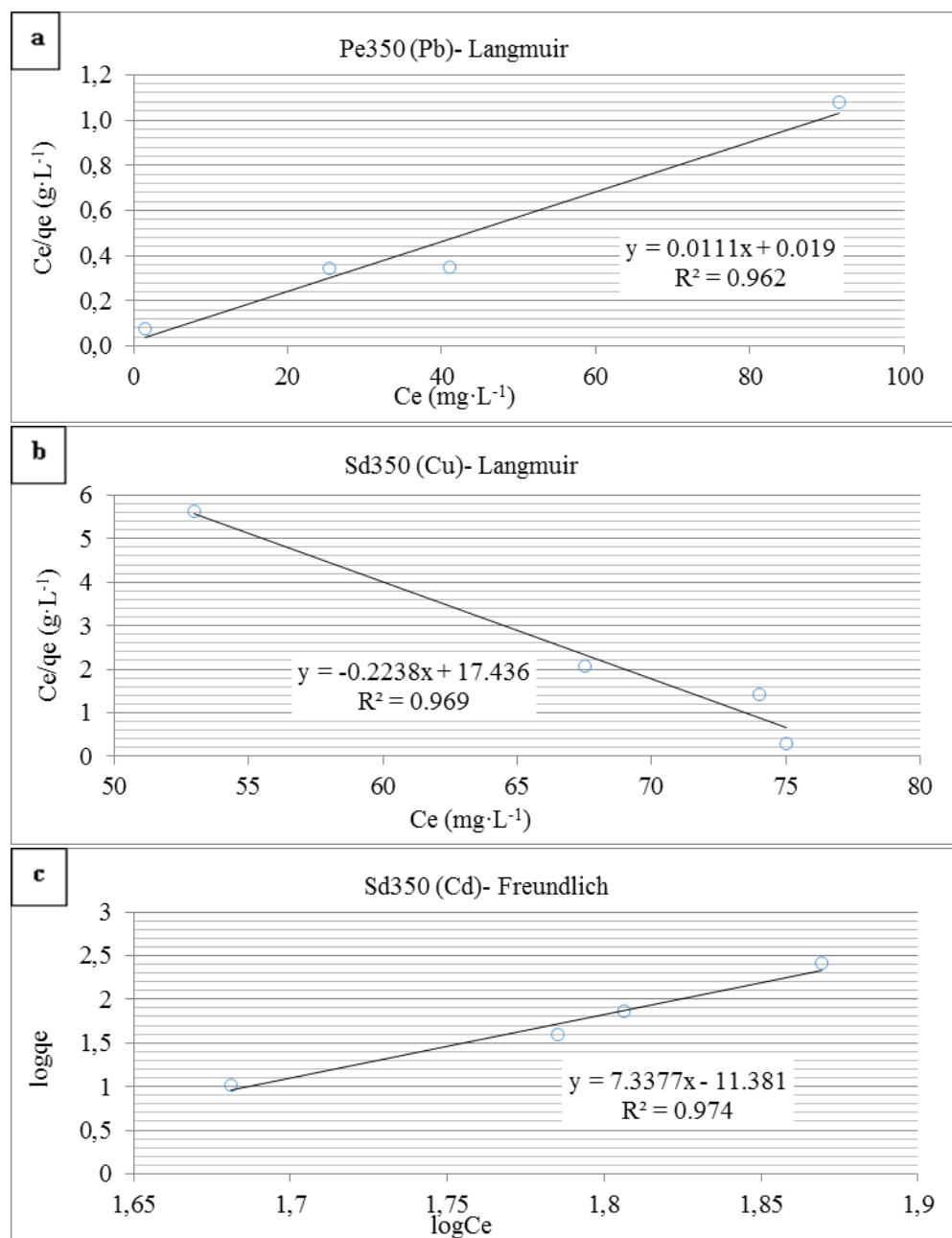

Fig 12. Linearized isotherms best-fitted to experimental data of equilibrium concentration of; **a** Pb adsorption onto Pe350, **b** Cu adsorption onto Sd350, **c** Cd adsorption onto Sd3

Te value of R_L indicated the type of Langmuir isotherm to be irreversible ($R_L=0$), linear ($R_L=1$), unfavorable ($R_L>1$), or favorable ($0< R_L<1$) *(Desta, 2013)*. Table 8 shows that for Pe350 (Pb), Ka is 0.584 and initial contaminant concentration is 100 mg·L^{-1}. For Sd350 (Cu) Ka equals to -0.013 while initial contaminant concentration is the same. Consequently, for Pe350 (Pb) R_L is equal to 0.017 while for Sd350 (Cu) R_L is equal to -3.33. Therefore, it can be only deduced that Pb adsorption onto Pe350 is favorable.

The n value of Freundlich equation indicates the degree of nonlinearity between solution concentration and adsorption as follows: if n=1, then adsorption is linear; if n<1, then adsorption is a chemical process; if n>1, then adsorption is a physical process. The 1/n value in Freundlich equation was found to be 7,338 for Cd adsorption onto Sd (Table 8). Therefore, n<1 is valid *(Desta, 2013)*. Moreover, if the value of constant n in Freundlich equation is larger than one then the adsorbate is positively adsorbed onto biochar *(Li et al., 2016)*.

3.2.4. Effect of heavy metal properties on their adsorption

The preference in heavy metal adsorption by Pe3350 or Sd350 is usually attributed by other researchers to the metal ion properties, such as ionic radius and electronegativity. Heavy metals in this study are consistent with the following serries Pb>Cd>Co>Cu as far as ionic radius is concerned. The ionic radius of Pb^{2+} (1.19 Å) is higher than that of Cd^{2+} (0.97 Å), Co^{2+} (0.745 Å) and Cu^{2+} (0.73 Å) and it is seen in Table 3 that in general the higher the ionic radius the higher the % adsorption onto biochar. Electronegativity of these metals follows the same serries. This means that the higher the electronegativity of a metal ion, the higher the adsorption *(Lao et al., 2005)*. Therefore, Pb^{2+} ions have a better electrostatic interaction with the functional groups on biochars than the other heavy metals examined in this study. A similar trend is also noticed between adsorption and hydration enthalpy for each metal ion. The enthalpy of hydration of an ion, H_{hyd}, in kJ·mole^{-1}, is the amount of energy released when a mole of the ion dissolves in a large volume of water forming thus an infinite dilute solution. It is shown that the higher the ionic radius the higher is the hydration enthalpy; hydration enthalpy of Pb^{2+} -1485 kJ/mole, considerably higher than that of Cd^{2+} (-1809 kJ·mol^{-1}), Co^{2+} (-2010 kJ·mol^{-1}) or Cu^{2+} (-2100 kJ/mole). These hypotheses seem to be verified in general for the most combinations of adsorbent material to adsorbent concentration. Co>Cu is verified concerning the % adsorption only for the half combinations (Pe350/1 g·L^{-1}, Pe350/5 g·L^{-1}, Sd350/0.1 g·L^{-1}), whereas Pb>Cu is not valid only for Pe350 at adsorbent concentration 0.1 g·L^{-1}. Variations from the series Pb>Cd>Co>Cu are attributed to experimental failures.

3.2.5. Reuse potential of biochars in Pb and Cu adsorption

Pb and Cu adsorption is important for estimating biochars reuse potential. Thus Pb and Cu desorption tests were performed using 0.1 N HCl and 0.1 N HNO_3 solutions (H^+ is a much stronger competitor for Pb^{2+} as *Ding et al. (2014)* mentioned). Results of the sequential 24 h adsorption and 24 h desorption experiments of 100 mg·L^{-1} Pb or Cu onto 5g·L^{-1} biochars are summarized in Table 9. Adsorbed mg of Pb or Cu onto biochars (mg·g^{-1}) was calculated as described in previous section 3.2.1. Similarly, adsorbed Pb or Cu amounts after 24 h second adsorption were computed. Fig 15 and 16 present these results. In Table 9, % adsorption (first and second metal adsorption) of Pb or Cu for each biochar was calculated using the following equation:

$$\% \text{ Adsorption} = \frac{C_0 - C_e}{C_0} \text{ x } 100 \qquad (11)$$

where C_o and C_e are the concentration of Pb or Cu (mg·L^{-1}) initially and at equilibrium time, respectively.
The % desorption of each heavy metal (Me) adsorbed onto biochar was estimated as:

$$\% \text{ Me}_{desorption} = \frac{m_D}{m_A} \text{ x } 100 \qquad (12)$$

where m_A and m_D are the adsorption rate and desorption rate of heavy metal to biochar (mg·g^{-1}), respectively.
The adsorption rate of each heavy metal adsorbed onto biochar is calculated using the following relationship:

$$A_{cap} = m_A - m_D + m_{A2} \qquad (13)$$

where m_{A2} is the adsorption rate of heavy metal to biochar (mg·g^{-1}) at second stage of adsorption and m_A and m_D are defined earlier.

Table 9. Adsorbed Pb or Cu onto biochar followed by desorption and second adsorption. Pb or Cu initial concentration 100 mg·L^{-1} before each adsorption experiment, 0 mg·L^{-1} before desorption experiment.

Heavy metal	Adsorbent	1st stage adsorption		Metal desorption	2nd stage adsorption	Adsorption rate, A_{cap}
		mg·g^{-1}	%	%	%	mg·g^{-1}
Pb	Pe350	18.3	97.3	86.9*	46.8	11.3
		16.9	89.9	63.3**	51.6	16.0
	Sd350	17.9	95.2	90.5*	94.7	19.7
		17.7	94.1	100**	94.2	35.6
Cu	Pe350	2.7	14.0	96,3*	11.3	2.3
		2.2	11.4	100**	14.9	2.9
	Sd350	6.5	33.7	86,1*	32.5	7.2
		6.8	35.2	73,5**	26.3	6.9

*Desorption using HCl
**Desorption using HNO$_3$

Biochar derived from both, pecan shells and sawdust feedstock material can adsorb Pb of initial concentration 100 mg·L^{-1} at an approximate percentage of 90 to 97 %, while can adsorb Cu of initial concentration of 100 mg·L^{-1} at a much lesser extent ranging from 11.4 to 35.2 % for Pe350 to Sd350 respectively (Table 9). In detail, Pb adsorption rate at first adsorption is estimated around 18 mg Pb per gram for both Pe350 and Sd350, while the Cu adsorption rate was estimated at 6.5 and 6.8 mg·g^{-1} for Sd350 and 2.2 and 2.7 mg·g^{-1} for Pe350 during first adsorption (Table 9).

24 h desorption followed the 24 h adsorption of Pb onto 5g·L^{-1} biochar. Pb desorbed from the biochars under the use of 0.1 M HCl or HNO$_3$ desorption solution is presented in Fig. 13. Similarly, Cu desorbed from the biochars under the use of 0.1 M HCl or HNO$_3$ desorption solution is presented in Fig. 14. Pb is desorbed more effectively from Sd350 than from Pe350 regardless the desorption treatment (Fig. 13) (e.g. extractable Pb from Sd350 equals to 100 instead of 63.3 % for Pe350 under the same desorption solution HNO$_3$). On the contrary, Cu is extracted more effectively from Pe350 than from Sd350 (Fig. 14), indicating that the % heavy metal desorption is not related to the desorption solution, but to the structure of biochars and the nature of heavy metal adsorbed. Finally, these results exhibited that only a small percentage of the adsorbed Pb in biochars remained immobilized except for Pe350 under HNO$_3$ that displayed larger immobilization (minimum desorption 63.3 %) (Table 9, Fig. 13). 86.9 % of the Pb on Pe biochar was desorbed by HCl within 24 h, while 90.5 and 100 % of the Pb on Sd biochar was desorbed by HCl and HNO$_3$ within 24 h respectively (Table 9, Fig.13). The amount of Pb that was not desorbed was probably trapped inside the pore spaces in the biochars, as *Ding et al. (2014)* supported. On the other hand, 86.1 and 73.5 % was desorbed from Sd350 under HCl and HNO$_3$ desorption, while almost the whole amount of the adsorbed Cu in biochars was desorbed from Pe350 accounting for 96.3 and 100 % under HCl and HNO$_3$ desorption respectively.
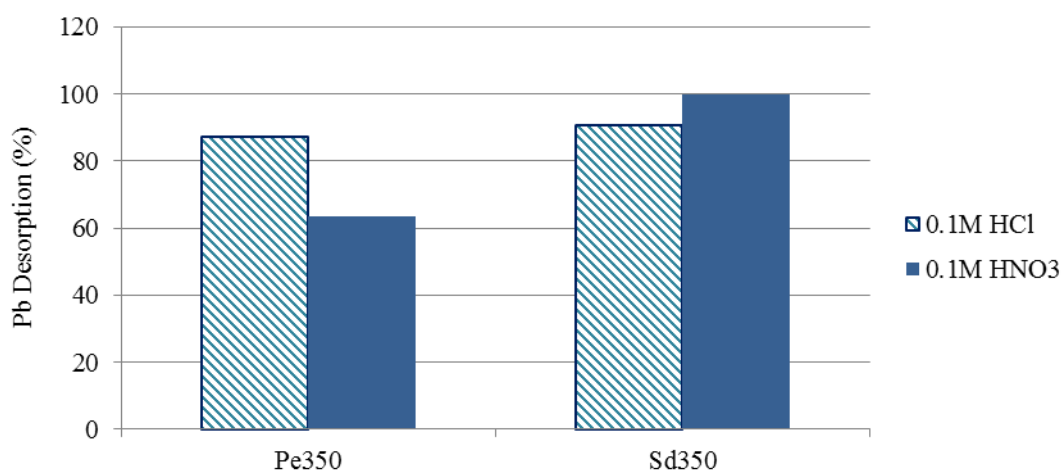
Fig. 13. Desorption of Pb from Pe350 and Sd350. Conc. of biochar 5 g L^{-1} biochar, conc. of Pb 100 mg L^{-1} Pb
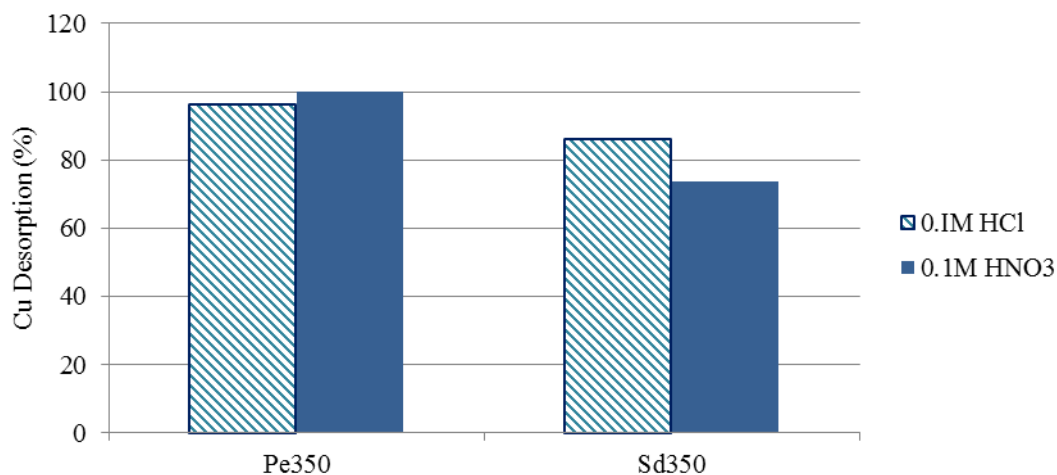
Fig. 14. Desorption of Cu from Pe350 and Sd350. Conc. of biochar 5 g L-1 biochar, conc. of Pb 100 mg L-1 Pb

Second adsorption experiments using the loaded biochars and a new 100 mg·L^{-1} solution of Pb or Cu for Sd350 and Pe350 indicated that they can be reused for adsorption. Particularly, second 24 h adsorption experiments using 5g·L^{-1} loaded Sd350 with Pb and a new 100 mg·L^{-1} solution of Pb indicated almost the same adsorption efficiency (94.2-94.7 %), while for Pe350 indicated % adsorption around half of the first stage (46.8-51.6 %) (Table 9). Second 24 h adsorption experiments using 5g·L^{-1} loaded biochar with Cu and anew 100 mg·L^{-1} solution of Cu extended adsorption procedure at a similar percentage for both Pe350 (11.3-14.9 %) and Sd350 (32.5-26.3 %). Fluctuation in Pb or Cu adsorbed amount is demonstrated in Fig. 15 and Fig 16. Finally, Sd350 showed the higher adsorption capacity for Pb under desorption with HNO$_3$ (35.6 mg·g^{-1}) followed by the extraction with HCl (19.7 mg·g^{-1}) prior to second adsorption experiment. On the other hand, Cu was better adsorbed by Sd350 under desorption with HCl (7.2 mg·g^{-1}) followed by desorption with HNO$_3$ (6.9 mg·g^{-1}). In any way, Sd350 is a better reuse adsorbent compared with Pe350.
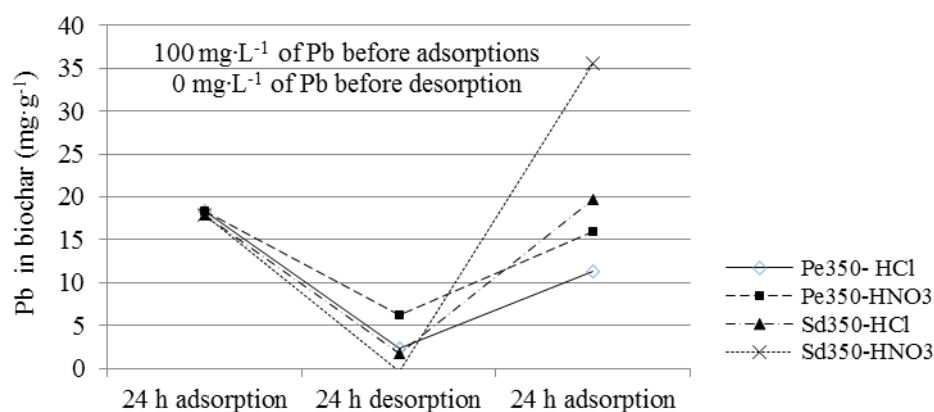
Fig. 15. Adsorbed Pb onto Pe350 and Sd350 under; 24 h first adsorption, 24 h desorption and 24 h second adsorption.
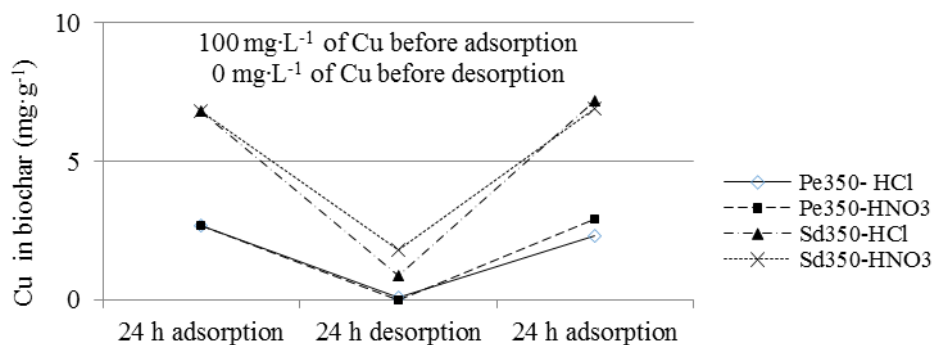
Fig. 16. Adsorbed Cu onto Pe350 and Sd350 under; 24 h first adsorption, 24 h desorption and 24 h second adsorption.

3.3. Phenols adsorption onto biochar and activated carbon

3.3.1. Effect of contact time and adsorbent dosage on phenols adsorption

Next experiments were conducted in order to examine biochars potential to adsorb phenols in flasks. Thus, solutions of 100 mg·L^{-1} phenols were agitated with 0.5, 1, 2.5 and 5 g·L^{-1} of biochars Pe350, Sd350 or PI350 respectively for up to 48 h in order to establish equilibrium, henceforth referred to as PePhe, SdPhe or PIPhe. Sampling was done at various times, namely 15 min, 2, 6, 24 and 48 h. Phenols adsorption increased rapidly within the first 6 h, followed by a gradual increase up to 48 h (Fig 17, 18, 19). The increase in adsorption at the initial stage is due to the large number of vacant adsorption sites, as also mentioned for metals before, which become saturated with time and as a consequence the adsorption is less efficient afterwards and assigned to slow migration of phenols into pore spaces inside the biochars. Most of phenols removal occurred within 24 h accounting for 67.4 to 98.6 % of total phenols adsorption. Table 10 presents the calculated % phenols adsorption in respective solutions at each interval time. The highest % adsorption of phenols is shown for 5 g·L^{-1} SdPhe at 48 h, namely 70 %, followed by PIPhe for 2.5 and 5 g·L^{-1} adsorbent concentration at 48 h, namely 62 and 54 % respectively. Higher adsorbent concentrations result in increased % adsorption as it can be concluded from Table 10 and Fig.17, 18. This behavior is mostly observed for PePhe and SdPhe over 24 h, where % phenols adsorption ranged from 37 to 57 % and 31 to 69 % respectively, while this trend is not clear for PIPhe (Fig 19). Finally, it can be assumed that equilibrium concentration of phenols is achieved after 48 h in comparison with the time required for equilibrium of heavy metals (24 h) indicating that different adsorbates involve different adsorption mechanisms (e.g., ion exchange, precipitation, physical adsorption and complexation, intraparticle diffusion).

Table 10. The effect of adsorbent (Pe350, Sd350 and PI350) concentration (0.5, 1, 2.5 and 5 g·L^{-1}) on phenols adsortpion.

% Phenols Adsorption						
Time (h)		*0.25*	*2*	*6*	*24*	*48*
Adsorbent	*Adsorbent concentration, mg·L^{-1}*					
Pe	*0.5*	18	16	23	37	46
	1	11	22	32	37	53
	2.5	17	34	42	50	48
	5	25	46	54	57	-
Sd	*0.5*	8	26	31	31	46
	1	17	30	39	41	48
	2.5	31	40	46	57	51
	5	34	38	58	69	70
PI	*0.5*	13	21	28	41	46
	1	18	33	35	35	48
	2.5	23	33	35	48	62
	5	19	29	34	47	54
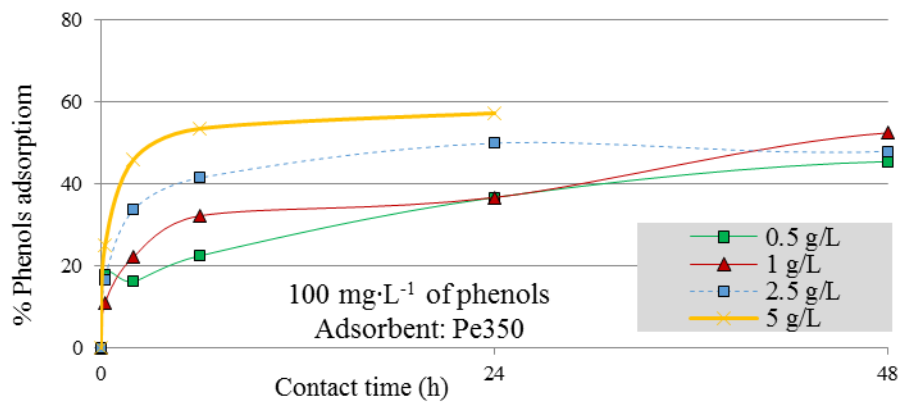
Fig. 17. The effect of adsorbent Pe350 concentration (0.5, 1, 2.5 and 5 g·L^{-1}) on phenols adsortpion.
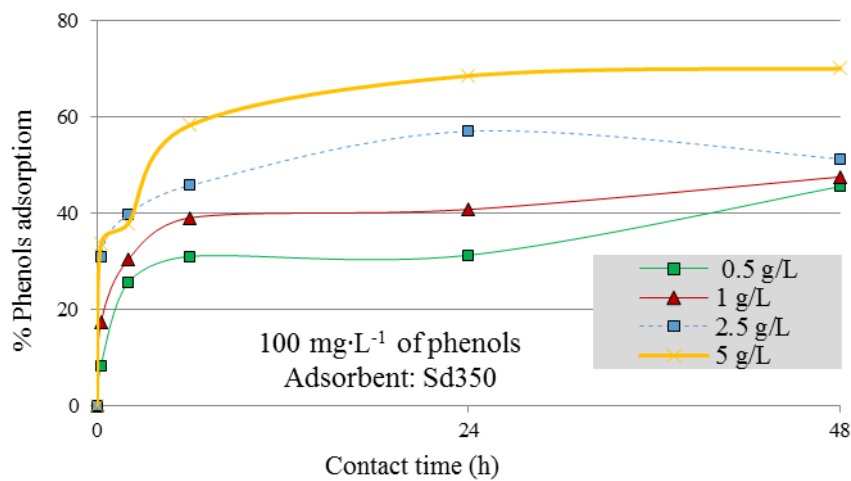
Fig. 18. The effect of adsorbent Sd350 concentration (0.5, 1, 2.5 and 5 g·L^{-1}) on phenols adsortpion.
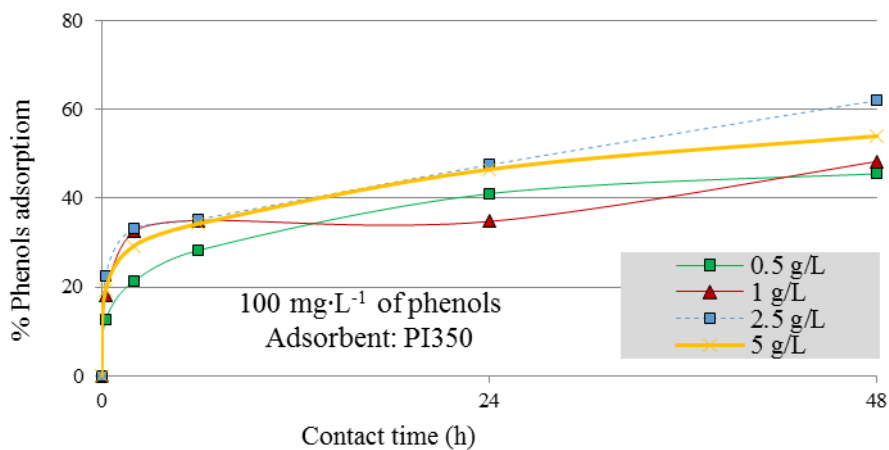
Fig. 19. The effect of adsorbent PI350 concentration (0.5, 1, 2.5 and 5 g·L^{-1}) on phenols adsortpion.

Subsequently, Fig. 20 presents the adsorption rates of all the adsorbent materials versus the adsorbent concentrations for phenols adsorption. For all the used adsorbents, the adsorption rate of phenols increases with decreasing adsorbent concentration. This result showed that as the adsorbent concentration increases, the amount of phenol bonds on biochars increases (increased % adsorption) but adsorption rate decreases and thus adsorption efficiency decreases as also mentioned in heavy metal adsorption in previous section.
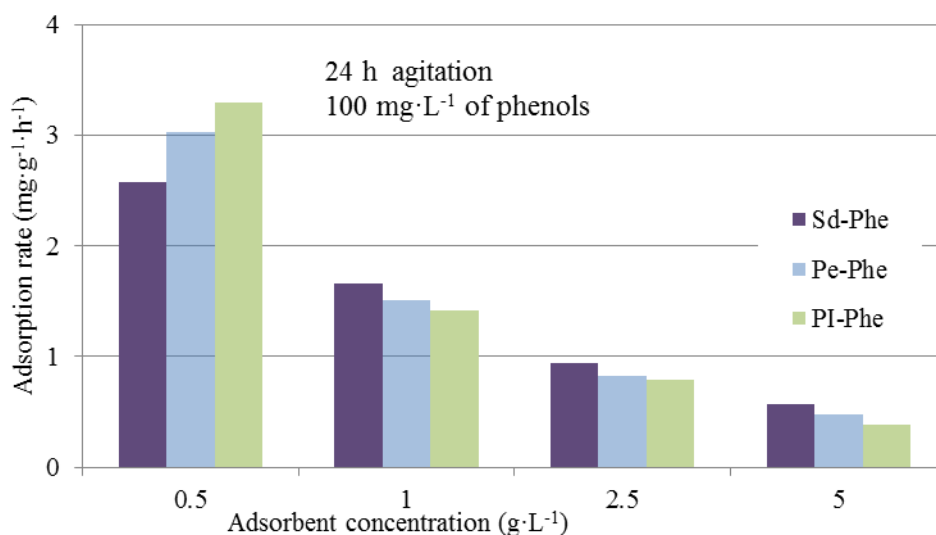
Fig. 20. Adsorption rates (mg·g^{-1}·h^{-1}) of phenols (concentration 100 g·L^{-1}) for each adsorbent (PePhe, SdPhe and PIPhe) concentration (0.5, 1, 2.5 and 5 g·L^{-1})

Thus, the highest adsorption rate was 3.3 followed by 3.02 and 2.57 mg·g^{-1}·h^{-1} for PIPhe, PePhe and SdPhe respectively, at 0.5 g·L^{-1} biochar concentration, while the lowest adsorption rate was 0.39, 0.48 and 0.57 mg·g^{-1}·h^{-1} respectively at 5 g·L^{-1} biochar concentration. Entirely opposite behavior is observed for the other biochar concentrations used, where the adsorption rate of phenols is higher for SdPhe, followed by PePhe and subsequently PIPhe. Experimental data as far as pH is concerned showed increase in pH for all adsorbents and adsorbent concentrations used, with the maximum increase from 6.69 to 8.35 for PePhe at a concentration 0.5 g·L^{-1} (Table 11). It is worth mentioning, however, that the higher the adsorbent concentration the lower the increase of pH for PePhe and SdPhe, while the higher the adsorbent concentration the higher the increase of pH for PIPhe (Table 11). These results combined with the calculated adsorption rates (Fid 20) demonstrate probably the priority of PePhe and SdPhe to bind H^{+} and subsequently to bind phenols.

Table 11. pH of phenol solutions (100 mg·L^{-1}) before and after agitation for Pe350, Sd350 and PI350. Adsorbent concentration 0.5, 1, 2.5 and 5 g·L^{-1}

pH			
Time, h		*0*	*24*
Adsorbent	*Adsorbent concentration, g·L^{-1}*		
Pe350	0.5	6.69	8.35
	1		8.15
	2.5		7.66
	5		6.65
Sd350	0.5	6.69	7.5
	1		6.78
	2.5		6.09
	5		7.21
PI350	0.5	6.69	7.33
	1		7.6
	2.5		7.62
	5		8.08

3.3.2. Kinetic studies

Kinetics of phenols adsorption was studied using the pseudo-first and pseudo-second order kinetic models (Lagergren) also used in section 3.2.2. The results presented in Tables 12 and 13 indicate that the pseudo-second-order kinetic model fits the data better than the pseudo-first one. The pseudo-second-order model exhibited correlation coefficient (R^2) values higher than 0.956 with most of them being higher than 0.99. On the other hand, the pseudo-first-order model exhibited much lower R^2 values ranging from 0.914 to very low values, 0.317. Moreover, experimental q_e values were comparable with those obtained from pseudo-second-order model, while differed from those obtained from pseudo-first-order model as expected. Under the assumptions of the pseudo-second-order model, the rate-limiting step may be chemical adsorption that involves chemical bonding between ionic form

of phenols and polar functional groups present on the adsorbent and the reaction rate is proportional to the number of active sites (functional groups) present on the adsorbent surface.

Table 12. Pseudo-first-order kinetic model parameters for the adsorption of phenols (concentration 100 $g \cdot L^{-1}$) onto Pe350, Sd350 or PI350 (0.5, 1, 2.5 or 5 $g \cdot L^{-1}$)

Adsorbent	Adsorbent concentration, $g \cdot L^{-1}$	$q_{e(Exp)}$, $mg \cdot g^{-1}$	Model q_e, $mg \cdot g^{-1}$	k_1, $l \cdot h^{-1}$	R^2
Pe350	0.5	91.0	68.6	0.06	0.914
	1	52.5	38.0	0.04	0.702
	2.5	19.2	14.5	0.30	0.914
	5	22.8	17.0	0.02	0.479
Sd350	0.5	91.0	59.3	0.04	0.474
	1	47.5	25.7	0.06	0.616
	2.5	20.5	12.0	0.30	0.802
	5	14.0	8.7	0.15	0.950
PI350	0.5	91.0	68.2	0.09	0.956
	1	48.3	40.4	0.01	0.317
	2.5	24.8	16.6	0.05	0.766
	5	10.8	7.3	0.07	0.880

Table 13. Pseudo-second-order kinetic model parameters for the adsorption of phenols (concentration 100 g·L^{-1}) onto Pe350, Sd350 or PI350 (0.5, 1, 2.5 or 5 g·L^{-1})

Adsorbent	Adsorbent concentration, g·L^{-1}	$q_{e(Exp)}$, mg·g^{-1}	Model q_e, mg·g^{-1}	k_2, g·µg^{-1}·h^{-1}	R^2
Pe350	0.5	91.0	100.0	2.50	0.980
	1	52.5	50.0	5.71	0.961
	2.5	19.2	20.0	83.33	0.999
	5	22.8	11.1	270.00	0.999
Sd350	0.5	91.0	100.0	3.33	0.956
	1	47.5	50.0	13.33	0.994
	2.5	20.5	11.1	90.00	0.996
	5	14.0	14.3	61.25	0.999
PI350	0.5	91.0	100.0	3.33	0.996
	1	48.3	20.0	25.00	0.966
	2.5	24.8	25.0	16.00	0.977
	5	10.8	11.1	40.50	0.993

3.3.3 Isotherm studies

Based on equilibrium concentrations regarding adsorption of phenols using Pe350, Sd350 or PI350 in a solution containing 100 mg·L^{-1} phenols, Langmuir and Freundlich isotherms described in previous section have been used to describe adsorption. Neither Langmuir nor Freundlich isotherms were found to fit data as it is seen in Table 14 below.

Table 14. Langmuir and Freundlich parameters and correlation coefficients for the adsorption of phenols onto Pe350, Sd350 or Pe350. Initial phenol concentration 100 mg·L^{-1}

	Langmuir			Freundlich		
	R^2	qmax	Ka	R^2	1/n	logK$_F$
Pe(Phenols)	0.036	36.900	3.115	0.227	3.316	-4.026
Sd (Phenols)	0.410	-20.747	-0.013	0.639	2.422	-2.485
PI (Phenols)	0.124	-12.594	-0.014	0.384	3.535	-4.397

3.3.4. Effect of pH on phenols adsorption

In order to examine the effect of pH on phenols adsorption 0.01 N HCl and 0.01 N NaOH solutions were used for pH adjustment of the 100 mg·L^{-1} phenol solution. Thus, 5 g·L^{-1} of Pe350, Sd350 or PI350 were added in phenols solutions of initial pH 4 or 9 to test their ability to reduce phenols concentration. Samples would be referred to as Pe4Phe, Pe9Phe and so forth. Aliquots of aqueous samples were measured for their phenols concentration at 15 min, 2, 4, 6, 24 and 48 h. The different pH conditions under which phenols adsorption occurred by Pe350, Sd350 or PI350 did not seem to influence the % adsorption at equilibrium (48 h) as it is presented in Fig. 21, 22, 23 below probably due to buffering capacity of biochar. In detail, experimental data are shown in Table 15. pKa is the pH at which half of the functional groups of the compounds present in solution are charged and half are neutral. The larger the value of pKa the smaller is the extent of dissociation at any given pH (Henderson–Hasselbalch equation). The distribution of molecular and ionized phenols varies as the solution pH is altered. pKa of phenols equals to 9.98. Phenols are hydrophobic but the ionic form is less hydrophobic and as a result adsorption decreases when pH is higher than pKa *(Mathialagan and Viraraghavan, 2009)* indicating that pH higher than 10 would probably lead to different adsorption results. The following adsorption experiments involve phenol solutions without pH alteration.
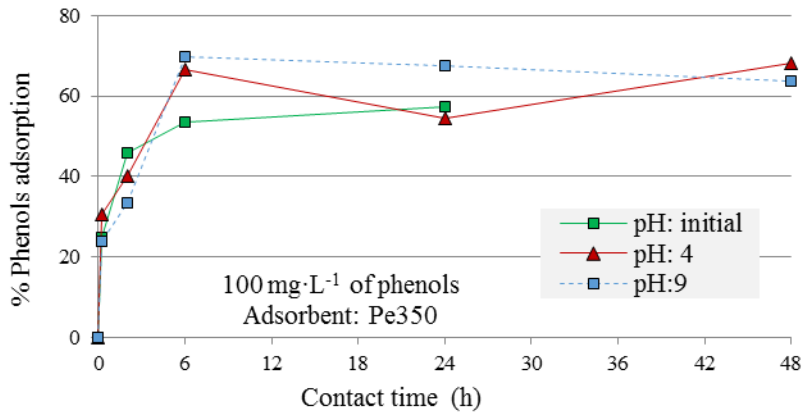
Fig. 21. The effect of pH on phenols adsorption onto Pe350. Adsorbent concentration 5 g·L⁻¹
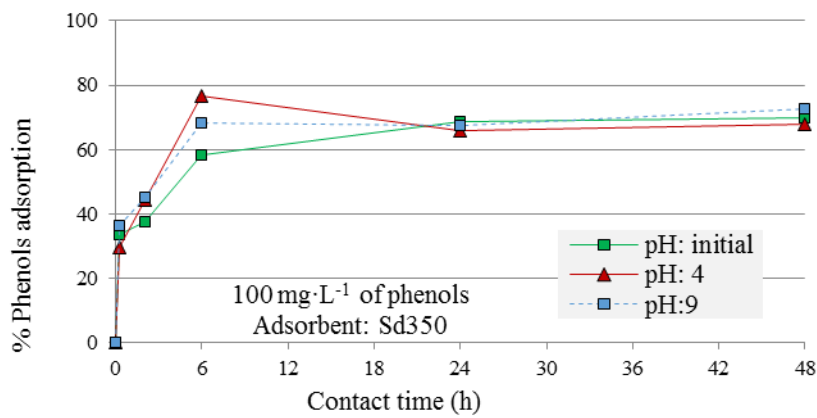
Fig. 22. The effect of pH on phenols adsorption onto Sd350. Adsorbent concentration 5 g·L⁻¹
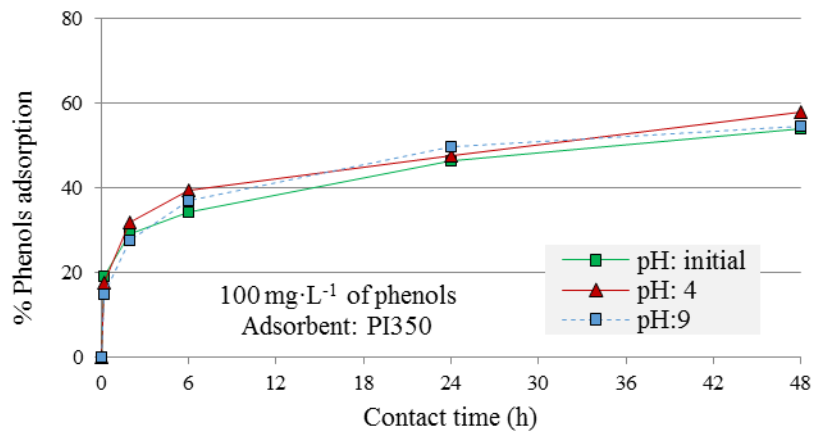
Fig. 23. The effect of pH on phenols adsorption onto Pl350. Adsorbent concentration 5 g·L⁻¹.

Table 15. The effect of pH on % phenols adsorption onto adsorbent Pe350, Sd350 or PI350. Adsorbent concentration 5 g·L^{-1}

	pH		% phenols adsorption				
Time, h	0	24	0.25	2	6	24	48
Adsorbent							
Pe350	6.3	6.65	25	46	54	57	-
	4	6.91	31	40	66	55	68
	9	7.27	24	34	70	67	64
Sd350	6.3	7.21	34	38	58	69	70
	4	6.97	30	44	77	66	68
	9	7	36	45	68	68	73
PI350	8.2	8.08	19	29	34	47	54
	4	6.35	18	32	40	48	58
	9	8.34	15	28	37	50	55

Before and after adsorption, pH did not show remarkable fluctuation in unmodified phenols solutions PePhe, SdPhe and PIPhe (maximum fluctuation from 6.3 to 7.21 for SdPhe). However, pH in modified phenol solutions differed before and after adsorption. Particularly, pH increased in acidic solution from 4 to 6.97 for Sd4Phe and decreased from 9 to 7 for Sd9Phe (Table 15). This fact indicates that biochars not only can be used for pollutant reduction in water solutions, but also for pH buffering.

3.3.5. Effect of activation on phenols adsorption

The selected biochars Pe350, Sd350 or PI350 were mixed and stirred with 1M KOH or 1M FeCl$_3$ solution with impregnation w/v ratio of biochar to activator 20:500 (g/mL) and hereafter referred to PeA350, SdA350 and PIA350. The adsorbent concentration with maximum % adsorption (5 g·L^{-1} in this study) was used for the following adsorption experiments with activated biochars. Solutions containing 100 mg·L^{-1} phenols were shaken with activated biochars for up to 48 h. Aliquots of aqueous samples were measured for their phenols concentration at 15 min, 2, 6, 24 and 48 h. Results are exhibited in Table 16 and respective graphs are illustrated in Fig. 24, 25, 26. For activated biochars, equilibrium time is estimated at 5 days (120 h), longer than that of non activated biochars (48 h). For all adsorbent materials, activated biochars with KOH solution demonstrated decreased % phenols adsorption.

Table 16. Effect on % phenols adsorption of activated biochars (PeA350, SdA350 and PIA350) with 0.1 M KOH or FeCl$_3$ in comparison with non activated biochars.

Time, h		0	0.25	2	6	24	48	72	120
Pe350	% Adsorption		25	46	54	57	-	-	-
	pH	6.3				6.65			
PeA350-KOH	% Adsorption		11	19	30	38	41	61	59
	pH	6.88					10.08		
PeA350-FeCl$_3$	% Adsorption		14	28	44	56	64	69	74
	pH	6.88					4.10		
Sd350	% Adsorption		34	38	58	69	70	-	-
	pH	6.3				7.21			
SdA350-KOH	% Adsorption		3	5	11	28	45	51	58
	pH	6.88					9.14		
SdA350-FeCl$_3$	% Adsorption		15	43	62	67	69	74	79
	pH	6.88					4.48		
PI350	% Adsorption		19	29	34	47	54	61	-
	pH	8.2				8.08			
PIA350-KOH	% Adsorption		14	17	29	42	41	52	68
	pH	6.88					9.55		
PIA350-FeCl$_3$	% Adsorption		23	34	49	60	68	74	78
	pH	6.88					4.65		

Moreover, KOH activated biochars showed lower % adsorption than FeCl$_3$ activated biochars did in all cases. Maximum % adsorption onto KOH activated biochar was achieved for PIA350-KOH (68 %) after 5 days. *Dehkhoda et al. (2016)* claimed that intermediate stages of activation process such as centrifuging and sample drying process after impregnation are key steps for the efficient adsorption

capacity of biochars. Centrifuging the samples provided better separation compared to filtration since using filter papers leads to shrinkage as a result of exposure to highly concentrated KOH solution and problematic separation. In addition, the sample drying process affects the porosity development due to the potential conversion of activating reagent KOH to its corresponding carbonate (K_2CO_3) in the presence of CO_2 in the air-dried. *Stavropoulos et al. (2008)* also report that KOH impregnation may exhibit more than desired erosive behavior for the surface of biochar. The increase of solution pH after phenols adsorption (48 h) by KOH activated biochars (Table 16) is probably attributed to the release of OH^- ions from KOH.
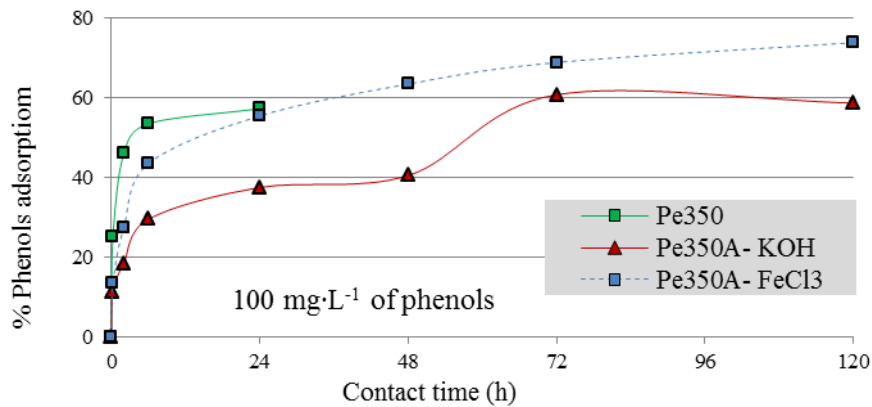
Fig. 24. Effect on phenols % adsorption of activated biochar Pe350A with 0.1 M KOH or $FeCl_3$ in comparison with non activated biochar Pe350.
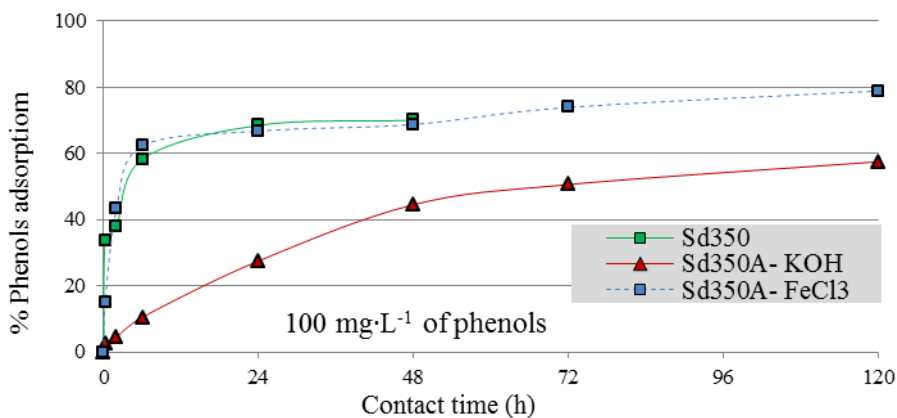

Fig. 25. Effect on phenols % adsorption of activated biochar Sd350A with 0.1 M KOH or $FeCl_3$ in comparison with non activated biochar Sd350.
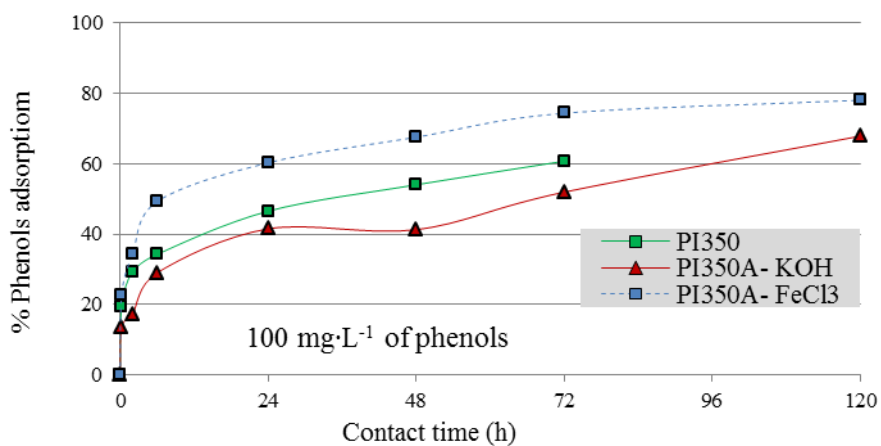

Fig. 26. Effect on phenols % adsorption of activated biochar PI350A with 0.1 M KOH or $FeCl_3$ in comparison with non activated biochar PI350.

On the other hand, SdA350-FeCl$_3$ showed similar results in % phenols adsorption with Sd350 after 2 h agitation, PeA350-FeCl$_3$ and Pe350 differed until the first 6 hours with a maximum variation at 2 hours (28 and 46 % respectively), while PIA350-FeCl$_3$ showed higher % phenols adsorption than PI350 during the entire time of the experiment with a maximum variation at 6 hours (49 instead of 34 % respectively). Maximum % adsorption onto FeCl$_3$ activated biochar was achieved for SdA350-FeCl$_3$ (79 %) at 5 days. Surface of activated biochars with FeCl$_3$ is positively charged with the form C-Fe(OH$_2$)$_5^{+3}$$_{(s)}$. Under the acidic conditions present in phenol solutions after 48 h adsorption (Table 16) the concentration of this form is elevated and thus ionic phenols are adsorbed onto PIA350-FeCl$_3$ explaining the small increase in phenols adsorption. As far as PeA350-FeCl$_3$ and SdA350-FeCl$_3$ are concerned, when *Li et al. (2016)* used FeCl$_3$ in order to activate biochar, biochar pores were blocked with excess iron and decreased the contact area of ionic adsorbate and iron (hydr)oxides. They found an optimal ratio of iron to biochar, which is probably unique for each biochar of different feedstock material or/and pyrolysis temperature. Thus, in our case the ratio might have exceeded the optimal one. The drop in pH shown in Table 16 may be attributed to the cation exchange between FeCl$_3$ and protons present on biochar's surface.

3.3.6. Phenols adsorption in fixed-bed columns

Biochars' potential for removing phenols was examined in 100 mL open-top transparent plexiglas free draining columns filled with 50-50 v/v quartz sand to Pe350 or Sd350. A control column, filled only with quartz sand was also set. Solution of 10 mg·L^{-1} phenols was left to percolate from the top of the columns; 35 and 57 mL percolated through 29 and 4.5 g Pe350 and Sd350 respectively. The % adsorption of phenols through Pe10Phe and Sd10Phe was estimated at 90 and 86 % respectively on first day and remained stable until the third day where sampling was done again, while % adsorption of phenols through C10Phe was estimated at 18.9 % on first day and at 88 % on third day indicating that physical adsorption takes place also onto quartz sand beside adsorption onto biochars. On the other hand, for the clean-up of a solution containing 150 mg·L^{-1} COD or 60mg·L^{-1} PO$_4$, % adsorption was negligible for both solutions at percentages not exceeding 0.7 %. For this reason the following experiments included only phenol adsorption on biochars.

The next experimental series was also set in order to estimate biochars potential to adsorb phenols using 1000 mL transparent plexiglas columns. Columns were filled with 75-25 v/v quartz sand to Pe350 or Sd350 and phenol solution of 200 mg·L^{-1} was pumped up-flow in the columns. At the end of the experiment (24 h), 1575 and 953 mL were pumped through the columns Sd200Phe and Pe200Phe respectively containing 17.5 and 99 g of the respective biochar. 64.4 % phenol adsorption was achieved for Pe200Phe, while a lower one was achieved for Sd200Phe (49 %). It is worth mentioning though that Sd200Phe shows better % adsorption than Pe200Phe in the middle (after ~2.5 h) and at the exit (after ~4 h) of the column when phenol solution reached these points for the first time; 83 and 98 % for Sd200Phe instead of 74 and 93 % for Pe200Phe. This difference is explained because a greater volume flows through the Sd200Phe than through Pe200Phe at the same time, as mentioned before. 28 hours after starting the experiment, samples was taken from the middle of the columns again. Sd200Phe showed better adsorption than Pe200Phe (53 instead of 31 %), indicating that Sd200Phe is more efficient in continuous phenol adsorption even if greater volume is treated. Sd200Phe is also more efficient than Pe200Phe because significantly less amount of biochar was used. As far as pH is concerned, pH of initial and final solution showed a minor change (~6.6 to 7.3 respectively). Therefore, pH does not affect phenols adsorption in fixed-bed columns, although biochars seem to ameliorate slightly solutions pH.

Double amount of biochar and a much lesser concentration of phenols were examined next in 1000 mL transparent plexiglas columns. Columns were filled with 50-50 v/v quartz sand to Pe350, Sd350 or PI350 and phenol solution of 20 mg·L^{-1} was pumped up-flow in the columns containing 142, 30 or 129 g of biochar respectively while the experiment took place continuously for 14 days. For all the biochars investigated (Pe350, Sd350,and PI350) experimental data shown in Table 17 revealed maximum phenol adsorption in the first day, reaching up to 96.1 % for Sd20Phe, followed by Pe20Phe and PI20Phe (93.3 and 92.9 % respectively). It is worth mentioning that Sd20Phe which exhibited the highest % adsorption treated higher volume of phenols solution than the other two (1.3 instead of 0.6 L). The % adsorption percentages at the days where similar volumes were treated are comparable; 57.3, 55.5 and 42.8 % with treated volumes of 6.5, 7.5 and 7.1 L for Pe20Phe, Sd20Phe and PI20Phe respectively and 41.8, 44.5 and 43.3 % with treated volumes of 9.1, 9.5 and 8.3 L respectively and furthermore 36.3 and 38 % with treated volumes of 10.7 and 10.6 L for Pe20Phe and Sd20Phe respectively. However, it is concluded that Sd20Phe is more efficient than Pe20Phe and PI20Phe because significantly less amount of biochar was used (30, 142 and 129 g respectively).

Table 17. % phenols adsorption, phenols concentration (mg·L^{-1}) and treated volume (mL) at several days in a period of 14 days.

Time d	Pe 350: quartz sand			Sd 350: quartz sand			PI 350: quartz sand		
	Concentration mg·L^{-1}	Adsorption %	Cumulative treated volume L	Concentration mg·L^{-1}	Adsorption %	Cumulative treated volume L	Concentration mg·L^{-1}	Adsorption %	Cumulative treated volume L
0	20	0.0	0.0	20	0.0	0.0	20	0.0	0
1	1.4	93.3	0.6	0.8	96.1	1.3	1.4	92.9	0.6
2	-	-		-	-		7.1	64.8	1.7
3	-	-		-	-		8.4	58.0	3.0
4	6.1	69.8	3.4	8.9	55.5	7.5	-	-	
5	7.2	64.0	4.3	11.1	44.5	9.5	-	-	
6	7.5	62.5	5.1	12.4	38.0	10.6	12.2	39.3	4.9
7	8.2	59.3	5.7	13.8	31.0	12.7	11.5	42.8	7.1
8	8.6	57.3	6.5	14.8	26.3	14.9	11.4	43.3	8.3
9									
10									
11	11.7	41.8	9.1	15.9	20.5	21.3	-	-	
12 d	11.5	42.5	10.1	20.0	0.0	23.5	-	-	
13 d	12.8	36.3	10.7	17.3	13.5	25.6	-	-	
14 d	12.9	35.5	12.2	19.9	0.7	27.7	-	-	

From the time perspective, it seems that Pe20Phe and secondly PI20Phe mixtures are more efficient in adsorbing phenols under continuous phenol flow. Particularly, Pe20Phe could still adsorb a percentage of 57.3 % on eighth day instead of 43.3 and 26.3 % for PI20Phe and Sd20Phe respectively. As far as Pe20Phe is concerned, it seems that it could adsorb at least 35 % of phenols on fourteenth day. On the other hand, adsorptive sites of Sd20Phe seem to be saturated on the twelfth day and phenols are thereafter adsorbed and desorbed. Intermediate values of phenols % adsorption are shown in Table 17 as well. Furthermore, Fig. 27 and 28 illustrate all these values after fourteen days. In conclusion, it can be concluded that Sd20Phe adsorbs phenols as much as Pe20Phe and PI20Phe do, but faster and with the advantage of much less quantity.
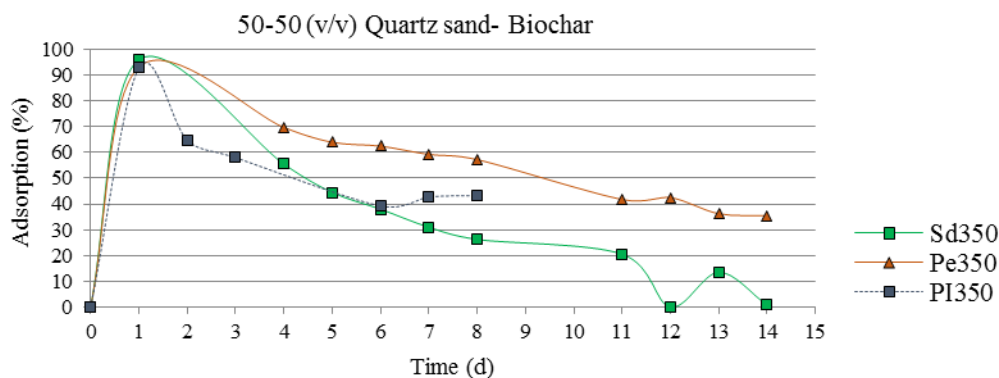
Fig. 27. % phenols adsorption in columns, at several days in a period of 14 days.
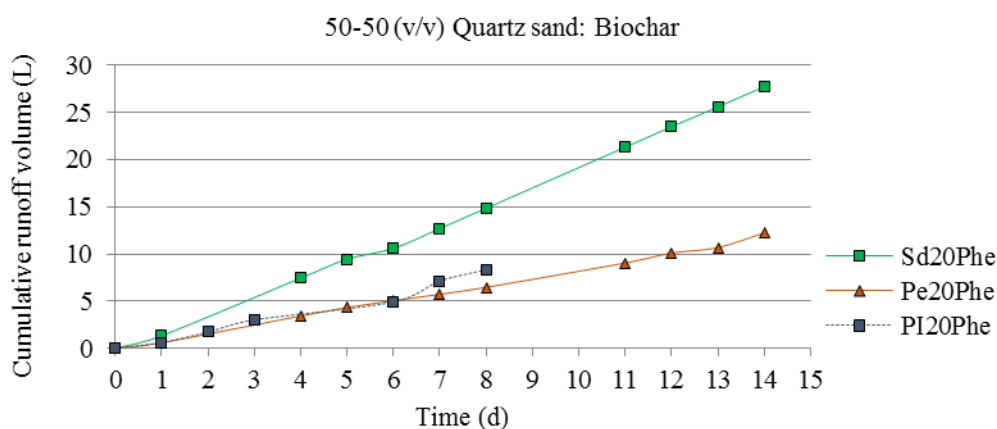
Fig. 28. Cumulative runoff volume during 14 days phenols adsorption in columns

Furthermore, in all experimental columns, pH did not fluctuate significantly before and after adsorption varying from 7.14 to 8.02 for Sd20Phe, 7.6 to 8 for Pe20Phe and 7.06 to 7.62 for PI20Phe. Tables 18 and 19 summarize the adsorption capacity and % phenols adsorption calculated from all tests carried out either in flasks or in columns.

Table 18. Adsorption capacity in all experiments in flasks and columns

		Biochar concentration.	Phenols concentration, $mg \cdot L^{-1}$	Adsorption rate, $mg \cdot g^{-1}$		
				Adsorbent		
				Pe350	Sd350	PI350
Flasks	pH initial	0.5 $g \cdot L^{-1}$	100	72.56	61.70	79.15
		1 $g \cdot L^{-1}$		36.22	39.93	34.00
		2.5 $g \cdot L^{-1}$		19.88	22.68	18.93
		5 $g \cdot L^{-1}$		11.40	13.65	9.26
	pH4	5 $g \cdot L^{-1}$		10.91	13.17	9.50
	pH9	5 $g \cdot L^{-1}$		13.44	13.49	9.92
	KOH		100	7.49	5.46	8.28
	FeCl₃		100	11.09	13.24	11.99
Columns	H/D: 20/2 (cm/cm)	50-50 v/v quartz sand to biochar (24 h)	10	0.01	0.13	
	H/D: 45/5 (cm/cm)	50-50 v/v quartz sand to biochar (24 h)	20	0.08	0.86	0.09

Table 19. % phenols adsorption in all experiments in flasks and columns

| | | Biochar dosage | Phenols concentration, $mg \cdot L^{-1}$ | Phenols adsorption, % | | |
| | | | | Adsorbent | | |
				Pe350	Sd350	PI350
Flasks	pHinitial	0.5 g·L⁻¹	100	36.75	31.25	41.00
		1 g·L⁻¹		36.75	40.75	34.75
		2.5 g·L⁻¹		50.00	57.00	47.50
		5 g·L⁻¹		57.30	68.50	46.50
	pH4	5 g·L⁻¹		54.60	65.90	47.50
	pH9	5 g·L⁻¹		67.40	67.50	49.75
	KOH	5 g·L⁻¹	100	37.50	27.50	41.50
	FeCl₃	5 g·L⁻¹	100	55.50	66.75	60.25
Columns	H/D: 20/2 (cm/cm)	50-50 v/v quartz sand to biochar (24 h)	10	85.96 (828 g·L⁻¹)	89.91 (79 g·L⁻¹)	
	H/D: 45/5 (cm/cm)	50-50 v/v quartz sand to biochar (24 h)	20	93.25 (236 g·L⁻¹)	96.05 (23 g·L⁻¹)	92.85 (215 g·L⁻¹)

Parentheses under the values of % phenols adsorption in Table 19 refer to the respective biochar concentration ($g \cdot L^{-1}$) needed to attain the displayed % adsorptions. Values of adsorbed phenols onto biochars in Table 18 show that in column experiments far bigger amount of biochar remains unexploited than in flask experiments. From the combined examination of the values displayed in both Tables 18 and 19, the ideal treatment of phenols solutions seems to be that in flasks and with 5 $g \cdot L^{-1}$ biochar concentration.

3.4. TG and DTG analysis

Fig. 29 shows the TG (weight loss) and DTG (weight loss rate) curves versus temperature, for Pe and biochars Pe350 and Pe550 (Figs. a and b, respectively) as well as for Sd and biochars Sd350 and Sd550 (Figs. c and d, respectively). The noise shown in some parts of the curves is due to instrumental difficulties. The total calculated weight loss decreases when pyrolysis temperature increases and reaches 73, 44 and 23% for Pe, Pe350 and Pe550 and 89, 49 and 43% for Sd, Sd350 and Sd550, respectively. A sharp weight loss is shown for Pe and Sd at the temperature range of 300-400 °C, while the weight loss is smooth for biochars produced at 350 and 550 °C. For PI and PI biochars (curves not shown), *Komnitsas et al. (2014)* also found the total weight loss to decrease with the increase of temperature from 86.3 (PI) to 41.7 (PI350) and 31.7 % (PI550). Similarly to Pe, Sd and their biochars, a sharp weight loss was shown for PI between 300 and 400 °C, while for PI350 and PI550 the weight loss is linear and smooth after 300 °C.

DTG curves in Figs. 1b and 1d show that the major weight loss was initiated at around 300 °C as also confirmed by the respective TG curves (Figs. 1a and 1c). In the DTG curve of Pe (Fig. 1b) two distinct peaks, typical for lignocellulose materials, are clearly shown. The first peak at around 300 °C represents the decomposition of hemicellulose which decomposes at 150-350 °C. The second peak at around 350 °C, which is also shown in the DTG curve of Sd (Fig. 1d), corresponds to the decomposition of cellulose which usually takes place in a relatively narrow temperature range of 275-350 °C. The gradual decomposition of lignin of Pe350, Pe550, Sd350 and Sd550 over a wider temperature range (usually at 275-500 °C) is represented by the flat section shown in Figs. 1b and 1d. Similar DTG curves (not shown) represented the decomposition of hemicelluloses and cellulose of PI in *Komnitsas et al. (2014)* study. They also found that biochar produced at temperature lower than 300 °C (PI250) was similar to Sd curve, while for biochars produced at higher temperatures (≥300 °C) the curves were similar to those of Pe350 and Sd350.
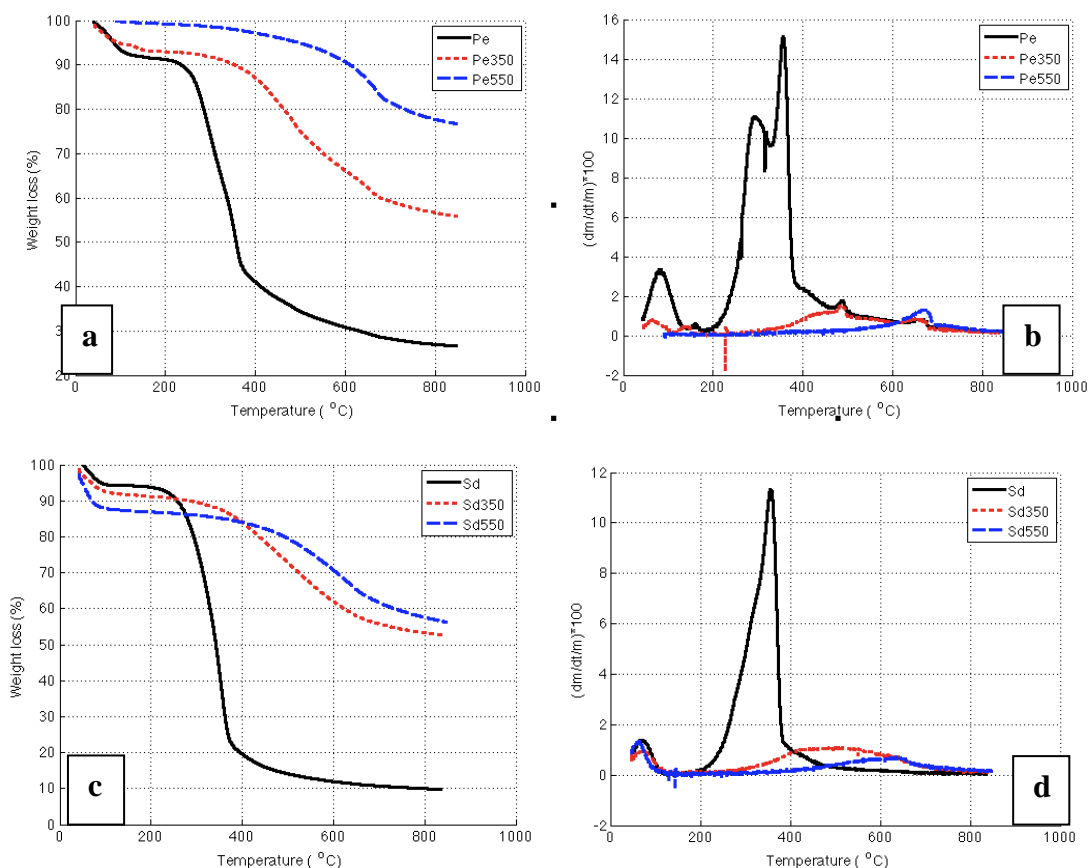
Fig. 29. TG and DTG curves versus temperature, for Pe and biochars Pe350, Pe550 (a and b) and Sd and biochars Sd350, Sd550 (c and d)

3.5. FTIR analysis

Feedstock materials Pe, Sd and PI as well as biochars Pe350, Pe550, Sd350, Sd550, PI350 and PI550 were characterized by FTIR spectroscopy. For brevity, only Sd phenol loaded biochars were examined in all experimental cases. Moreover, Pe20Phe and PI20Phe derived from column experiments were also examined. Fig. 30 concentrates all these FTIR spectra, while Figs. 31, 32 and 33 show in detail the spectra concerning Pe, Sd and PI respectively. The respective FTIR spectra band assignments are summarized in Table 20. The different energy absorption values indicate difference in aromaticity and amount of functional groups in biochar *(Purakayastha et al., 2015).* All feedstocks, (Pe, Sd and PI) spectra are characteristic of a generic oxygenated hydrocarbon due to their cellulose content. The presence of cellulose is also confirmed by XRD analysis, as reported below. As pyrolysis temperature increases FTIR spectra show a loss of chemical diversity, mainly for Pe and Sd (Fig. 30), compared to the raw materials and major bands disappear. The broad band seen for Pe, Sd and PI spectra at around 3400 was ascribed to the mixed stretching vibration adsorption of amino and hydroxyl groups (Figs. 31, 32, 33). This band disappears when feedstocks are pyrolyzed, indicating the absence of amino and hydroxyl content and increase of hydrophobicity of biochars, while it reappears for the SdA350-KOH but not for SdA350-FeCl$_3$ indicating the reformation of hydroxyl groups due to OH$^-$ derived from KOH (Fig 32). The peak at 3690 cm^{-1} appeared at loaded biochars of Pe (Fig 31), Sd (Fig 32) and PI (Fig 33) is attributed to stretching vibration of hydroxyl groups due to phenols adsorption. The respective peak 3722 cm^{-1} is observed for SdA350-KOH. The peaks at 2932, 2882 and 2900 cm^{-1}, shown only in Pe and Sd (Fig 31 and 32 respectively) and not in the respective biochars, are due to aliphatic C−H stretching vibration. For PI the respective bands 2850 and 2920 disappear at the PI350 spectra and reappear at the Pe550 spectra but slightly reduced, while for the phenols loaded biochars of column experiments Pe20Phe and PI20Phe irregularities in the spectra at this wave range are present (Fig 31, 33). The small band at 2398 cm^{-1} shown only in Pe20Phe and Sd spectras is due to the presence of atmospheric carbon dioxide. A near band for PI20Phe (2378 cm^{-1}) is also observed (Fig 33).
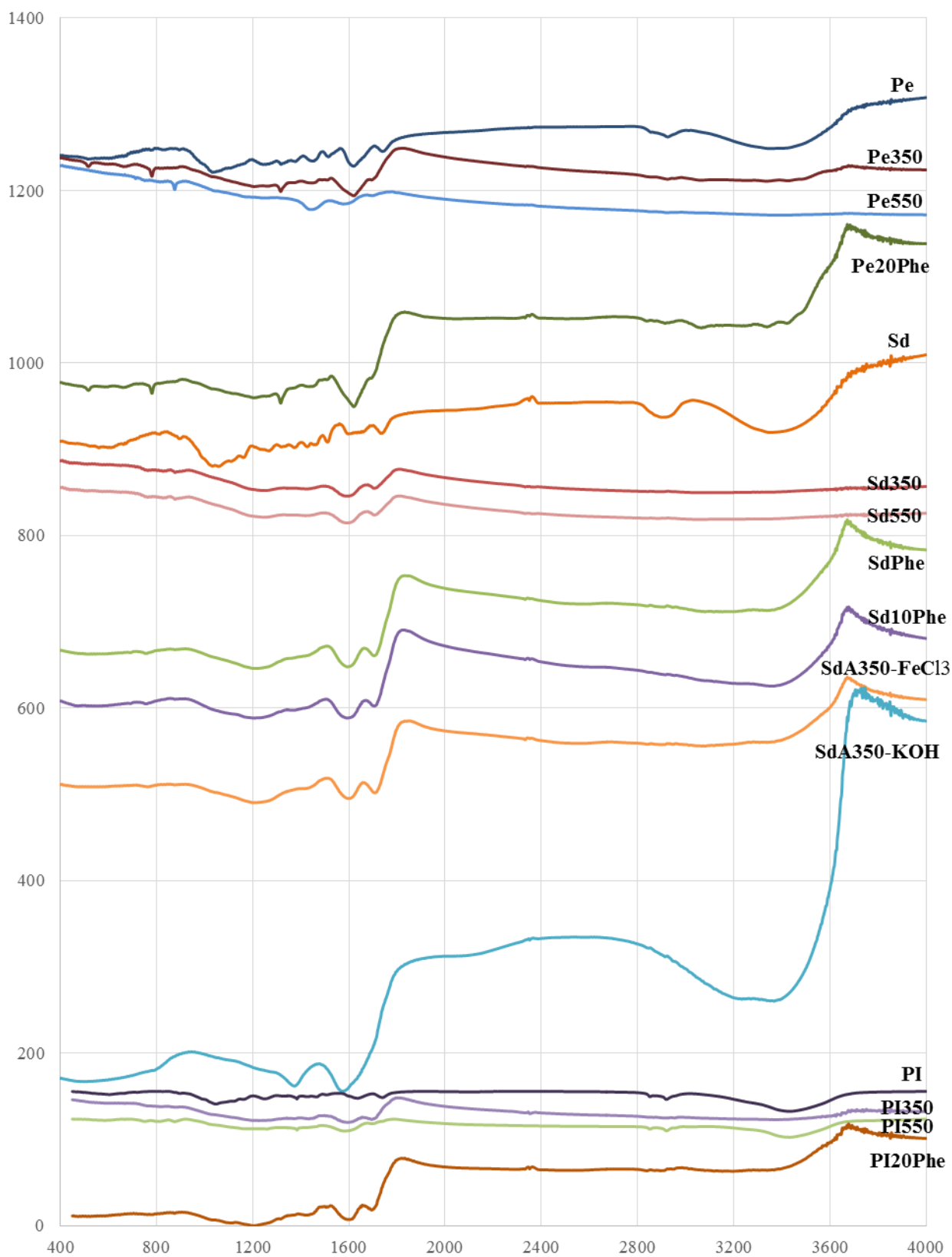
Fig. 30. FTIR spectra of feedstocks Pe, Sd and PI, biochars Pe350, Pe550, Sd350, Sd550, PI350 and PI550, loaded with phenols biochars
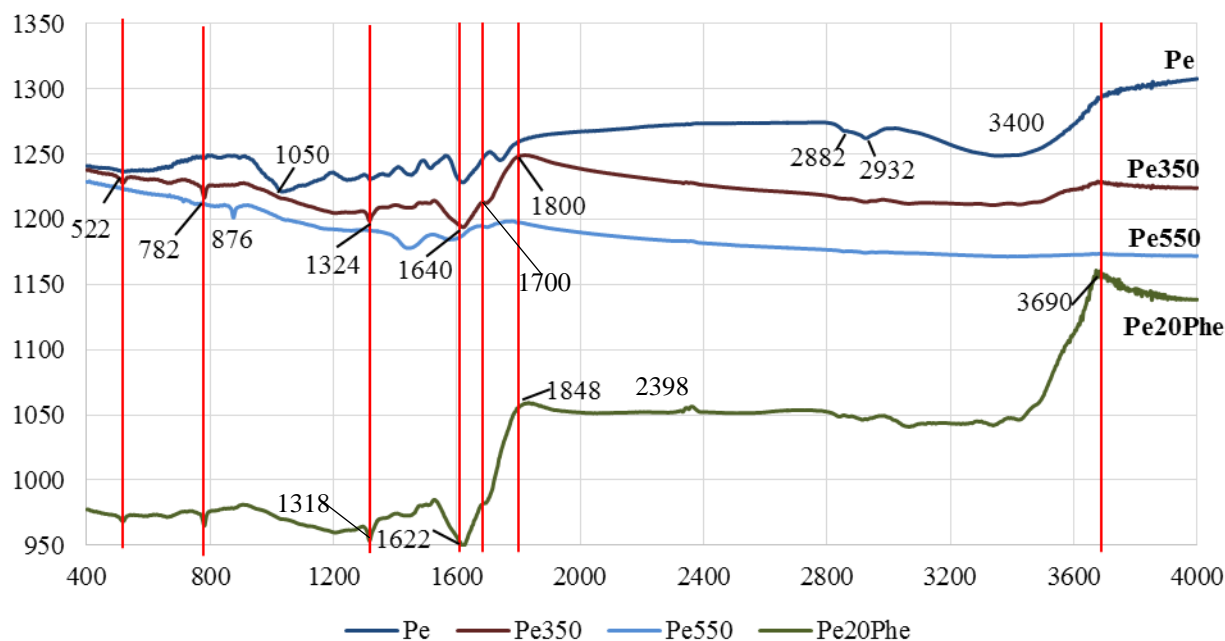
Fig. 31. FTIR spectra of feedstock Pe, biochars Pe350 and Pe550, loaded with phenols pecan shells biochar
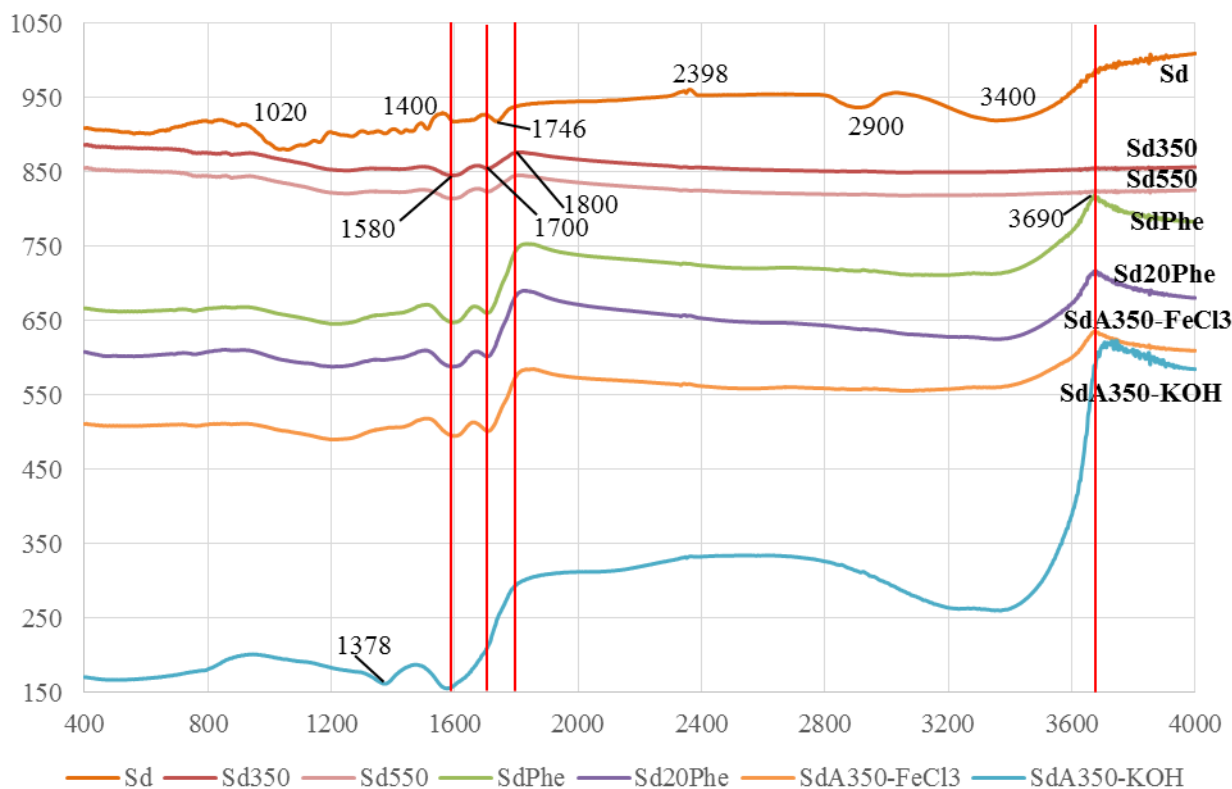
Fig. 32. FTIR spectra of feedstock Sd, biochars Sd350 and Sd550, loaded with phenols biochars in column and flask experiments

The band around 1700-1800 cm^{-1} shown in all spectra is attributed to ν(C=O) vibration in carbonyl group or the presence of carboxylic bonds. The intensity of these bands for Pe and PI biochars decreases slightly at higher temperatures due to the decomposition of carbonate compounds (Fig 31, 33). Moreover, these bands are slightly shifted and become more intence after phenols adsorption. The changes at this wave range indicate changes in carbonyl or carboxyl groups probably due to phenols

complexation with these groups. For SdA350-KOH the band 1700 completely disappears probably due to the erosive impact of KOH.
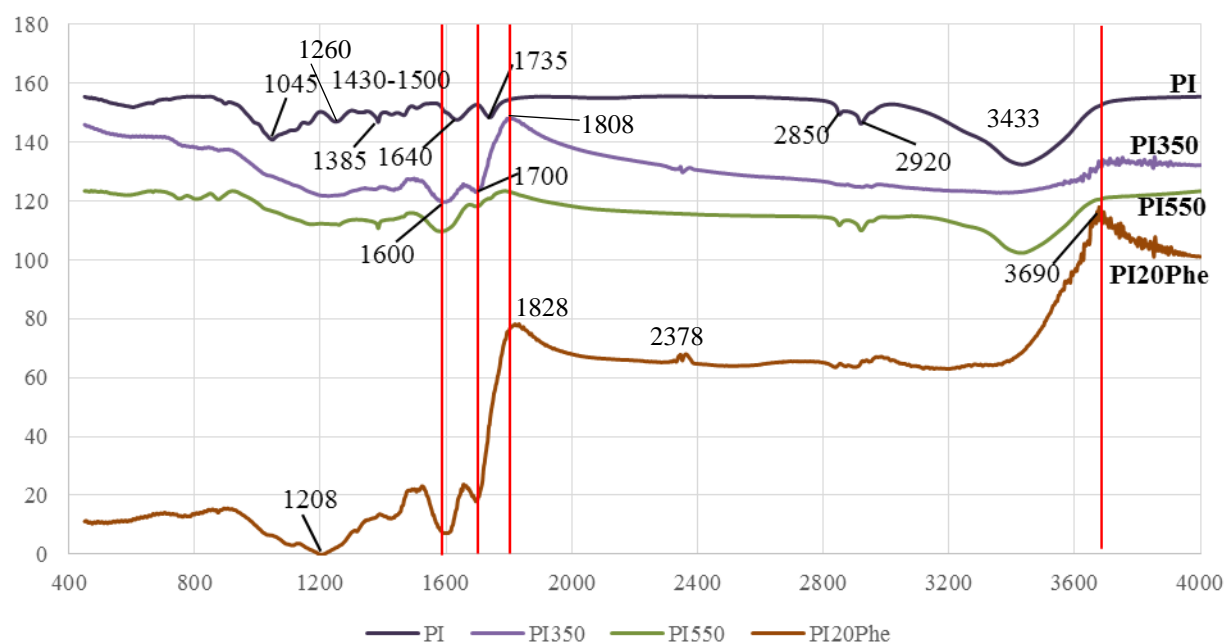
Fig. 33. FTIR spectra of feedstock PI, biochars PI350 and PI550, loaded with phenols biochar;

The bands ranging from 1580 to 1640 cm^{-1} seen in all spectra are due to the presence of aromatic C=O ring stretching (likely –COOH) or C=C stretching of aromatic groups in lignin. If carbonyl groups are in conjunction with aromatic ring peaks they are detected below 1700 cm^{-1}. The ratio of these peaks has been also found to reflect the degree of charring of cellulose *(Pastorova et al., 1994; Chen et al., 2011)*. The presence of these bands after pyrolysis implies the presence of residual lignin after decomposition. These bands are becoming more intence for all loaded biochars indicating greater amount of these functional groups. After phenols adsorption these bands are also shifted marginally to the lower (Fig. 31) or higher wave numbers (Fig. 32, 33) probably suggesting that chemical interactions or complexation occurred between the phenols and these groups on biochar surfaces. For SdA350-KOH the smoothing in the FTIR spectra between 1580 and 1700 cm^{-1} reveals the loss of C=O or C=C groups due to the erosive behavior of KOH. The characteristic group of peaks which appears at 1400-1500 cm^{-1} in raw materials Pe, Sd and PI, biochars and all the loaded biochars is attributed to phenolic O–H bending. The band at 1378 cm^{-1} for SdA350-KOH, 1385 cm^{-1} for PI and PI550 and the band at 1324 cm^{-1} for Pe350 which is moved at lower wavelength (1318 cm^{-1}) in Pe20Phe are attributed to δ(C=H) vibration in alkanes and alkyl groups or stretching vibration of the phenolic O−H or C−O of carboxylate anion. This band is weakly moved likely due to the coordination between these groups and phenols. It seems that for Sd350 the phenols adsorption involves the same bonds of phenols onto functional groups of biochar in all the experimental layouts except SdA350-KOH (Fig. 32). The band at 1260 cm^{-1}, which is seen in PI and disappears in PI350 and PI550, is attributed to C=C stretching. This band decreases with increasing temperature, as also shown by *CaO and Harris (2010)*. The intense bands occurring at 1020 and 1050 cm^{-1}, for Sd and Pe respectively, and bands at 1045 cm^{-1} for PI are characteristic of a C−C−O or C−O−C asymmetric stretch or due to aliphatic ether, alcohol C−O or aromatic stretching, O−H deformation vibrations or b-glycosidic bonds in cellulose and hemicelluloses. These peaks disappear in all biochars indicating the decomposition of hemicellulose and cellulose and are consistent with the results of elemental analysis (reduced O %). The band at 1208 cm^{-1} seen in PI20Phe is likely attributed to C−H bending in plane. Pe350 shows a small peak at around 782 cm^{-1} which is attributed to the aromatic and heteroaromatic compounds and is confirmed by C−H wagging vibrations. This band is remained after phenols adsorption in Pe20Phe. Pe, Sd, PI biochars and loaded biochars mostly for Pe and PI show peaks in the region 800-600 cm^{-1} also attributed to aromatic and heteroaromatic compounds. The intensity of these peaks increases for PI550 due to the stability of these compounds and possible cyclisation *(Komnitsas et al., 2014)*. *Angin et al. (2013)* attributed bands in this range to the presence of primary, secondary and tertiary alcohols, phenols, ethers and esters showing C−O stretching and O−H deformation vibrations. Pe350 shows also a small peak at 522 cm^{-1} due to −OH out of plane bending modes.

Table 20. FTIR spectra band assignments corresponding to Figs. 30, 31, 32, 33

Assignment		References
3722, 3690, 3433, 3400	Amino and hydroxyl groups (−OH) stretching	*[Yaman et al., 2004; Liu et al., 2013; Zhenyu et al., 2015]*
2932, 2920, 2900, 2882, 2850	Aliphatic C−H stretching vibration	*[Ghani et al., 2013; Angin & Şensöz, 2014; Purakayastha et al., 2015]*
2398, 2378	Atmospheric carbon dioxide	*[Socrates, 2001]*
1800, 1746, 1735, 1700	ν(C=O) vibration in carbonyl group or presence of carboxylic bonds	*[Sharma et al., 2004; Cao et al., 2010]*
1600-1580	Aromatic C=O ring stretching (likely –COOH) or C=C stretching of aromatic groups in lignin	*[Chen et al., 2011, Gray et al., 2014; Zhenyu et al., 2015; Purakayastha et al., 2015]*
1500-1400	C6 ring modes (phenolic O−H bending)	*[Ghani et al., 2013; Caglar et al., 2000; Purakayastha et al., 2015]*
1385, 1378, 1324	δ(C=H) vibration in alkanes and alkyl groups Stretching vibration of the phenolic O−H or C−O of carboxylate anion	*[Caglar et al., 2000]* *[Wang et al., 2011a]*
1260	C≡C stretching	*[CaO and Harris, 2010]*
1208	C−H bending in plane	*[Dokken et al., 2002]*
1050, 1045, 1020	Aliphatic ether, alcohol C−O or aromatic stretching peak, O−H deformation vibrations, b-glycosidic bond in cellulose and hemicellulose	*[Ghani et al., 2013]*
600- 800	C–H stretching vibrations	*[Angin & Şensöz, 2014; Purakayastha et al., 2014]*
522	−OH out of plane bending modes	*[Ghani et al., 2013]*

3.6. XRD analysis

The XRD patterns of Sd and biochars Sd350 and Sd550, are presented in Fig. 34 and are characterized by the elevated background between 16 to 26° 2-theta, due to the presence of organic matter. Similar XRD patterns are obtained for Pe, Pe350 and Pe550, while PI, PI300 and PI550 (Fig 35) exhibited a lower characteristic peak on their XRD patterns *(Komnitsas et al., 2014)*. In all raw materials (Pe, Sd and PI) the characteristic amorphous peaks of cellulose, which is one of the important structural components of the primary cell wall of green plants, are detected. However, after pyrolysis these peaks are quite lower and slightly shifted. PI XRD patterns also show a small peak attributed to thermonatrite, the naturally occurring evaporite mineral form of sodium carbonate as a result of atmospheric carbonation, while this phase is not present in biochars PI300 and PI550 due to the higher pyrolysis temperature *(Komnitsas et al., 2014)*.
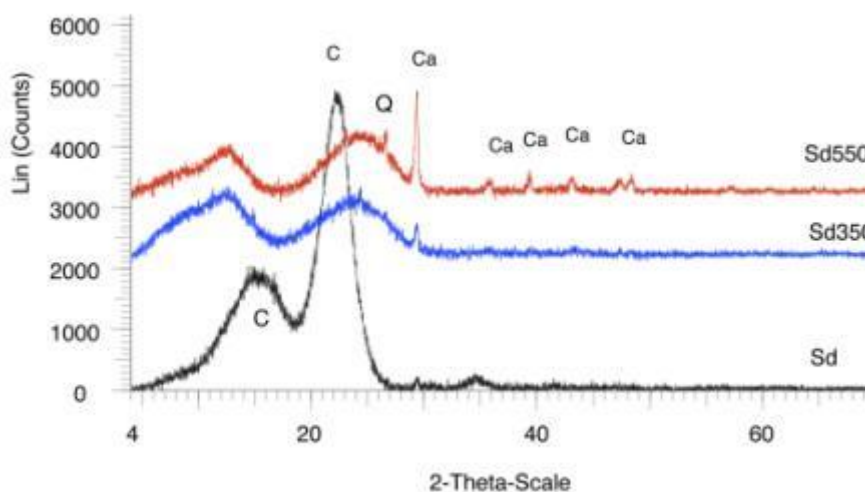
Fig. 34. XRD patterns of sawdust (Sd) and biochars Sd350 and Sd550 (C: cellulose $(C_6H_{10}O_5)_n$, Ca: calcite $CaCO_3$, Q: quartz SiO_2)
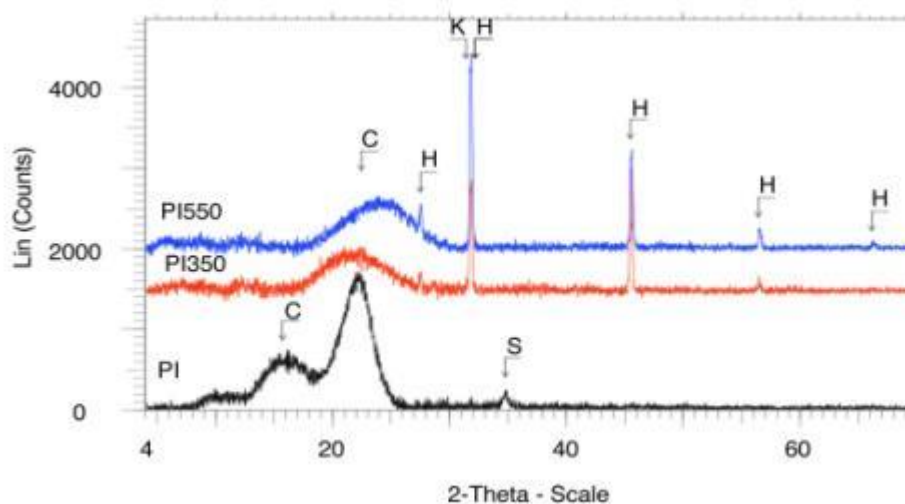
Fig. 35. XRD patterns of pistachio shells (PI) and biochars PI300, PI550 (C: cellulose $(C_6H_{10}O_5)_n$, H: halite (NaCl), K: kalicinite $(KHCO_3)$, S: thermonatrite $(Na_2CO_3H_2O)$) (Adapted from reference *Komnitsas et al. (2014)*)

The peaks of residual inorganic phases, calcite, quartz and halite in Pe, Sd and PI biochars, are more easily detected by XRD as a result of decomposition of organic phases in temperatures higher than 350 °C. The presence of calcite and quartz is due to impurities, such as atmospheric deposition of dust which may be present on trees as also reported elsewhere *(Houben et al., 2014),* while the presence of halite is due to residual salt that was not fully removed during PI soaking at the preparation stage prior to pyrolysis. The presence of kalicinite, detected in PI300 and PI550, improves the quality of biochar. Kalicinite, which is mainly formed in nature after decomposition of dead trees, is a highly soluble mineral phase and may be involved in a) release of K in soil when biochar is added as amendment and b) exchange of K with divalent ions if biochar is used as adsorbent.

3.7. SEM analysis

In Fig. 36 and 37, SEM backscattered electron images (BSI) of Pe and biochars Pe350 and Pe550 as well as of Sd and biochars Sd350 and Sd550 are shown, respectively. It is seen from Fig. 36 that the matrix of raw Pe is quite homogeneous. When Pe is pyrolyzed for the production of Pe350 a microporous structure is formed, due to the release of volatiles, with particle size varying between 7 and 18 μm. Increase of pyrolysis temperature from 350 to 550 °C also results in increased pore diameter and the development of new pores.
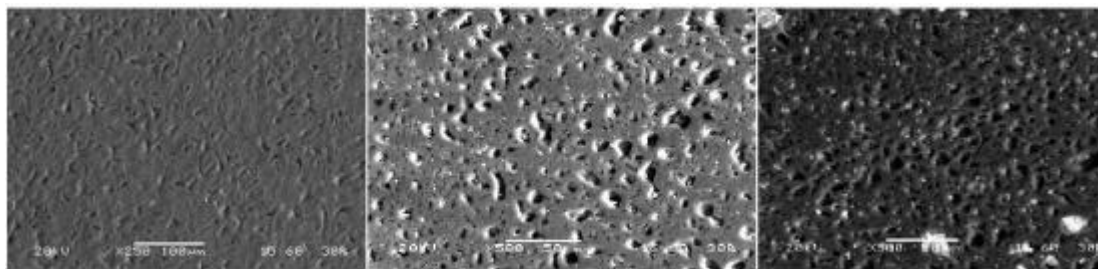
Fig. 36. SEM-BSI images of the Pe (x250), Pe350 (x500) and Pe550 (x500) structures (left to right)

According to Fig. 37, the fiber structure of Sd is slightly altered when pyrolysis takes place at 350 °C or 550 °C. The increase of pyrolysis temperature from 350 to 550 °C also increases pore diameter from 9-16 μm (micropores) to 21-48 μm (mesopores), respectively as a result of the continuous release of other high-molecular-weight volatiles. It is evident, that when the pyrolysis temperature is increased from 350 to 500 °C, very fine and oriented cellular mesopores with sharp and curvy edges are formed, suggesting clear development of pore structure.
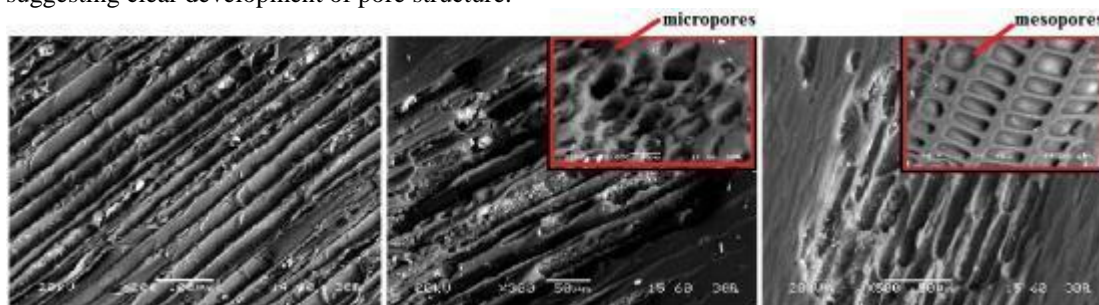
Fig. 37. SEM-BSI images of the Sd (x200), Sd350 (x300 and x2000) and Sd550 (x500 and x1000) structures (left to right)

On the other hand, SEM analysis of PI in *Komnitsas et al. (2014)* study showed that the matrix of PI is heterogeneous containing particles with varying size (27.5-228 μm), while after pyrolysis PI300 and PI550 exhibit some agglomeration revealing a distribution of macropores with varying size and shape between 51.9 and 565 μm. These macropores with a bigger size in biochars compared to PI enclose a network of irregularly scattered micropores in the surface due to the release of volatiles. If the pyrolysis temperature is further increased to 550 °C, a more homogenous matrix is obtained and the grain size becomes smaller and varies between 6.25 and 35.7 μm. This can be attributed to the decomposition of more volatile fractions that were not fully decomposed in temperatures below 500 °C.

4. Discussion

4.1. Feedstock and biochar characteristics

The pyrolysis yield of Pe, Sd and PI was found to decrease (e.g from 77 to 7.9 % for Sd) as pyrolysis temperature increases, more from 250 to 350 °C due to the destruction of the cellulose and hemicelluloses, and less from 450 to 550 °C due to condensation of aliphatic compounds and loss of volatiles CH_4, H_2 and CO *(Agrafioti, 2014)*. This trend is consistent with other researches' findings as seen in Table 21 and explains the decrease of volatile matter content and increase of char content with the increase of pyrolysis temperature as seen also in Table 21. *Agrafioti (2014)* also reported that different yields may be also attributed to ash content which prevents the loss of volatile matter. Volatile matter ranged from 23 to 35.7% for biochars produced at 550 °C, while lower values were reported by *Novak et al. (2009)* for biochars produced at 700 °C from pecan shells and poultry litter (10- 15%). Increase of pyrolysis temperature results also in increased char content ranging from 71.7 to 77 % at 550 °C in this study. The condensation of aliphatic-C structures at higher temperatures as *Manya (2012)* and *Deenik et al. (2010)* reported enhances the potential of biochar as soil amendment. The different degree of decrease in pyrolysis yield from 250 to 350 °C among biochars derived from different feedstocks is attributed to different lignocellulosic composition of the feedstocks (greater reduction for Sd and PI than for Pe biochars). In addition, Sd biochars showed lower pyrolysis yields than Pe and PI biochars for the entire temperature range, except for 250 °C, where Sd showed the highest pyrolysis yield. Increase of pyrolysis yield with the decrease of pyrolysis time, from77 to 7.9 % for Pe biochars and 74.2 to 21.7 % for Sd biochars for 60 min retention time instead of 92.1 to 28.7 %

and 90.8 to 18.3 % respectively with no retention time, is due to incomplete pyrolysis reaction at lower retention time *(Agrafioti, 2014)*.

pH as well as EC were found to increase slightly as pyrolysis temperature increases. pH was acidic to neutral for all feedstocks and biochars produced; 4.9- 6.9 for Pe and Pe biochars, 3.8- 6.6 for Sd and Sd biochars, 4.3- 7.2 for PI and PI biochars. EC of PI and PI biochars ranged from 7.7 to 29.7 mS·cm^{-1}, while the other feedstocks and biochars ranged from 0.18 to 0.46 mS·cm^{-1} similarly to results of *Srinivasan and Sarmah (2015)* (Table 21). This trend in pH and EC change has been also observed by other researchers (Table 21) while when biochars are produced from maize stover, pearl millet stalk, rice and wheat straw, leaves and pomelo peel pH values can be as high as 11 *(Purakayastha et al., 2015, Dai et al., 2013)*. *Liu et al. (2012)* correlated this trend also to the type of feedstock and the retention time. *Ding et al. (2014)* attributed the pH increase to alkali salts accumulation during pyrolysis, as increase of pyrolysis temperature for bagasse biochar production increased substantially mineral elements (Na, K, Ca, Fe, Mg) concentration. Finally, it can be deduced that biochars produced from pyrolysis at approximate 350 °C may be used as additives in alkaline soils, while biochars produced at approximate 550 °C may be applied in acidic soils as soil amendment.

Carbon content also increased as pyrolysis temperature increased reaching 77.3 % for PI550 followed by Pe550 (76.4 %) and Sd550 (68 %), while the hydrogen content indicated the opposite trend; from 5.4 to 1.9, 5.8 to 1.5 and 6 to 2.1 % for Pe, Sd and PI feedstocks and the respective biochars. Carbon and hydrogen contents of the biochar used in this study are in conformity with those reported for biochars produced from peanut shells, pine chips, maize stover, pearl millet stalk, rice and wheat straw etc (Table 21). *Purakayastha et al. (2015)* and *Sanchez et al. (2009)* found sulfur traces (~0.2 %) in biochars (Table 21), while for all biochars used in this study, the sulfur content was below the detection limit and thus they could be used in adsorption and purification processes. Nitrogen content was almost stable with the increase of pyrolysis temperature for Pe, Sd and PI biochars and values recorded in this study are similar to those mentioned by other researches (Table 21). Oxygen content was found to decrease with the increase of temperature as expected, from approximate 40 % to approximate 20 % for all biochars produced, while those reported from other researchers were lower for all temperatures ranging from 29 to 6 % (Table 21). As far as feedstocks used in this study are concerned, they were found to have similar characteristics with other feesdtocks shown in Table 21.

All feedstocks (Pe, Sd and PI) spectra are characteristic of a generic oxygenated hydrocarbon due to their cellulose content. The presence of cellulose is also confirmed by XRD analysis. For Pe, Sd and PI amino and hydroxyl groups, aliphatic C−H stretching vibration as well as phenolic O–H bending were observed. Moieties characteristic of a C−C−O or C−O−C asymmetric stretch or due to aliphatic ether, alcohol C−O or aromatic stretching, O−H deformation vibrations or b-glycosidic bonds in cellulose and hemicelluloses or even phenols or esters were also observed for raw materials. Aromatic and heteroaromatic compounds were observed as well. For PI δ(C=H) vibration in alkanes and alkyl groups or stretching vibration of the phenolic O−H or C−O of carboxylate anion, as well as C=C stretching were observed. In all spectra, ν(C=O) vibration in carbonyl group or carboxylic bonds, as well as aromatic C=O ring stretching (likely –COOH) or C=C stretching of aromatic groups in lignin were found. As pyrolysis temperature increases FTIR spectra, mainly for Pe and Sd biochars, show a loss of chemical diversity compared to the raw materials and major bands disappear. Hydroxyl groups disappear when Pe and Sd are pyrolyzed, indicating the absence of hydroxyl content and increase of hydrophobicity of biochars. On the other hand, for PI the respective band disappears in low temperature biochar, while reappears in high temperature biochar, though slightly reduced. For Pe and Sd aliphatic C−H stretching vibration disappear with the raise of temperature, while for PI the respective bands are present to the higher temperature produced biochars as well but slightly reduced. C=C stretching, C−C−O or C−O−C asymmetric stretch or aliphatic ether, alcohol C−O or aromatic stretching, O−H deformation vibrations or b-glycosidic bonds in cellulose and hemicelluloses, all disappear in all biochars indicating the decomposition of cellulose and hemicellulose. Moreover, the intensity of ν(C=O) vibration in carbonyl group or the carboxylic bonds decrease slightly for Pe and PI higher temperature biochars due to the decomposition of carbonate compounds.

Table 21. Characterization of biochars derived from various feedstock materials

	Material	Heating rate, °C·cm^{-1}	Pyrolysis time, h	Feedstock	Biochar 250- 350 °C	Biochar 350- 450 °C	Biochar 450- 550°C	Biochar 550- 700 °C	Reference
y_p, %	Pistachio nut, Reed, Fishscale bamboo, Sugarcane bagasse	10	1-2		32- 77	31- 32-50	28-32	17- 30	Komnitsas et al., 2014; Dai et al., 2013; Ding et al., 2014; Purakayastha et al., 2015; Zhongmin Dai et al., 2013
EC, mS·cm^{-1}	Pistachio nut, Maize stover, Pearl millet stalk, Rice, Wheat straw	10	1/2, 1	7.7	13- 22	3.84- 22	26- 30		Komnitsas et al., 2014 ; Purakayastha et al., 2015 Srinivasan and Sarmah (2015)
	Greenwaste (leaves, grass clippings, twigs and plant prunings.), Corncob, Pinus radiata sawdust		1/3		0.17	0.09	0.18	1.57-4.63	
pH	Pecan shell, Peanut hull, Pistachio nut, , Sugarcane Bagasse, Coniferous & Hardwood chips, Greenwaste (leaves, grass clippings, twigs and plant prunings.), Corncob, Pinus radiata sawdust, Maize stover, Pearl millet stalk, Rice , Wheat straw	10	1/3-1/2, 1-2, 36	4.3	4.7- 5.9	5.8- 10.7	6.7- 8.6	7.1- 9.7	Jeffrey et al., 2013; Komnitsas et al., 2014; Ding et al., 2014 ; Rees et al., 2014; Srinivasan and Sarmah, 2015;
	Reed, Water canna, Fishscale bamboo, Ravenna grass, Yalan leaf, Palm leaf, Weaner manure, Sow manure, Pineaple peel, Pomelo peal				7-8.9		8.1-11.23		Purakayastha et al., 2015; Zhongmin Dai et al., 2013
Eh, mV	Pistachio nut	10	1		111- 135	19- 111	-6- 19		Komnitsas et al., 2014
% C	Pistachio nut, Peanut hull, Pecan shell, Safflower seeds, Rape, Sunflower, Coniferous & Hardwood chips, Pine chips, Greenwaste (leaves, grass clippings, twigs and plant prunings.), Corncob, Pinus radiata sawdust Maize stover, Pearl millet stalk, Rice, Wheat straw	10- 30	1/60, 1/3, 1-2	44- 50	54- 65	60- 78	62- 82	63- 91	Komnitsas et al., 2014; Jeffrey et al., 2013; Angın et al., 2013; Sanchez et al., 2009; Rees et al., 2014; Gaskin et al., 2008; Srinivasan and Sarmah, 2015; Purakayastha et al., 2015; Zhongmin Dai et al., 2013
% H	Pistachio nut, Safflower seeds, Rape, Sunflower, Greenwaste (leaves, grass clippings, twigs and plant prunings.), Corncob, Pinus radiata sawdust	10- 30	1/60, 1/3	6- 7	3- 5	2- 3.28	0- 2.83	1.31-2.15	Komnitsas et al., 2014; Angın et al., 2013; Sanchez et al., 2009; Zhongmin Dai et al., 2013

Table 21. Characterization of other biochars derived from various feedstock materials (continued)

	Feedstock								References
% N	Pistachio nut, Peanut Hull, Pecan shell, Safflower seeds, Rape, Sunflower, Coniferous & Hardwood chips, Maize stover, Pearl millet stalk, Rice , Wheat straw, Greenwaste (leaves, grass clippings, twigs and plant prunings.), Corncob, Pinus radiata sawdust	10- 30	1/60, 1/2, 1/3	0- 3	0-1	0- 3	0- 4	0- 2	*Komnitsas et al., 2014; Jeffrey et al., 2013; Angın et al., 2013; Sanchez et al., 2009; Zhongmin Dai et al., 2013; Rees et al., 2014; Srinivasan and Sarmah, 2015; Purakayastha et al., 2015*
% O	Greenwaste (leaves, grass clippings, twigs and plant prunings.), Corncob, Pinus radiata sawdust, Maize stover, Pearl millet stalk, Rice , Wheat straw		1/2, 1/3		29.3	25.4-29.6	19.8	6.1-8.1	*Srinivasan and Sarmah, 2015; Purakayastha et al., 2015*
% S	Rape, Sunflower, Maize stover, Pearl millet stalk, Rice , Wheat straw	30	1/2, 1/60	0- 1		0.05-0.29			*Sanchez et al., 2009; Zhongmin Dai et al., 2013; Purakayastha et al., 2015*

4.2. Heavy metal adsorption

The adsorption of Cu, Pb, Cd and Co increased rapidly within the first 30 min with most of metal ion removal occurring within 2 h (95.9, 85.6 and 82.1 % of Pb adsorption by 5 and 1 $g \cdot L^{-1}$ of Pe350 and by 5 $g \cdot L^{-1}$ of Sd350 respectively) due to the large number of vacant adsorption sites which eventually become saturated with time; adsorption continues up to 24 h due to slow migration of heavy metal into biochar pore spaces *(Ding et al., 2014)*. Similar trend was observed for Pb adsorption onto bagasse biochar accounting for 51- 81 % up to 2 h *(Ding et al., 2014)*, while more time (12 h) was reported for the adsorption of 78.1% of Pb by peanut shell biochar *(Wang et al., 2015)* indicating the different kinetics of Pb adsorption onto different biochars. In this study, the pseudo-second-order kinetic model fits the heavy metals adsorption data better (almost all R^2 = 0.999-1) than the pseudo-first-order kinetic model (R^2 = 0.438- 0.995) except for Pb adsorption onto 0.1 $g \cdot L^{-1}$ Sd350 where R^2 was higher (R^2 =0.999) than that of pseudo-second-order kinetic model indicating the slower adsorption when the adsorbent concentration is low. Similarly, other researchers *(Ding et al., 2014; Wang et al., 2014; Elaigwu et al., 2013; Zhang et al., 2013)* also found that the pseudo-second-order kinetic model fits Pb and Cd adsorption data (R^2 >0.99) better than the pseudo-first-order kinetic one (0.82- 0.96), when they used prosopis Africana shell, peanut shell and bagasse biochars. Thus, the adsorption mechanism is chemical adsorption that involves chemical bonding between divalent metal ions and polar functional groups present on the adsorbent *(Elaigwu et al., 2013)* in all cases except the Pb adsorption onto 0.1 $g \cdot L^{-1}$ Sd350. Oxygen-containing functional groups, namely carboxyl (R−COOH) and alcoholic or phenolic hydroxyl groups (R−OH) are the main groups contributing to coordination between heavy metals and the sorbent surface. Moreover, it seems that the reaction rate is proportional to the number of active sites (functional groups) present on the adsorbent surface *(Mohan et al., 2011)*. *Ding et al. (2014)* assigned the Pb adsorption onto bagasse biochar pyrolyzed at 250 °C to hydroxyl, carboxyl and ether which exist on biochar and bound with Pb through complexation and cation exchange. *Lu et al. (2012)* found up to 42 % of the total sorbed Pb was removed due to hydroxyl and carboxyl functional groups and up to 61 % due to complexation with mineral surfaces. In this study, functional groups like the above mentioned are present in all biochars, viz Pe350, Sd350 and PI300 as the FTIR analysis revealed, and thus the respective interactions are all possible.

As *Wang et al. (2014)* reported, adsorption can be also affected by the released anions (e.g., PO_4^{3-} and CO_3^{2-}) from minerals in biochars which can precipitate with heavy metal cations. The XRD analysis in our study revealed the presence of calcite ($CaCO_3$) which due to acidic solution may be dissociated to Ca^{+2} and CO_3^{-2} and form new precipitates with the divalent metal ions such as $PbCO_3$ and $Pb_3(CO_3)_2(OH)_2$ *(Lu et al., 2012)*. Cation exchange mechanism of Pb adsorption onto low temperature biochar was confirmed by the parallel release of cations Ca, Na and K in *Ding et al. (2014)* study. The same researchers also reported that biochars owe 5.8- 9.7% of their sorption capacity to their high P content, if so, through Pb-P co-precipitation. As *Agrafioti et al. (2014)* claimed, the main mechanisms regarding heavy metal removal from aqueous solutions were electrostatic interactions between biochar negative surface charge and metal cation as well as metal precipitation for the case of anionic metal. The higher carbon content found in biochars produced at higher temperatures is also believed to contribute to biochars higher heavy metal adsorption capacity *(Sarmah, 2015; Komnitsas et al., 2014; Dai et al., 2013; Cao and Harris, 2010)*. In others researches *(Uchimiya et al., 2010; Wang et al., 2015)*, coordination of Pb^{2+} with p electrons (C=C) of carbon is referred as a possible mechanism of Pb^{2+} sorption. Fig. 38 illustrates all the potential mechanisms proposed in this research.

If biochars are produced at higher temperatures (e.g. 500 °C) the intraparticle diffusion through pore spaces is assumed to mainly determine Pb adsorption *(Cao and Harris, 2010; Dai et al., 2013; Komnitsas et al. 2014; Sarmah 2015)*. *Han et al. (2013)* agreed that the pore structure is not the sole determining factor of heavy metal adsorption as many heavy metal ions (Zn^{+2} and Cu^{+2}) accumulated on the surface of the samples but not deep within the pores as expected (SEM analysis); *Agrafioti (2014)* reported that rice husk biochar exhibited the lower heavy metal (As^{+5}, Cr^{+3}, Cr^{+6}) adsorption among other adsorbents despite its higher surface area.

pH before and after adsorption experiments are comparable and it can be assumed that solution pH variation did not have a significant impact on heavy metal adsorption mechanisms. Slight reduction in pH is attributed to H^+ release after coordination between functional groups (COOH or OH) with metal ions *(Wang et al., 2014)*. Eh and EC where not found to differ notably as well. However, greater Eh is probably related to higher heavy metal adsorption capacity.

Results indicated monolayer adsorption of Pb onto Pe350 (Langmuir model best fitted data), while laminate adsorption of Cd onto Sd350 (Freundlich model fitted best data) which indicate heterogeneous energetic distribution of active sites, accompanied by interactions between adsorbed

ions. On the other hand, monolayer adsorption of Cu or Co onto Sd350 was observed. *Agrafioti (2014)* found the Freundlich model to better fit the data confirming the heterogenous surface of biomass and consequently of biochar.
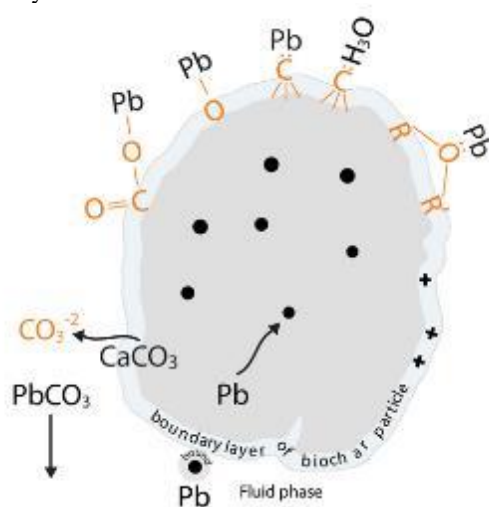

Fig. 38. Schematic representation of heavy metal (Pb) adsorption onto biochar

In general, the higher the adsorbent concentration, the higher is the % adsorption of heavy metal. The same behavior was reported in a previous study of *Komnitsas et al. (2014)* when Pb and Cu (15-150 mg·L^{-1}) adsorption onto PI300 and PI550 (1- 10 g·L^{-1}) was examined. Irregularities in the proportion of adsorbent concentration and % adsorption indicate that beside the fact that the number of adsorption sites plays a predominant role in adsorption of heavy metals, it is not the only one. In all cases, the higher the adsorbent concentration the lower is the adsorption rate, despite the fact that the higher the adsorbent concentration the higher is the % adsorption. The same trend was also reported by *Komnitsas et al. (2014)* who found the adsorption rate to increase with the increase of heavy metal concentration despite the fact that the higher the heavy metal concentration the lower the % adsorption. These results show that as the adsorbent concentration increases, the amount of heavy metal adsorbed on biochars increases (increased % adsorption) but with much reduced adsorption rate. In addition, as the heavy metal concentration increases, the bonds are created with increased adsorption rate, but the competition of metal ions to be attached onto biochars prevents intraparticle diffusion of ions because of metal ions boundaries and thus reduced metal bonds onto biochars are formed (decreased % adsorption). *Wand et al. (2014)* concluded that apart from intraparticle diffusion, transfer of Pb^{2+} from fluid phase to biochar particles across its own boundary layer could also affect sorption. Adsorption rates recorded in this study are comparable to those recorded in *Komnitsas et al. (2014)* study for adsorbent concentration 1 g·L^{-1}; 2.91 and 1.54 mg·g^{-1}·h^{-1} were recorded for Pe350 and Sd350 (100 mg·L^{-1} adsorbate concentration), while around 1.2 mg·g^{-1}·h^{-1} was recorded for PI300 (70 mg·L^{-1} adsorbate concentration). A lower adsorption rate (7.5 mg·g^{-1}) was reported in *Elaigwu et al., (2013)* study when prosopis Africana shells biochar produced at 350 °C was used for Pb adsorption explained by its lower initial Pb concentration (10 mg·L^{-1}). However, the last authors observed proportional relationship between adsorbed amount of metal ions and the amount of adsorbent used, probably due to the nature of biochar and its structure. Both Pe350 and Sd350 seem to adsorb more effectively Pb and Cd than Cu and Co. Similarly, in *Komnitsas et al., (2014)* study, Pb is adsorbed more efficiently compared to Cu onto PI, PI300 and PI550. Pb exhibited the maximum % adsorption and is much better removed by pecan shell biochar compared to the next highest adsorption onto sawdust biochar at 1 and 5 g·L^{-1} adsorbent concentrations (74.5 and 98.5 % adsorption for Pe350 compared to 35 and 72.5 % adsorption respectively for Sd350). Regarding Cu, Cd and Co they seem to be better adsorbed onto sawdust biochar. It is worth mentioning though that the adsorption rate of Pb onto Pe350 is far lower than those calculated for the other heavy metals' onto both 0.1 g·L^{-1} biochars because of the competition of Pb ions, with the higher ionic radius among all heavy metals examined in this study, to be attached onto biochars. The 0.5 g·L^{-1} adsorbent concentration seems to be crucial for the best adsorption rate of Pb onto Pe350, while for the other combinations of heavy metals and biochars the crucial adsorbent concentration maybe 0.1 g·L^{-1} or less.

4.3. Desorption studies

Both biochars, Pe350 and Sd350 can adsorb Pb or Cu (100 mg·L^{-1}) at an approximate percentage of 90 to 97 % or 11 to 35 % respectively. Nearly the same percentage of Cu was adsorbed onto both biochars and Pb onto Sd350 during the two adsorption cycles, while Pe350 indicated Pb adsorption around half of the first adsorption. Pb is desorbed more effectively from Sd350 than from Pe350 regardless the desorption treatment. *Ding et al. (2014)* explained that irreversible Pb adsorption onto bagasse biochar was due to trapped Pb inside the pore spaces. On the contrary, Cu is desorbed more effectively from Pe350 than from Sd350, indicating that the % heavy metal desorption is related to the structure of biochars and nature of heavy metal adsorbed and not to the desorption solution. After 24 h of desorption, using 0.1 M HNO$_3$, Pe350 showed the lowest desorption (63.3 %). For the rest, when 0.1 M HCl was used for Pb desorption from Pe350 and both desorption agents for Pb and Cu desorption from Sd350 and both biochars respectively, desorption ranged from 73.5 to 100 %. The adsorption capacities revealed that Sd350 is a better adsorbent to reuse compared with Pe350 (e.g. 35.6 and 16mg of Pb per g of Sd350 and Pe350 respectively both under HNO$_3$ treatment, while the initial adsorption capacity was similar for the two biochars; 17.7 and 16.9 mg·g^{-1} respectively). From an environmental perspective, the low desorption could mean immobilization of heavy metals in waters without the need of removing biochar from the ecosystem. However, Pe350 and Sd350 do not seem to be appropriate for removing Pb or Cu from an aquatic system in this way. Moreover, the possibly contaminant release due to the mineral content of biochars needs to be examined when biochars are used, although *Zhand et al. (2013)* found acceptable release of Cu, Cr, Ni, Zn or Pb ($\leq$0.05 mg·L^{-1}) when they are applied on wastewater treatment.

4.4. Phenols adsorption

Rapid increase of phenols adsorption in flasks was observed within the first 6 h due to the large number of vacant adsorption sites which become saturated with time up to 48 h due to slow migration of phenols into pore spaces present inside the biochars. Most phenols removal occurred within 24 h accounting for 67.4 to 98.6 %, while for pentachlorophenol removal an equilibrium time of 2 h was observed when switchgrass and woody biomass were used for biochar production (500 °C); 70 % of adsorption achieved within the first minute *(Han et al., 2013)*. This huge difference in equilibrium time is probably assigned to the easier dissolving of pentachlorophenols (pKa= 4.75) in water compared to phenols (pKa= 9.98) as the larger the value of pKa, the smaller is the extent of dissociation at any given pH (Henderson–Hasselbalch equation). The highest % adsorption was shown for 5 g·L^{-1} SdPhe at 48 h, namely 70 %, followed by PIPhe for 2.5 and 5 g·L^{-1} adsorbent concentration at 48 h, namely 62 and 54 % respectively. A similar % adsorption (76.4 %) but only just after 30 min has been recently observed for 3 g·L^{-1} pomelo peel biochar when 100 mg·L^{-1} phenols solution was used *(He and Chen, 2014)*. Higher adsorbent concentrations result in increased % phenols adsorption. This behavior is mostly observed for PePhe and SdPhe for 24 h (% phenols adsorption increase from 37 to 57 % and 31 to 69 % respectively), while this is not observed for PIPhe.

The pseudo-second-order kinetic model fit the data better than the pseudo-first-order kinetic model, with R^2 values higher than 0.956 with the most of them to be higher than 0.99, indicating chemical bonding between ionic phenols and polar functional groups on the adsorbent and that the reaction rate is proportional to the number of active sites (functional groups) present on the adsorbent surface. The different contact time needed for equilibrium for heavy metals (24 h) and phenols (48 h) shows that different adsorbates involve different combinations of adsorption mechanisms onto biochars (e.g., ion exchange, precipitation, physical adsorption, complexation and intraparticle diffusion). Combination of micropore surface area, pore structure and functional groups, rather than the specific surface area alone are the dominant factors that significantly impact adsorption of phenols *(Han et al., 2013; Mathialagan and Viraraghavan, 2009; Qiu et al., 2009)*. The phenols adsorption was also found to be physical and transient in nature and eliminated by heating and storage, while if the pore structure of biochars is similar, the carboxylic, lactonic and phenolic groups play a more prominent role due to the ionization state of the available functional groups at neutral pH *(Han et al., 2013)*. *Mathialagan and Viraraghavan (2009)* reported that among the surface functional groups present on the fungal biomass, carboxyl, amide and hydroxyl groups seem to have played a role in pentachlorophenols biosorption and also reported that most of the pentachlorophenols were irreversibly bound to the biomass. Regarding isotherms, neither Langmuir nor Freundlich isotherms were found to fit phenols adsorption data in this study. However, *Han et al. (2013)* found the Freundlich isotherm to be a better representation for phenol adsorption for all biochars produced at 500 °C from switchgrass, hardwood and softwood with R^2 values ranging from 0.981 to 0.997.

For all the adsorbent materials, the adsorption rate of phenols increases with decreasing adsorbent concentration. This result showed that as the adsorbent concentration increases, the amount of phenol bonds on biochars increases (increased % adsorption) but with much reduced adsorption efficiency as also mentioned in a previous section. A similar trend was also observed in *Lang et al. (2014)* when they used wheat straw and peanut hull biochars for the removal of pentachlorophenols from aqueous solution. In this study, the highest adsorption rate was 3.3 followed by 3.02 and 2.57 mg·g^{-1}·h^{-1} for PIPhe, PePhe and SdPhe respectively, at 0.5 g·L^{-1} biochar concentration, while for 5 g·L^{-1} biochar concentration the adsorption rate was 0.39, 0.48 and 0.57 mg·g^{-1}·h^{-1} respectively. *Han et al. (2013)* found adsorptive capacities above 100 mg·g^{-1} (>4.17 mg·g^{-1}·h^{-1}) when examined phenols (200-2000 mg·L^{-1}) adsorption onto 10 g·L^{-1} biochars from switchgrass, hardwood and softwood pyrolyzed at 500 °C for 1 h. This probably means that biochars pyrolyzed at higher temperatures adsorb more effectively phenols or simply that higher initial pollutant concentration results in higher adsorption rate onto biochar. For the 1, 2.5 and 5 g·L^{-1} biochar concentration used in this study, the adsorption rate of phenols is higher for SdPhe, followed by PePhe and subsequently PIPhe, thus completely different behavior than at 0.5 g·L^{-1} biochar concentration is shown. This is probably correlated to the different surface and pore structure of the three biochars as it is deduced from SEM analysis; Pe350 and Sd350 characterized by a microporous structure, while the PI300 by a macroporous structure maybe revealing the priority of phenols to penetrate into pore spaces. Moreover, increase in pH was observed for all adsorbents and adsorbent concentrations (maximum increase from 6.69 to 8.35 for PePhe at adsorbent concentration 0.5 g·L^{-1}). It is worth mentioning, however, that the higher the adsorbent concentration the lower the increase of pH for PePhe and SdPhe, while the higher the adsorbent concentration the higher is the increase of pH for PIPhe. These results combined with the calculated adsorption rates demonstrate probably the priority of PePhe and SdPhe to bind H$^+$ and subsequently to bind phenols probably explaining also the longer time needed for equilibrium concentration as discussed above. From an environmental perspective, the biochars not only can be used for phenols removal from solutions, but also for pH amelioration.

The distribution of molecular and ionized phenols varies as the solution pH is altered. Phenol is a weak acid and at high pHs gives the phenolate anion C$_6$H$_5$O$^-$ (also called phenoxide) (Fig. 39) *(Smith and Jerry, 2007)*. The alteration of initial solution pH did not affect phenols adsorption in this study, but did affect pentachlorophenols adsorption onto fungal biomass when pH was altered to be higher than pKa (4.75) *(Mathialagan et al., 2009)* indicating that an increased pH over phenols pKa (9.98) would probably also result in different (reduced) % phenols adsorption because of the less hydrophobic nature of ionic form of phenols present in these pHs *(Lazo-Cannata et al., 2011; Mathialagan and Viraraghavan, 2009). Lazo-Cannata et al. (2011) f*ound that the adsorption capacity of phenolic compounds onto carbon nanospheres prepared from benzene (C$_6$H$_6$) pyrolysis (CNS) was very influenced by the acidity of the solution. It is also reported that the addition of inorganic salts affected (NaCl) the removal of phenolic compounds from carbon nanospheres prepared from benzene (C$_6$H$_6$) pyrolysis (CNS) *(Lao-Cannata et al., 2011)*, while did not affect (NaCl, Na$_2$SO$_4$, NaNO$_3$, CaSO$_4$, MgSO$_4$) the removal of pentachlorophenols from aqueous solutions *(Mathialagan and Viraraghavan, 2009)*.
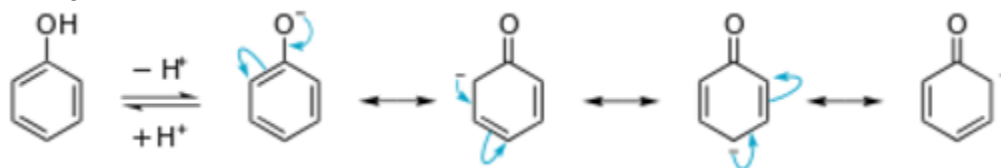
Fig. 39. Formation of phenoxide anion in aqueous solution

Adsorption via acid–base interaction and hydrogen binding between phenol and the functional groups was proposed to explain the process *(Liu et al., 2011)*. Moreover, it has been widely documented that hydrophobic organic contaminants adsorption on biochars was heavily dependent on its high surface area via pore-filling mechanism *(Ji et al., 2011; Zhang et al., 2013). Peng et al. (2016)* summarized that hydrophobic partition, pore-filling process, electron donor-acceptor interaction, hydrogen bonds and hydrophobic interactions are the primary mechanisms for controlling pentachlorophenols adsorption behavior. *Ahmad et al. (2014)* report that polar compounds are adsorbed by H bonding between the compounds and the O-containing moieties of the biochars, whereas non-polar compounds access hydrophobic sites on biochar surfaces in the absence of H-bonding between water and O-containing functional groups.

In fixed-bed column experiments, in Pe10Phe and Sd10Phe the % phenols adsorption was estimated at 90 and 86 % respectively on first day and stayed stable until the third day where sampling

was done again, while % adsorption of phenols through C10Phe was estimated at 18.9 % on first day and at 88 % on third day indicating that physical adsorption takes place also onto quartz sand beside adsorption onto biochars. Sd200Phe shows better % adsorption in the middle (~2.5 h) and at the exit (~4 h) of the column when phenol solution reaches these points for the first time; 83 and 98 % for Sd200Phe instead of 74 and 93 % for Pe200Phe, while higher phenol adsorption (64.4 %) was achieved for Pe200Phe than for Sd200Phe (49 %), because different volumes of the solution were collected at the exit of column after 24 h (953 and 1575 mL respectively) because of the different porosity of the mixture quartz sand-pecan shells biochar and quartz sand-sawdust biochar. After more 4 h, Sd200Phe is more efficient in continuous phenol adsorption than Pe200Phe (53 instead of 31 % adsorption, respectively), since greater volume was treated and less biochar was used for Sd200Phe (17.5 instead of 99 g). As far as pH is concerned, pH of initial phenol solution and final solutions after 24 h did not vary considerably (~6.6 to 7.3 respectively). Therefore, pH does not seem to affect phenols adsorption, although biochars seem to meliorate slightly solutions pH.

Maximum phenol adsorption was observed in the first day during phenol up-flow tests reaching up to 96.1, 93.3 and 92.9 % for Sd20Phe, Pe20Phe and PI20Phe respectively (1.3 and 0.6 L treated volume for Sd20Phe and the rest respectively). Similar % adsorption was observed during the days at which similar volumes were treated (e.g 57.3, 55.5 and 42.8 % with treated volumes of 6.5, 7.5 and 7.1 L for Pe20Phe, Sd20Phe and PI20Phe respectively). However, it is concluded that Sd20Phe is more efficient than Pe20Phe and PI20Phe because significantly less amount of biochar was used (30, 142 and129 g respectively). From the time perspective, Pe20Phe could still adsorb a percentage of 57.3 % on eighth day instead of 43.3 and 26.3 % for PI20Phe and Sd20Phe respectively for the same day. Pe20Phe is found to adsorb at least 35 % of phenols at the fourteenth day. Sd20Phe seems to be saturated on the twelfth day and then equilibrium is reached. Furthermore, in all the experimental columns, pH did not fluctuate significantly before and after adsorption and its values varied from 7.14 to 8.02 for Sd20Phe, 7.6 to 8 for Pe20Phe and 7.06 to 7.62 for PI20Phe. Previous researches were not found to be published for phenols adsorption in fixed-bed columns containing biochars. However, the FTIR analysis of Sd loaded biochars revealed that phenols adsorption includes the same bonds of phenols onto functional groups of biochar regardless experimental setup.

The peak at 3690 cm^{-1} in the FTIR spectra appeared at all polluted biochars of Pe and Sd is attributed to stretching vibration adsorption of hydroxyl groups due to phenols adsorption. *Pakula et al. (2007)* also found the presence of hydroxyl groups in samples of activated carbon used for phenols adsorption. In this study, these bands are slightly shifted and become more intence after phenols adsorption. The changes at this wavelength range indicate changes in carbonyl or carboxyl groups probably due to phenols complexation with these groups. In column experiments Pe20Phe and PI20Phe irregularities were observed in the spectras at the wavelength range of aliphatic C−H stretching vibration. The bands around 1700-1800 cm^{-1} seen in all spectra are attributed to ν(C=O) vibration in carbonyl group or the presence of carboxylic bonds. Structural oxygen species were also found in *Pakula et al. (2007)* study attributed to the respective wavelength range 1705-1730 cm^{-1} (carboxylic, ester, lactonic or anhydride groups). The bands ranging from 1580 to 1640 cm^{-1} seen in all spectra are due to the presence of aromatic C=O ring stretching (likely –COOH) or C=C stretching of aromatic groups in lignin. These bands are also present in the spectra of loaded biochars, but to a lesser degree. After phenols adsorption these bands are becoming more intence indicating greater amount of these functional groups. After phenols adsorption these bands are also shifted marginally suggesting that chemical interactions or complexation occurred between the phenols and these groups on biochar surfaces. *Han et al. (2013)* found bands ranging from 1525 to 1731 cm^{-1} indicative of the binding with phenol molecules. The characteristic group of peaks at 1400-1500 cm^{-1} in raw materials and all the loaded biochars is attributed to phenolic O–H bending.

The band at 1324 cm^{-1} for Pe350 which is moved at lower wave (1318 cm^{-1}) in Pe20Phe is attributed to δ(C=H) vibration in alkanes and alkyl groups or stretching vibration of the phenolic O−H or C−O of carboxylate anion. This band is weakly moved likely due to the coordination between these groups and phenols. Respective wave number ranges for aromatic and alkyl moieties were also found in other studies (*Pakula et al., 2007)*. The band at 1208 cm^{-1} appeared in PI20Phe is likely attributed to C−H bending in plane. Raw materials, biochars and loaded biochars mostly for Pe and PI show peaks in the region 800-600 cm^{-1} attributed to aromatic and heteroaromatic compounds.

The shift of all the above wavelenghts for loaded biochars as well as the coexistence of the absorption bands originated from aromatic stretchings and phenolic O−H bending are indicative of the bindings with phenol molecules *(Han et al., 2013)*. Fig 40 in next section represents the possible bonds of phenols onto biochar arising from all these observations.

4.5. Activation

Activated biochars with KOH solution (PeA350-KOH, SdA350-KOH and PIA350-KOH) not only did not demonstrate enhancement in % phenols adsorption, but showed lower % adsorption than the ones recorded without activation and lower than $FeCl_3$ activated biochars in all cases. This reduction in % phenols adsorption is attributed to the prevention of KOH attached onto biochars. Activated biochars with KOH in *Jin et al. (2014)* study enhanced As^{+5} removal from aqueous solution over a shorter period of time than in non activated biochars (less than 3 h instead of 10 h). For the phenols adsorption in our study, 5 days were needed to reach equilibrium, longer time even than that in respective experiments with non activated biochars. KOH improved As^{+5} adsorption capacity (30.98 mg·g^{-1}) more than 1.3 times compared to non activated biochar *(Jin et al., 2014)*. The proposed base-leaching procedure that they used enhanced surface area, pore volume (development of mesoporosity) and adsorptive capacity of activated carbons produced from sugar cane bagasse and sunflower seed hull biochars pyrolyzed at 500 °C. According to the literature, chemical activation using KOH results in high surface area activated carbon with mostly microporous structure *(Dehkhoda et al., 2016)*. A significant reduction in the pore structure development was observed in *Stavropoulos et al. (2008)* when they used nitric acid for biochar activation. The micropore volume was higher for samples treated at short reaction time, namely 3 h, while additional treatment resulted in the reduction of pore volume due to the incorporation of oxygen functionalities in pore walls and the erosive effect of nitric acid on the carbon structure. Similarly, in our study, KOH <u>may</u> exhibit erosive behavior for the surface of biochar more than desired due to elevated reaction time. In *Han et al. (2013)* study in which steam activation was used, activation not only significantly reduced the surface functional groups, but also assumed a fast adsorption and desorption process for phenols. *Stavropoulos et al. (2008)* propose that urea modification could introduce N functional groups and increase the surface basicity, thus enhancing π-π dispersion forces for phenol uptake. *Pakula et al. (2007)* concluded that the carbon modification procedure affects the final FTIR spectra after phenols adsorption and moreover that the kind of co-adsorbed cation also leads in different spectra. *Jin et al. (2014)* found that after KOH treatment the phenolic and hydroxyl groups as well as the C and O contents increased, but the H content decreased meaning that KOH activation increased O- containing groups but not the polarity. On the other hand, *Angin et al. (2013)* found the H content to increase, but the O content to decrease when biochar was modified with KOH. In their study, C content was also found to increase.

In the FTIR analysis of this study, the peak 3722 cm^{-1} observed for SdA350-KOH is attributed to stretching vibration adsorption of hydroxyl groups due to phenols adsorption. 3400 cm^{-1} peak reapears for the SdA350-KOH indicating the reformation of hydroxyl groups due to OH$^-$ derived from KOH and the increased solution pH also confirmed the increased concentration of OH$^-$ in SdA350-KOH. Moreover, the bands between 1580 and 1700 cm^{-1} are completely disappeared revealing the loss of C=O or C=C groups probably due to the erosive impact of KOH. *Dehkhoda et al. (2016)* claimed that intermediate stages of activation process such as centrifuging and sample drying process after impregnation are key steps for the efficient adsorption capacity of biochars. Centrifuging the samples provided better separation compared to filtration since the use of filter papers led to shrinkage as a result of exposure to highly concentrated KOH solution and problematic separation. In addition, the sample drying process affects porosity development due to the potential conversion of KOH to its corresponding carbonate (e.g. K_2CO_3) due to the presence of CO_2 in the air-dried *(Dehkhoda et al., 2016)*. Moreover, the air dried activated biochars resulted in mixed micro- and meso-porous structures with a decreasing trend of surface area and micropore volume with increasing drying time as *Dehkhoda et al. (2016)* refer. On the other hand, the same researchers found that N_2-dried samples showed mainly microporous structure independent of drying time. Further investigation of the different drying conditions on the conversion of KOH to K_2CO_3, including the presence or absence of CO_2 in the drying atmosphere (i.e., drying under air vs N_2) and its role in tailoring the porosity at specific temperatures needs to be done. This way, KOH modified biochars could be a more efficient, easy and low-cost process for tailoring the biochars porous structure. Fig. 40 also illustrates the phenols adsorption mechanisms onto KOH activated biochar as they arise from this study.

--- hydrogen bonds
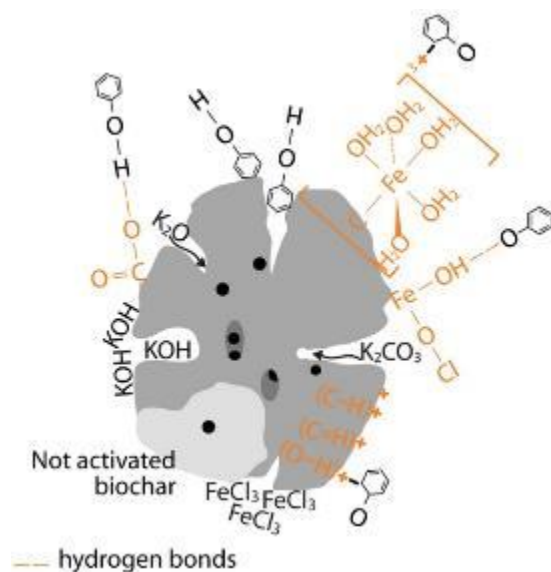
Fig. 40. Schematic representation of phenols adsorption onto biochar

As far as pH is concerned, the increase of pH after phenols adsorption by KOH activated biochars is probably attributed to the release of OH⁻ ions as mentioned before. In the research of *Jin et al. (2014)* the drop in pH value significantly increased when municipal solid wastes KOH activated biochar was used for As^{+5} removal indicating that adsorption of more As^{+5} onto biochars causes the release of more H^+ from the surface site of biochar into solution.

On the contrary with KOH activation, *Chen et al. (2011b)* found that materials activated with Fe^{2+}/Fe^{3+} before pyrolysis adsorbed efficiently organic pollutants from aqueous solutions. In this study, not activated and activated biochars with $FeCl_3$ had similar results for % phenols adsorption, except for PIA350-$FeCl_3$ that exhibited higher % phenols adsorption than PI350 did. Akaganeite can be formed in the ferric chloride solutions because of the interaction of chloride ions with the surface of the hydrous iron. In this case, amorphous FeOOH can be the active substance of biochar *(Li et al., 2016)* (Fig. 40). The surface of PIA350-$FeCl_3$ is positively charged with the form C-Fe(OH$_2$)$_5^{+3}$$_{(s)}$ which retained in the solid matrix of biochar contributing therefore to the electrostatic power developed between adsorbent and adsorbate. Under acidic conditions in solution the concentration of this form is elevated and thus ionic phenols are adsorbed onto PIA350-$FeCl_3$ explaining the small increase in phenols adsorption. However, in acidic pH the concentration of ionic form of phenols is not as high as in elevated pH (pH>pKa) as explained before in 4.4 section indicating that this modification would be more beneficial for contaminants that exist mostly in ionic form when the pH is acidic. As far as PeA350-$FeCl_3$ and SdA350-$FeCl_3$ are concerned, excess iron probably blocked their microporous structure and decreased the contact area of ionic adsorbate and iron (hydr)oxides. In PeA350-$FeCl_3$ and SdA350-$FeCl_3$ the pores seemed to be blocked by iron, while in PIA350-$FeCl_3$ not, probably due to their different porous structure which is microporous and macroporous, respectively, as the SEM analysis revealed. When *Li et al. (2016)* used $FeCl_3$ in order to coat biochar they found that a mass ratio of iron to biochar equal to 0.70 was the optimal for nitrogen adsorption, viz 125 mL of 1 mol·L⁻¹ $FeCl_3$ ($FeCl_3$·$6H_2O$) with 10 g biochar. In our study, 500 mL of the same concentration of $FeCl_3$ where mixed with 20 g biochar. However, removal percentage in *Li et al. (2016)* research began to decline at a mass ratio of 0.84, viz 150 mL solution with 10 g biochar indicating that an optimal ratio of iron to biochar should be used which is probably unique for each biochar of different feedstock material or/and pyrolysis temperature.

Drop in pH after phenols adsorption by iron coated biochars is attributed to H^+ released by phenols attached onto C-Fe(OH$_2$)$_5^{+3}$$_{(s)}$. Moreover, pursuant to following hydrolytic reactions, increase of solution pH would lead to [C-Fe(OH$_2$)$_4$(OH)]$^{+2}$$_{(s)}$ and [C-Fe(OH$_2$)$_3$(OH)]$^+$$_{(s)}$ *(Li et al., 2016)* and thus to less phenols adsorbed.

$$C-Fe(OH_2)_5^{+3} + H_2O \leftrightarrow [C-Fe(OH_2)_4(OH)]^{+2}_{(s)} + H_3O^+$$

$$[C-Fe(OH_2)_4(OH)]^{+2}_{(s)} + H_2O \leftrightarrow [C-Fe(OH_2)_3(OH)]^+_{(s)} + H_3O^+$$
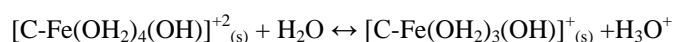
According to this, *Li et. al (2016)* found the most effective pH values for nitrate and phosphate removal by $FeCl_3$ activated biochar equal to 3 and 6, respectively. They used KNO_3 which is fully

dissociated in water solution and KH_2PO_4 which has three pKa, namely 2.15, 6.82 and 12.38 (phosphoric acid), while phenols have a pKa of 9.98, meaning that potential adsorbate phenol ions will exist in higher concentration at pH higher than 10. However, phenols are hydrophobic and the ionic form of phenols is less hydrophobic *(Mathialagan and Viraraghavan, 2009)* which may cause reduction of phenols adsorption via the reduced pore filling of biochar. Another opinion says that at low pH (e.g. 2) the surfaces of activated carbons are protonated and have acidic surfaces with positive charges which interact by dispersion electron donor-acceptor interaction with phenols which in that case behave as weak base *(Dehkhoda et al., 2016)*. In contrary, at pH 12 the surfaces of activated carbons have negative charges and the molecules of phenol are in the form of the phenolic anion. These cause the electrostatic repulsion between the biochar surfaces and phenolic anions. From the above it is concluded that impregnation of biochar with $FeCl_3$ is not appropriate procedure for adsorption of contaminants with high pKa (e.g. over 6).

4.6. Quality of biochar

For all biochars used in this study, high surface area values are shown when biochars are produced at higher temperatures reaching 298.7 $m^2 \cdot g^{-1}$ for Pe550 far higher than that shown mainly for Pe250, namely 3.2 $m^2 \cdot g^{-1}$. Similar results have been reported for sewage sludge biochar produced at 300 °C, namely 4.4 $m^2 \cdot g^{-1}$ *(Agrafioti, 2014)* and switchgrass biochar produced at 500°C, namely 3.62 $m^2 \cdot g^{-1}$ *(Han et al., 2013)*, while for both materials pyrolyzed at higher temperatures surface area increased at 18.4 (500°C) and 73.24 $m^2 \cdot g^{-1}$ (700°C) respectively. Moreover, a surface area of 795 $m^2 \cdot g^{-1}$ has been reported for pinus radiate sawdust produced at 700 °C *(Srinivasan and Sarmah, 2015)*. The progressive increase in biochar surface area at higher temperatures may be attributed to chemical changes such as decomposition of organic substances and improve of aromaticity of biochars which lead to the creation of micro and mesopores directly correlated to high surface areas *(Ding et al., 2014; Agrafioti, 2014)*. It seems, however, that different feedstock materials (e.g. with different composition, ash content and pore structure) produce biochars with different pore structure even if they are derived from same pyrolysis temperatures. The surface area is also related to the production procedure as mentioned in the previous section. Other factors such as heating rate and pyrolysis time are also said to influence surface area *(Agrafioti, 2014)*. Extremely higher surface area of 1277 $m^2 \cdot g^{-1}$ for activated carbon with potassium hydroxide prepared from safflower seed cake biochar at 500 °C was reported for a high heating rate of 50 °C·min^{-1} *(Angin et al., 2013)*. As a consequence of different feedstock materials and different pyrolysis conditions, the pore volumes and pore structures differ. The SEM images of raw Pe and Sd were quite homogeneous, while for Pe350 and Sd350 a microporous structure (particle size 9- 18 μm) was formed, due to the release of volatiles. Increase of these pores (mesopores) and development of new pores was observed for Pe550 and Sd550 (particle size 21- 48 μm) as a result of the continuous release of other high-molecular-weight volatiles. In *Jin e al. (2014)* study a rougher surface was also observed for biochar produced from municipal solid waste biochar at higher temperatures. *Gray et al. (2014)* have reported that as temperature increases, porosity increases as well due to the transformation of aliphatic C structures to aromatic C structures. Furthermore, the formation of new and well structured pores may contribute to the use of biochar as soil amendment as it can provide habitats for symbiotic microorganisms *(Hernandez-Mena et al., 2014)*. The matrix of raw PI was heterogeneous containing particles with varying size (27.5-228 μm), while PI300 revealed macropores with varying size and shape (51.9- 565 μm) due to irregularly scattered micropores because of the release of volatiles. For PI550, a more homogenous matrix was observed and the grain size became smaller (6.25- 35.7 μm) due to decomposition of more volatile fractions that were not fully decomposed at temperatures below 500 °C. Oil palm empty fruit bunch biochar produced at 350 °C exhibited uniform micropores (≤10 μm) with smooth wall surfaces, while rice husk biochar produced at the same temperature exhibited heterogeneous porous structure with rough surface *(Norazlina et al., 2014)*. Moreover, the activation with KOH of municipal solid waste biochar resulted in 10 times higher pore volume due to KOH etching that lead to destruction of some nanopore structures and deformation from nanopores into meso-/macropores *(Jin et al. 2014)* as revealed a more intensive porous structures formed on the surface as a result of organic matters or ash having been removed from the surface or small-sized pores.

    Jin et al. (2014) found that the activation procedure produce biochars with significantly increased surface area and total pore volume and partly changed functional groups on the surface of biochars. Activated carbon with steam exhibited much higher surface area than switchgrass biochar produced at 500°C in *Han et al. (2013)* study, namely 167.83 and 3.62 $m^2 \cdot g^{-1}$, respectively. Similar trend was observed by *Angin et al., (2013)* who found that the activated carbon produced by chemical activation with KOH of biochar produced by safflower seed press cake at 800 °C had a surface area of 1277

$m^2 \cdot g^{-1}$, extremely higher than that of 14.14 $m^2 \cdot g^{-1}$ found for respective biochar produced at 500 °C. Moreover, they found a well developed uniform pore structure for activated biochar, with a new matrix compared to biochar. The surface areas of activated carbon produced from sugar cane bagasse and sunflower seed hull biochars using H_3PO_4 and $ZnCl_2$ at 500 °C was similarly as high as 1611 and 2289 $m^2 \cdot g^{-1}$ for the first material and 1543 and 2240 $m^2 \cdot g^{-1}$ for the second one (*Liou et al., 2010*). Activation has been also found by *Liou et al. (2010)* to significantly influence the pore structure (development of mesoporosity) and adsorptive capacity of biochars. Thus, modification of biochars could be an efficient, easy and low-cost process for tailoring the biochars' porous structure adsorptive capacity.

5 Conclusions

The pyrolysis yield of Pe, Sd and Pl was found to decrease primarily with the increase of pyrolysis temperature and to a lesser degree with the raise of pyrolysis time. Other factors, such as the presence of lignocellulosic constituents seem to also affect the pyrolysis yield. pH, EC and carbon content were found to increase with increasing temperature, while oxygen content was found to decrease. All the feedstocks (Pe, Sd and Pl) spectra are characteristic of a generic oxygenated hydrocarbon, while lose these moieties with the pyrolysis due to decomposition of hemicellulose and cellulose.

Pecan shells and sawdust biochars were found to adsorb more effectively Pb and Cd compared to Cu and Co. Pb is much better removed by pecan shells biochar (98.5 %) compared to sawdust biochar (72.5 %) while for Cu, Cd and Co sawdust biochar was a better adsorbent. In general, the higher the adsorbent concentration the higher is the % adsorption of heavy metal and most of metal ions removal occurred within 2 h in all cases. Moreover, it seems that there is a crucial adsorbent concentration for the best adsorption rate of metals onto biochars which is dependent on biochar structure and metal ions boundaries. The pseudo-second-order kinetic model was found to fit better heavy metals adsorption data and the principal adsorption mechanism of adsorbate onto adsorbent is chemical adsorption of divalent metal ions onto polar functional groups of adsorbent namely hydroxyl, carboxyl and ether which are bound with metals through complexation and cation exchange. If biochars are produced at higher temperatures the intraparticle diffusion through pore spaces is assumed to mainly determine metal adsorption. However, other factors such as released anions (CO_3^{2-}) from minerals present in biochars and high C content are considered to contribute to metal ions removal. The % heavy metal removal is related to the structure of biochars and nature of heavy metal adsorbed and not to the washing solution. After 24 h of desorption, using 0.1 M HNO_3 as desorbing agent, Pe350 showed the lowest desorption of Pb (63.3 %). For the rest, the use of 0.1 M HCl as desorbing agent resulted in Pb desorption from Pe350 while the use of HNO_3 or HCl as desorption agents resulted in Cu desorption from both biochars, ranging from 73.5 to 100 %. The adsorption capacities obtained after second adsorption revealed that Sd350 is a better adsorbent compared with Pe350.

Higher adsorbent concentrations result in increased % phenols adsorption. The highest % adsorption was 70 % shown for 5 $g \cdot L^{-1}$ SdPhe at equilibrium time of 48 h, while most phenols removal occurred within 24 h accounting for 67.4 to 98.6 % of total phenols adsorption. Different combinations of adsorption mechanisms are involved when different adsorbates are adsorbed onto biochars. Micropore surface area, pore structure and functional groups, rather than the specific surface area alone are the dominating factors that significantly impact adsorption of phenols. The pseudo-second-order kinetic model fit the data better than the pseudo-first-order kinetic model indicating chemical bonding between ionic phenols and polar functional groups such as carboxyl and OH groups on the adsorbent also verified by the FTIR analysis. It seems, however, that there is a priority for phenols to penetrate into pore spaces. Moreover, PePhe and SdPhe seem to bind H^+ first and subsequently phenols probably explaining the longer time needed for equilibrium concentration. From an environmental perspective, the biochars not only can be used for phenols reduction in water solutions, but also for pH amelioration. The alteration of initial solution pH did not affect phenols adsorption, probably due to the buffering capacity of biochars. In fixed-bed columns, Sd biochar is more efficient in continuous phenol adsorption experiments than Pe and Pl biochar because a much lesser amount of biochar is used to achieve similar % adsorption.

Activated biochars with KOH solution not only did not demonstrate enhancement in % phenols adsorption, but showed lower than $FeCl_3$ activated biochars and lower than the ones without activation, mainly due to the erosive impact of KOH. Further investigation of the different drying conditions should be also examined. For activated biochar PlA350-$FeCl_3$ the % phenols adsorption was higher than that for not activated biochar, while for the other activated biochars adsorption was similar. Functional groups such as carboxyl and OH groups as well as the amorphous FeOOH and the Fe complexes were the active substances of activated biochars contributing to the electrostatic power developed between adsorbent and adsorbate. However, it seems that impregnation of biochar with

FeCl$_3$ is not appropriate procedure for enhanced adsorption of contaminants with high pKa when the pH of solution is acidic.

Surface area and pore structure of biochars depends on the nature of feedstock materials and can be quite different for biochars of common origin when they are produced at different temperatures or when they have been subjected to activation. Moreover, the properties of biochar are different from those of chemical activated carbon, though both of them are carbon-rich materials. Higher surface area is obtained, when biochars are produced at higher temperatures, reaching 298.7 m$^2 \cdot$g^{-1} due to chemical changes occurring on the biochar surface such as decomposition of organic substances and improvement of aromaticity, which lead to the creation of micro and mesopores.

All the above findings are important for selecting biochars and activated carbons that may be suitable for heavy metal or phenols adsorption from wastewaters and treatment of industrial waste containing phenolic compounds. However, the direct comparison of experimental results with literature data is complicated due to the diversity of experimental conditions and parameters. A great number of additional experiments needs to be done in the future.

References

Abdel-Fattah T. M., Mahmoud M. E., Ahmed S. B., Huff M. D., Lee J. W., Kumar S.: Biochar from woody biomass for removing metal contaminants and carbon sequestration. Journal of Industrial and Engineering Chemistry 22, 103–109 (2015)

Agegnehua G., Nelson P. N., Bird M. I.: Crop yield, plant nutrient uptake and soil physicochemical properties under organic soil amendments and nitrogen fertilization on Nitisols. Soil & Tillage Research 160, 1–13 (2016)

Agrafioti E., Kalderis D., Diamadopoulos E.: Arsenic and chromium removal from water using biochars derived from rice husk, organic solid wastes and sewage sludge. Journal of Environmental Management 133, 309−314 (2014)

Ahmad M., Lee S.S., Oh S.-E., Mohan D., Moon D.H., Lee Y.H., Ok Y.S.: Modeling adsorption kinetics of trichloroethylene onto biochars derived from soybean stover and peanut shell wastes. Environmental Science and Pollution Research 20, 8364−8373 (2013)

Angin D., Şensöz S.: Effect of Pyrolysis Temperature on Chemical and Surface Properties of Biochar of Rapeseed (Brassica napus L.). International Journal of Phytoremediation 16, 684−693 (2014)

Barceloux D. G. and Barceloux D.: Cobalt. Journal of Toxicology: Clinical Toxicology 37, 201–216 (1999)

Barrow C.J.: Biochar: Potential for countering land degradation and for improving agriculture. Applied Geography 34, 21−28 (2012)

Brewer G. J. MD, MACN: The Risks of Copper Toxicity Contributing to Cognitive Decline in the Aging Population and to Alzheimer's Disease. Journal of the American College of Nutrition 28 (3), 238–242 (2009)

Brewer G. J.: Copper excess, zinc deficiency, and cognition loss in Alzheimer's disease. BioFactors (Oxford, England) 38(2), 107–113 (2012)

Caglar A., Demirbas A.: Conversion of cotton cocoon shell to liquid products by pyrolysis. Energy Conversion and Management, 41, 1749–1756 (2000)

Cao X., Harris W.: Properties of dairy-manure-derived biochar pertinent to its potential use in remediation. Bioresource Technology, 101, 5222−5228 (2010)

Centers for Disease Control and Prevention (CDC)

Chen B., Chen Z., Lv S.: A novel magnetic biochar efficiently sorbs organic pollutants and phosphate. Bioresource Technology, 102, 716−723 (2011)

Dai Z., Meng J., Muhammad N., Liu X., Wang H., He Y., Brookes P. C., Xu J.: The potential feasibility for soil improvement, based on the properties of biochars pyrolyzed from different feedstocks. Journal of Soils and Sediments 13, 989–1000 (2013)

Deenik J.L., McClellan, T., Uehara, G., Antal, M.J., Campbell, S.: Charcoal volatile matter content influences plant growth and soil nitrogen transformations. Soil Science Society of America. J. 74, 1259−1270 (2010)

Dehkhoda A. M., Gyenge E., Ellis N.: A novel method to tailor the porous structure of KOH-activated biochar and its application in capacitive deionization and energy storage. Biomass and Bioenergy 87, 107–121 (2016)

Deichmann W.B., Gerarde H.W.: Toxicology of drugs and chemicals. Phenol (carbolic acid). Academic Press 463-464 (1969)

Desta M. B.: Batch Sorption Experiments: Langmuir and *Freundlich* Isotherm Studies for the Adsorption of Textile Metal Ions onto Teff Straw (Eragrostis tef) Agricultural Waste. Journal of Thermodynamics 2013 (2013)

Ding W., Dong X., Ime I. M., Gao B., Ma L. Q.: Pyrolytic temperatures impact lead sorption mechanisms by bagasse biochars. Chemosphere 105, 68–74 (2014)

Ding W., Dong X., Ime I., Gao B., Ma L.: Pyrolytic temperatures impact lead sorption mechanisms by bagasse biochars. Chemosphere 105, 68–74 (2014)

Dokken K., Davis L. C., Erickson L. E. and Castro S.: Fourier-Transform Infrared spectroscopy as a tool to monitor changes in plant structure in response to soil contaminants. Waste Research Technology (2002)

Doumer M. E., Rigol A., Vidal M., Mangrich A. S.: Removal of Cd, Cu, Pb, and Zn from aqueous solutions by biochars. Environmental Science and Pollution Research 23, 2684–2692 (2016)

Elaigwu S., Rocher V., Kyriakou G., Greenway G.: Removal of Pb^{2+} and Cd^{2+} from aqueous solution using chars from pyrolysis and microwave-assisted hydrothermal carbonization of Prosopis africana shell. Journal of Industrial and Engineering Chemistry 20, 3467–3473 (2014)

EPA. United States Environmental Protection Agency

Gaskin J.W., Steiner C., Harris K., Das K.C., Bibens B.: Effect of low-temperature pyrolysis conditions on biochar for agricultural use. Transactions of the ASABE 51, 2061–2069 (2008)

Ghani W.A.W.A.K., Mohd A., Da Silva G., Bachmann R.T., Taufiq-Yap Y.H., Rashid U., Al-Muhtaseb A.H.: Biochar production from waste rubber-wood-sawdust and its potential use in C sequestration: Chemical and physical characterization. Industrial Crops and Products 44, 18−24 (2013)

Gopal K., Srivastava S.B., Shukla S., Bersillon J.L.: Contaminants in drinking water and its mitigation using suitable adsorbents: An overview. Journal of Environmental Biology 25, 469–475 (2004)

Gray M., Johnson M.G., Dragila M.I., Kleber M.: Water uptake in biochars: The roles of porosity and hydrophobicity. Biomass and Bioenergy 61, 196−205 (2014)

Han Y., Boateng A. A., Qi P. X., Lima I. M., Chang J.: Heavy metal and phenol adsorptive properties of biochars from pyrolyzed switchgrass and woody biomass in correlation with surface properties. Journal of Environmental Management 118, 196−204 (2013)

Han Y., Boateng A., Qi P., Lima I., Chang J.: Heavy metal and phenol adsorptive properties of biochars from pyrolyzed switchgrass and woody biomass in correlation with surface properties. Journal of Environmental Management 118, 196-204 (2013)

Hansen V., Müller-Stöver D., Munkholm L. J., Peltre C., Hauggaard-Nielsen H., Jensen L. S.: The effect of straw and wood gasification biochar on carbon sequestration, selected soil fertility indicators and functional groups in soil: An incubation study. Geoderma 269, 99–107 (2016)

He Q., Chen Z.: Characterization and kinetics of biochar prepared from pomelo peel for adsorption of phenol. Chinese Journal of Environmental Engineering 8, 3853−3859 (2014)

Hernandez-Mena L.E., Pécora A.A.B., Beraldo A.L.: Slow Pyrolysis of Bamboo Biomass: Analysis of Biochar Properties. Chemical Engineering Transactions 37, 115–120 (2014)

Houben, D., Sonnet, P., Cornelis, J.-T.: Biochar from Miscanthus: a potential silicon fertilizer. Plant Soil 374, 871–882 (2014)

Jeffrey M. N., Keri B. C., Donald W. W., Warren J. B. & Mark G. J.: Designing relevant biochars as soil amendments using lignocellulosic-based and manure-based feedstocks. Journal of Soils and Sediments 11368, 0680−8 (2013)

Jin H., Capareda S., Chang Z., Gao J., Xu Y., Zhang J.: Biochar pyrolytically produced from municipal solid wastes for aqueous As(V) removal: Adsorption property and its improvement with KOH activation. Bioresource Technology 169, 622–629 (2014)

Jin H., Hanif M. U., Capareda S., Chang Z., Huang H., Ai Y.: Copper(II) removal potential from aqueous solution by pyrolysis biochar derived from anaerobically digested algae-dairy-manure and effect of KOH activation. Journal of Environmental Chemical Engineering 4, 365–372 (2016)

Kan T., Strezov V., Evans T.: Lignocellulosic biomass pyrolysis: A review of product properties and effects of pyrolysis parameters. Renewable and Sustainable Energy Reviews 57, 1126–1140 (2016)

Karhu K., Mattila T., Bergström I., Regina K.: Biochar addition to agricultural soil increased CH_4 uptake and water holding capacity - Results from a short-term pilot field study. Agriculture, Ecosystems and Environment 140, 309–313(2011)

Komnitsas K., Zaharaki D., Pyliotis I., Vamvuka D., Bartzas G.: Assessment of pistachio shell biochar quality and its potential for adsorption of heavy metals. Waste and Biomass Valorization 6, 805–816 (2015)

Lang Y.-H., Liu W., Wang H.: Adsorption efficiencies of pentachlorophenol from aqueous solution onto biochars Zhongguo Huanjing Kexue/China Environmental Science 34, 2017−2023 (2014)

Lao C., Zeledon Z., Gamisans X., Sole M.: Sorption of Cd(II) and Pb(II) from aqueous solutions by a low-rank coal (leonardite). Separation and Purification Technology 45, 79–85(2005)

Lazo-Cannata j., Márquez A., Jacoby A., Paredes-Doig A., Romero A., Sun-Kou M., Valverde J.: Adsorption of phenol and nitrophenols by carbon nanospheres: Effect of pH and ionic strength. Separation and Purification Technology 80, 217–224 (2011)

Lefaux R.: Practical toxicology of plastics. Chemical Rubber 329 (1978)

Lehmann, J., & Joseph, S.: Biochar for environmental management: science and technology. London: Earthscan (2009)

Li J., Lv G., Bai W., Liu Q., Zhang Y., Song J.: Modification and use of biochar from wheat straw (Triticum aestivum L.) for nitrate and phosphate removal from water. Desalination and Water Treatment, 4681–4693 (2014)

Liou T.-H.: Development of mesoporous structure and high adsorption capacity of biomass-based activated carbon by phosphoric acid and zinc chloride activation. Chemical Engineering Journal. 158, 129−142 (2010)

Liu Z., Quek A., Hoekman S.K., Balasubramanian R.: Production of solid biochar fuel from waste biomass by hydrothermal carbonization. Fuel 103, 943–949 (2013)

Liu, Xiang-Hong, Zhang, Xing-Chang: Effect of biochar on pH of alkaline soils in the loess plateau: results from incubation experiments. International Journal of Agricalture and Biology 14, 745–750 (2012)

Machida M., Mochimaru T., Tatsumoto H.: Lead (II) adsorption onto the graphene layer of carbonaceous materials in aqueous solution. Carbon 44, 2681−2688 (2006)

Manifold I.H., Platts M.M., Kennedy A.: Cobalt cardiomyopathy in a patient on maintenance haemodialysis. British Medical Journal 6152, 1609 (1978)

Manyà J.: Pyrolysis for Biochar Purposes: A Review to Establish Current Knowledge Gaps and Research Needs. Environmental Science & Technology 46, 7939−7954 (2012)

Manyà J.: Pyrolysis for Biochar Purposes: A Review to Establish Current Knowledge Gaps and Research Needs. Environmental Science and Technology 46, 7939−7954 (2012)

Marschner, H.: Marschner's Mineral Nutrition of Higher Plants (Third Edition). Academic Press 369–388 (2012)

Mathialagan T., Viraraghavan T.: Biosorption of pentachlorophenol from aqueous solutions by a fungal biomass. Bioresource Technology. 100, 549–558 (2009)

Mohan D., Rajput S., Singh V.K., Steele P.H., Pittman C.U.: Modeling and evaluation of chromium remediation from water using low cost bio-char, a green compost. Journal of Hazardous Materials. 188, 319−333 (2011)

Mohan D., Sarswat A., Ok Y. S, Pittman Jr C. U.: Organic and inorganic contaminants removal from water with biochar, a renewable, low cost and sustainable adsorbent – A critical review. Bioresource Technology 160, 191–202 (2014)

Niandou M. A. S., Novak J. M., Bansode R. R., Yu J., Rehrah D. and Ahmedna M.: Selection of Pecan Shell–Based Activated Carbons for Removal of Organic and Inorganic Impurities from Water. Journal of Environmental Quality 42, 902−911 (2013)

Norazlina A.S., Ishak C.F., Bakar R.A.: Characterization of oil palm empty fruit bunch and rice husk biochars and their potential to adsorb arsenic and cadmium. American Journal of Agricultural and Biological Sciences 9 (3), 450-456 (2014)

Novak J.M., Lima I., Xing B., Gaskin J.W., Steiner C., Das K.C., Ahmedna M., Rehrah D., Watts D.W., Busscher W.J., Schomberg H.: Characterization of designer biochar produced at different temperatures and their effects on a loamy sand. Annals of Environmental Science 3, 195–206 (2009)

Organization WH: Guidelines for drinking-water quality: incorporating 1st and 2nd addenda.

Pakula M., Walczyk M., Biniak S., Swiatkowski A.: Electrochemical and FTIR studies of the mutual influence of lead(II) or iron(III) and phenol on their adsorption from aqueous acid solution by modified activated carbons. Chemosphere 69, 209–219 (2007)

Panumati S., Chudecha K., Vankhaew P., Choolert V., Chuenchom L., Innajitara W., Sirichote O.: Adsorption of phenol from diluted aqueous solutions by activated carbons obtained from bagasse, oil palm shell and pericarp of rubber fruit. Songklanakarin Journal of Science and Technology 30 (2), 185–189 (2008)

Pastorova I., Botto R.E., Arisz P.W., Boon J.J.: Cellulose char structure: a combined analytical Py-GC-MS, FTIR, and NMR study. Carbohydrate Research 262, 27−47 (1994)

Peng P., Lang Y., Wang X.: Adsorption behavior and mechanism of pentachlorophenol on reed biochars: pH effect, pyrolysis temperature, hydrochloric acid treatment and isotherms. Ecological Engineering 90, 225–233(2016)

Purakayastha T.J., S., Pathak H.: Characterisation, stability, and microbial effects of four biochars produced from crop residues. Geoderma 239–240, 293–303 (2015)

Qiu Y.P., Zheng Z.Z., Zhou Z.L., Sheng G.D.: Effectiveness and mechanisms of dye adsorption on a straw-based biochar. Bioresource Technology 100, 5348–5351 (2009)

Rajapaksha A. U., Chen S. S., Tsang D. C.W., Zhang M., Vithanage M., Mandal S., Gao B., Bolan N. S., Ok Y. S.: Engineered/designer biochar for contaminant removal/immobilization from soil and water: Potential and implication of biochar modification. Chemosphere 148, 276−291 (2016)

Recommendations WHO (2008)

Sánchez M.E., Lindao E., Margaleff D., Martínez O., Morán A.: Pyrolysis of agricultural residues from rape and sunflowers: Production and characterization of bio-fuels and biochar soil management. Journal of Analytical and Applied Pyrolysis 85, 142–144 (2009)

Sharma R.K., Wooten J.B., Baliga V.L., Lin X., Geoffrey Chan W., Hajaligol M.R.: Characterization of chars from pyrolysis of lignin. Fuel 83, 1469–1482 (2004)

Singh R., Gautam N., Mishra A. and Gupta R.: Heavy metals and living systems: An overview. Indian Journal of Pharmacology 43, 246–253 (2011)

Smith M. B., Jerry M.: Advanced Organic Chemistry: Reactions, Mechanisms and Structure (6th ed.). Wiley-Interscience (2007)

Socrates G.: Infrared and Raman Characteristic Group Frequencies. John Wiley & Sons Ltd, 3rd ed. (2001)

Sohi, S.P., Krull, E., Bol, R.: A review of biochar and its use and function in soil. Advances in Agronomy. 105, 47–82 (2010)

Soil Association: Introduction to biochar. Information sheet. Carbon Gold

Sparkes J. and Stoutjesdijk P.: Biochar: implications for agricultural productivity. Technical report 11.06. Department of Agriculture, Fisheries and Forestry (2011)

Srinivasan P., Sarmah A. K.: Characterisation of agricultural waste-derived biochars and their sorption potential for sulfamethoxazole in pasture soil: A spectroscopic investigation. Science of the Total Environment 502, 471–480 (2015)

Stavropoulos G., Samaras P., Sakellaropoulos G.: Effect of activated carbons modification on porosity, surface structure and phenol adsorption. Journal of Hazardous Materials 151, 414–421 (2008)

Sun H., Hockaday W., Masiello C., Zygourakis K.: Multiple Controls on the Chemical and Physical Structure of Biochars. Industrial & Engineering Chemistry Research 51, 3587−3597 (2012)

Tang J., Lv H., Gong Y., Huang Y.: Preparation and characterization of a novel graphene/biochar composite for aqueous phenanthrene and mercury removal. Bioresource Technology 196, 355–363 (2015)

Tox FAQs: CABS/Chemical Agent Briefing Sheet: Lead. Agency for Toxic Substances and Disease Registry/ Division of Toxicology and Environmental Medicine (2006)

Tripathi M., J.N. Sahu, Ganesan P.: Effect of process parameters on production of biochar from biomass waste through pyrolysis: A review. Renewable and Sustainable Energy Reviews 55, 467–481 (2016)

Uchimiya M., Chang SeChin, Klasson T. K.: Screening biochars for heavy metal retention in soil: Role of oxygen functional groups. Journal of Hazardous Materials 190, 432–441(2011)

Van Zwieten L., Singh B., Joseph S., Kimber S., Cowie A., Chan K.Y.: Biochar and emissions of non-CO_2 greenhouse gases from soil. Biochar for Environmental Management – Science and Technology 227–249 (2009)

Vasanth Kumar K., Sivanesan S.: Isotherm parameters for basic dyes onto activated carbon: Comparison of linear and non-linear method. Journal of Hazardous Materials B129, 147–150 (2006)

Wang X., Lu Z., Miao H., He W., Shen H.: Kinetics of Pb (II) adsorption on black carbon derived from wheat residue. Chemical Engineering Journal 166, 986–993 (2011a)

Weber M., Weber M., Kleine-Boymann M.: Ullmann's Encyclopedia of Industrial Chemistry (2004)

Wu Y., Zhang P., Zhang H., Zeng G., Liu J., Ye J., Fang W., Gou X.: Possibility of sludge conditioning and dewatering with rice husk biochar modified by ferric chloride. Bioresource Technology (2015)

Xiang-Yang Yu, Guang-Guo Ying, & Kookana, R. S.: Reduced plant uptake of pesticides with biochar additions to the soil. Chemosphere 76, 665−671 (2009)

Yaman S.: Pyrolysis of biomass to produce fuels and chemical feedstocks. Energy Conversion and Management 45, 651–671 (2004)

Zeng Z., Zhang S., Li T., Zhao F., He Z., Zhao H., Yang X., Wang H., Zhao J., Rafiq M. T.: Sorption of ammonium and phosphate from aqueous solution by biochar derived from phytoremediation plants. Journal of Zhejiang University-SCIENCE B 14, 1152−1161 (2013)

Zhang A., Bian R., Hussaina Q., Li L., Pana G., Zheng J., Zhang X., Zheng J.: Change in net global warming potential of a rice–wheat cropping system with biochar soil amendment in a rice paddy from China. Agriculture, Ecosystems and Environment 173, 37–45 (2013)

Zhenyu W., Guocheng L., Hao Z., Fengmin Li, Huu Hao Ngo, Wenshan Guo, Cui L., Lei Chen, Baoshan X.: Investigating the mechanisms of biochar's removal of lead from solution. Bioresource Technology 177, 308–317 (2015)

Ελληνική βιβλιογραφία

Αγραφιώτη Ε.: Παραγωγή εξανθρακώματος από βιομάζα για περιβαλλοντικές εφαρμογές. Διδακτορική διατριβή. Σχολή μηχανικών Περιβάλλοντος, Πολυτεχνείο Κρήτης (2014)

Υγειονομική διάταξη Υ2/2600/21-6-2001 (ΦΕΚ 892/Β/11-7-2001 και ΦΕΚ 1082/Β/14-8-2001), "Ποιότητα του νερού ανθρώπινης κατανάλωσης" σε συμμόρφωση προς την Οδηγία 98/83/ΕΚ του Συμβουλίου της Ευρωπαϊκής Ένωσης της 3ης Νοεμβρίου 1998, όπως τροποποιήθηκε από την Αριθμ,. ΔΥΓ2/Γ.Π.οικ 38295 Κ.Υ.Α. (ΦΕΚ 630/Β/26-4-2007), με διόρθωση σφαλμάτων (ΦΕΚ 986/Β/18-06-2007).